Infrared and millimeter waves, Vol. 13, pp. 171-263, Orlando, FL, Academic Press, Inc. (1985)

Far-infrared properties of inhomogeneous materials

G.L. Carr and S. Perkowitz

Department of Physics
Emory University
Atlanta, Georgia 30322

D.B. Tanner

Department of Physics
University of Florida
Gainesville, Florida 32611

CONTENTS

I. Introduction....1

II. Example: Gold black....3

A. The material....3

B. Infrared measurements....3

C. Discussion of gold black data....4

III. The basic theory....5

A. The effective response functions....5

1. The dielectric function of a homogeneous substance....5

2. The Drude dielectric function....9

3. The response of an inhomogeneous medium....11

4. The effective medium....13

B. Response of a single grain....15

1. Quasistatic model: Electric dipole moment....15

2. Eddy currents: Magnetic dipole moment....16

3. Mie theory....18

C. Effective medium theories....22

1. Average fields....22

2. Maxwell-Garnett dielectric function....23

3. Maxwell-Garnett permeability....26

4. Mie expressions for the dielectric function....26

5. The effective medium approximation....27

6. Effective medium permeability....29

IV. Discussion of the theory....31

A. Numerical examples....31

B. Expansion at small volume fraction and low frequency.....34

C. Other shapes, other constituents, other sizes.....37

1. Ellipsoidal particles.....37

2. Dielectric function for oriented ellipsoids.....39

3. Dielectric function for randomly oriented ellipsoids....40

4. Many constituents.....42

5. Size distributions.....44

D. Modern theories of small particle composites.....46

1. Effective medium theories.....46

2. Percolation theory.....49

3. Mean free path and non-local effects.....51

V. Experiments on normal-metal and insulator composites.....55

A. Near infrared and visible studies.....56

1. Very dilute systems.....56

2. Discontinuous films.....57

3. Granular metal films.....58

4. Gas evaporated particles.....60

B. Far infrared studies.....63

1. Unsupported smoke.....63

2. Metal-particle/insulator composities.....64

3. Other systems.....67

VI. Superconductivity.....68

A. Homogeneous superconductors.....68

1. The frequency-dependent conductivity of a superconductor.....68

2. Thin superconducting films.....70

3. Deviations from Mathis Bardeen prections.....71

B. Theories for inhomogeneous superconductors.....74

1. Small dimensions....74

2. Effective-medium theories for superconductiny-particle composites....76

3. Thin granular films....78

4. Superconducting/normal-metal composites....79

C. Experimental studies of inhomogeneous superconductors....80

1. Superconducting small particles....81

2. Granular films....84

VII. Discussion of the anomalies....89

A. Oxides....89

B. Interactions and clustering....91

C. Hopping conduction....93

D. Quantum size effects....96

1. The gap....97

2. The static dielectric constant....100

3. The frequency-dependent dielectric function....101

4. Comparison with classical models....105

5. Observation of quantum size effects....106

VIII. Another inhomogeneous material: Layered semiconductor systems...108

IX. Summary....112

Acknowledgement....114

References....115

Figure Captions....122

Figures....127

I. Introduction.

The subject of this review is the far-infrared properties of randomly inhomogeneous media consisting of mixtures of two or more kinds of small particles. The size of an individual particle (approximately 100 Å) is large compared with atomic dimensions but small compared to the wavelength of far-infrared radiation (50 to 1000 μm). On the scale of the wavelength, these inhomogeneous media appear to be homogeneous and to have a well-defined effective dielectric response function. One of the goals of research in this area is to understand the ways in which the effective properties of an inhomogeneous medium depend upon the properties of the constituents and their geometric arrangement in the medium.

The field of inhomogeneous materials has been an active area of research in recent years, both on account of the intrinsic interest of the subject and due to possible technological applications of these materials. An area of basic interest is the insulator to conductor transition or "percolation transition" which occurs in these materials and which resembles in many ways a second-order thermodynamic phase transition. A possible important application is in the design of materials with useful infrared properties, such as efficient photothermal solar energy collectors. The far-infrared absorption in small particles is another interesting issue. For nearly ten years it has been known that this absorption is substantially larger than the predictions of classical electromagnetic theory. A central focus of this review will be this long-standing problem, which at present remains unexplained.

The next section of this review describes the far infrared properties of gold black. This substance has been used for many years to increase the performance of thermal infrared detectors. It is a good example

of the qualitative behavior of small particle systems in the far infrared. With this material as background, we discuss in detail theoretical models for inhomogeneous media in the third and fourth sections. Section V reviews experimental studies of normal metal and insulator composite systems whereas Section VI gives both theoretical and experimental details of granular superconducting systems. The anomalous properties and theoretical attempts to resolve the anomalies are discussed in Section VII. Section VIII gives a brief description of layered semiconductor systems. Lastly, Section IX is a summary of current problems in the area.

There have been no previous reviews specifically about this subject. The general area of inhomogeneous materials has been reviewed by Landauer (1977) while the properties of granular films have been described by Abeles et al (1975). A detailed review of the electronic properties of small metallic particles was recently made by Perenboom, Wyder, and Meier (1981). Other articles which have touched on the subjects with which we are concerned include studies of surface phonons by Ruppin (1973), by Genzel and Martin (1973), and, recently, by Martin (1983), the reviews of percolation by Kirkpatrick (1973) and Shklovskii and Efros (1975), a review of disordered solids by Bottger and Bryksin (1976), a survey of the properties of interstellar dust by Huffman (1977), a discussion of the bounds upon the dielectric constant by Bergman (1978), an article about amorphous solids by Zallen (1979), and a review of quantum size effects in small particles by Marzke (1979). Reviews of the far-infrared properties of homogeneous materials which bear on our analysis include Mitra and Nudelman (1970), Chantry (1971), Hughes (1971), Möller and Rothschild (1971), Robinson (1973), Wyder (1976), and Perkowitz (1983).

II. Example: Gold black.

A. The material.

Gold black has been used for many years as a coating for thermal receivers of infrared radiation (Harris et al, 1948, Harris and Beasley, 1952, Harris and Loeb, 1953, Harris, 1961). These samples are prepared by evaporation of gold metal in the presence of 0.1 to 10 Torr pressure of an inert gas. The gases used include N, Ar and He, sometimes with an admixture of oxygen. This procedure allows the production of a highly absorbing layer of gold small particles. The performance of infrared detectors is enhanced by the application of gold black, because the black increases the amount of radiation absorbed without adding greatly to the heat capacity of the detector.

Electron microscope examination of these materials (Harris and Beasley, 1952) show that they consist of small gold particles about 100 Å in diameter, aggregated into chains. Samples made without the presence of oxygen are usually found to be conducting and to be highly absorbing in the infrared; this class of materials is called "gold black". Those made with the oxygen are usually electrical insulators and, although absorbing in the visible, are relatively transparent in the infrared; this second type is called "gold smoke".

B. Infrared measurements.

Harris and Loeb (1953) reported the transmittance and reflectance of gold black from 22 to 100 cm^{-1} while Harris (1961) gave data from 100 to 700 cm^{-1}. In these conducting blacks, the transmittance below 100 cm^{-1} is nearly constant, determined by the sheet impedance of the sample; at higher frequencies the absorption increases as a roughly linear or perhaps somewhat slower function of frequency. The magnitude of the absorption coefficient at

a frequency of 200 cm^{-1} was $\alpha \approx 200\ cm^{-1}$. Typical data for three samples are shown in Fig. 1, after Harris (1961).

Harris and Beasley (1952) showed mid-infrared transmission data, covering 700 cm^{-1} to 10,000 cm^{-1}, for gold blacks and for gold smokes. The absorption of the blacks is strong at all frequencies. It increases slightly with increasing frequency and has a broad maximum around 2000-3000 cm^{-1}. In contrast, the smokes have high transmission at low frequencies but show an intense absorption above 5000 cm^{-1}, with a maximum at 12,000 cm^{-1}.

C. Discussion of the gold black data.

The gold black and gold smoke samples differ primarily in that the blacks are conducting and the smokes are not. Thus, the blacks are above their percolation transition; their far-infrared absorption is governed by the effective conductivity (1 to 10 $\Omega^{-1}cm^{-1}$, relatively low for a metal but still large enough to dominate the optical properties). The smokes, with an insulating oxide coating on each metal particle, are well below their percolation point and the absorption is characteristic of isolated grains. The strong absorption in the infrared is a resonant absorption of a small particle. Theoretical models for both types of absorption processes are discussed in the next section.

III. The basic theory

A. The effective response functions

1. The dielectric function of a homogeneous substance.

We begin by considering a pure, isotropic, homogeneous substance which is subjected to an external electromagnetic field of frequency ω. The response of this medium to the applied field can be characterized quite generally by a frequency-dependent permeability, $\mu(\omega)$ and complex dielectric function, $\varepsilon(\omega)$. We write the latter quantity in terms of its real and imaginary parts as:

$$\varepsilon(\omega) = \varepsilon_1(\omega) + \frac{4\pi i}{\omega}\sigma_1(\omega) \tag{1}$$

The quantity $\varepsilon_1(\omega)$ appearing in Eq. (1) is called the real dielectric function while $\sigma_1(\omega)$ is the frequency-dependent conductivity. In the zero-frequency limit, $\varepsilon_1(0)$ becomes the static dielectric constant and $\sigma_1(0)$ the ordinary dc electrical conductivity.

That this definition of $\varepsilon(\omega)$ is a reasonable one can be shown easily. In the absence of free charges, Maxwell's equations are:

$$\nabla\cdot\vec{D} = 0 \tag{2a}$$

$$\nabla\cdot\vec{B} = 0 \tag{2b}$$

$$\nabla\times\vec{E} = -\frac{1}{c}\frac{\partial\vec{B}}{\partial t} \tag{2c}$$

$$\nabla\times\vec{H} = \frac{4\pi}{c}\vec{J} + \frac{1}{c}\frac{\partial\vec{D}}{\partial t} \tag{2d}$$

with the usual definitions of $\vec{E}$ (electric field), $\vec{D}$ (displacement vector), $\vec{B}$ (magnetic field), $\vec{H}$ (magnetic intensity), and $\vec{J}$ (electric current density). For linear materials (as we will assume throughout) linear relations exist among these quantities:

$$\vec{D} = \epsilon_1 \vec{E} = \vec{E} + 4\pi\vec{P} \tag{3a}$$

$$\vec{J} = \sigma_1 \vec{E} \tag{3b}$$

$$\vec{H} = \vec{B}/\mu = \vec{B} - 4\pi\vec{M} \tag{3c}$$

where $\vec{P}$ is the electric dipole moment per unit volume, $\vec{M}$ is the magnetic dipole moment per unit volume, and μ is the magnetic permeability.

These equations may be simplified further by assuming plane wave solutions for $\vec{E}$ and $\vec{B}$:

$$\vec{E} = \vec{E}_o e^{i(\vec{k}\cdot\vec{r} - \omega t)} \tag{4a}$$

$$\vec{B} = \vec{B}_o e^{i(\vec{k}\cdot\vec{r} - \omega t)} \tag{4b}$$

where $\vec{k}$ is the wave vector of the light. When Eqs. (3) and (4) are substituted into Maxwell's equations, we find

$$\vec{k}\cdot\vec{E}_o = 0 \tag{5a}$$

$$\vec{k}\cdot\vec{B}_o = 0 \tag{5b}$$

$$\vec{k}\times\vec{E}_o = \frac{\omega}{c}\vec{B}_o \tag{5c}$$

$$-\vec{k}\times\vec{B}_o = \mu\left(\frac{4\pi i}{\omega}\sigma_1\vec{E}_o + \frac{\omega}{c}\epsilon_1\vec{E}_o\right) \tag{5d}$$

Eqs. (5a) and (5b) show that the light is transverse, with $\vec{k}$ perpendicular to $\vec{E}$ and $\vec{B}$. The vector parts of (5c) and (5d) show that $\vec{E}$ and $\vec{B}$ are likewise perpendicular, with $\vec{k}$, $\vec{E}$, and $\vec{B}$ forming a right-handed set. Simultaneous solution of the scalar parts of these last two equations, gives

$$k = \frac{\omega}{c}\left[\mu\left(\epsilon_1 + \frac{4\pi i}{\omega}\sigma_1\right)\right]^{1/2} = N\frac{\omega}{c} \tag{6a}$$

$$B_o = NE_o \tag{6b}$$

where $N=n+i\kappa$ is the complex refractive index of the substance; n is called the refractive index and κ the extinction coefficient.

Finally, with the definition of the complex dielectric function given in Eq. (1), there is a simple relationship between N, ϵ, and μ

$$N = \sqrt{\epsilon\mu} \tag{7}$$

The flow of energy through the system is governed by the Poynting vector, $\vec{S}$:

$$\vec{S} = \frac{c}{8\pi}\mathrm{Re}(\vec{E}\times\vec{B}^*) \quad = \frac{c}{8\pi}\hat{k}|E_o|^2 n\, e^{-2\frac{\omega}{c}\kappa(\hat{k}\cdot\vec{r})} \tag{8}$$

where $\hat{k}$ is a unit vector in the propagation direction. Taking $\hat{k}=\hat{x}$ the intensity $I=(4\pi/c)|\vec{S}|$ is

$$I = I_o e^{-\alpha x} \tag{9}$$

where α is the absorption coefficient, defined to be

$$\alpha = 2\frac{\omega}{c}\kappa = 2\frac{\omega}{c}\mathrm{Im}(\sqrt{\mu\varepsilon}) \tag{10}$$

Thus, the absorption coefficient of a substance--a commonly measured quantity--is governed by the dielectric function and the permeability of that substance.

As might be expected the real and imaginary parts of the complex dielectric function are not independent quantities. First, they are related by the Kramers-Kronig relations (for a discussion, see Wooten, 1972):

$$\varepsilon_1(\omega) = 1 + 8P\int_0^\infty \frac{\sigma_1(\omega')}{\omega'^2 - \omega^2}d\omega' \tag{11}$$

where P means "principal part". Second, they satisfy certain sum rules, the most important of which is the f-sum rule:

$$\int_0^\infty \sigma_1(\omega')d\omega' = \frac{\pi}{2}\frac{ne^2}{m} \tag{12}$$

where n is the total electron density in the medium, e is the electronic charge, and m is the mass of the electron. Subject to these constraints, $\varepsilon(\omega)$ depends primarily upon such properties of the medium as the free carrier density and lifetime, the phonon spectrum, any electronic band gaps, and the details of the band structure. If the material is inherently anisotropic, as for example a one-dimensional conductor or a good metal in a strong magnetic field, the dielectric function becomes a tensor quantity. So long as the

medium is perfectly homogeneous, however, its response to external fields is still well characterized.

2. The Drude dielectric function

The simplest model for the dielectric function of a metal is due to Drude and Sommerfeld (See Kittel, 1976). According to this model, when the electrons in a metal are subjected to an electric field the entire Fermi surface is displaced rigidly in a direction opposite to the field direction (because the electronic charge is negative) by an amount proportional to the current density. This displacement is caused by a balance between the force exerted on each electron by the external field and the scattering of electrons across the Fermi surface. The relaxation rate is $1/\tau = v_F/\ell$, where v_F is the Fermi velocity and ℓ the total electron mean free path, which is determined by the probability of collisions between electrons and imperfections such as phonons (giving ℓ_p), impurities (ℓ_i), and the sample surfaces (ℓ_d). If the scattering processes are independent, then the rates add, so that

$$\frac{1}{\ell} = \frac{1}{\ell_p} + \frac{1}{\ell_i} + \frac{1}{\ell_d} + \cdots \tag{13}$$

The Drude dielectric function is

$$\varepsilon(\omega) = \varepsilon_\infty - \frac{\omega_p^2}{\omega^2 + i\omega/\tau} \tag{14}$$

where ε_∞ is the dielectric constant of the atomic cores (typically $1 < \varepsilon_\infty < 3$) and ω_p is the plasma frequency of the electron gas,

$$\omega_p = \sqrt{\frac{4\pi ne^2}{m^*}} \tag{15}$$

Using Eq. (1), the real dielectric function within the Drude model is

$$\varepsilon_1(\omega) = \varepsilon_\infty - \frac{\omega_p^2}{\omega^2 + 1/\tau^2} \tag{16}$$

while the frequency dependent conductivity becomes

$$\sigma_1(\omega) = \frac{\omega_p^2 \tau/4\pi}{1 + \omega^2\tau^2} \tag{17}$$

Typical values for the plasma frequency for ordinary metals are in the range 5 to 12 eV (40,000 to 100,000 cm^{-1}). At room temperature, electronic mean free paths are 50 to 500 Å, making the relaxation rate 300 to 3000 cm^{-1}. (Note that in cm^{-1}, $1/\tau = v_F/2\pi c\ell$.) Pure metals at low temperatures have mean free paths often 1000 times the room-temperature value, so that the relaxation rate can be <1 cm^{-1}. For many of the systems considered here, however, the mean free path is limited by surface scattering to 100 Å or so, making the relaxation rate larger than typical far infrared frequencies (2-200 cm^{-1}). Thus the far infrared is often equivalent to zero frequency, where the dc conductivity is

$$\sigma_o = \frac{\omega_p^2 \tau}{4\pi} \tag{18}$$

and the static dielectric function is

$$\varepsilon_o = \varepsilon_\infty - \omega_p^2\tau^2 \simeq -\omega_p^2\tau^2 \tag{19}$$

(Note that with ω_p and $1/\tau$ in cm^{-1}, the conductivity in practical units, Ω^{-1}-cm^{-1}, is $\sigma_o = \omega_p^2\tau/60$.)

In metals physics, and particularly for superconductors, a complex

conductivity, $\sigma(\omega) = \sigma_1 + i\sigma_2$, is often defined. This quantity is related to the complex dielectric function by

$$\varepsilon(\omega) = \varepsilon_\infty + \frac{4\pi i}{\omega}\sigma(\omega) \tag{20}$$

or

$$\sigma(\omega) = -\frac{\omega i}{4\pi}[\varepsilon(\omega)-\varepsilon_\infty] \tag{21}$$

Clearly σ_1 is still given by Eq. (17). The imaginary part of the complex conductivity within the Drude model is

$$\sigma_2 = \frac{\omega\omega_p^2\tau^2/4\pi}{1+\omega^2\tau^2} \tag{22}$$

(Finally, we note that in this review we have taken an $e^{-i\omega t}$ time dependence for the electric and magnetic fields. Had we chosen an $e^{+i\omega t}$ time dependence, the sign of every imaginary part would be changed; the complex conductivity would be $\sigma=\sigma_1 - i\sigma_2$, for example. This latter time dependence was often used in optics in the past; in quantum mechanics the convention that we have chosen is the more common.)

3. The response of an inhomogeneous medium.

The situation is greatly complicated if the medium is not spatially homogeneous, but instead has physical properties which vary throughout the material. The manner of the variation may be random, may be periodic, or may be ordered in some other way; in all cases the dielectric function and permeability become functions of position

$$\varepsilon = \varepsilon(\vec{r},\omega) \tag{23a}$$

$$\mu = \mu(\vec{r},\omega) \tag{23b}$$

In writing Eq. (23) (or Eq. (3) for that matter) we have used a local response function; namely, we assumed that the response of the medium at point $\vec{r}$ depends only on the values of the fields at that point. This assumption is equivalent to taking the scale over which the dielectric function fluctuates to be large compared to such quantities as the electronic mean free path.

As an example of an inhomogeneous medium, consider a random composite made from metal small particles and insulating grains. The dielectric response function of each constituent is assumed to be well understood. The metal could be approximated by a Drude dielectric function with $\tau=\infty$ while the insulator has a dielectric function that is mostly real and nearly unity. Thus the spatially varying dielectric function has two possible values:

$$\varepsilon(\vec{r},\omega) = \begin{cases} 1 - \dfrac{\omega_p^2}{\omega^2} \simeq -10^{10}/\omega^2 (\text{in cm}^{-1}) & \vec{r} \text{ in metal} \\ \varepsilon_i \simeq 1 & \vec{r} \text{ in insulator} \end{cases} \tag{24}$$

Obviously, the local properties of this material will vary dramatically depending upon whether $\vec{r}$ is in the metallic or insulating component of the composite.

Although it is true that the functions $\varepsilon(\vec{r},\omega)$ and $\mu(\vec{r},\omega)$ completely describe the electromagnetic response of the medium, this description is not a very useful one because to employ it would require a knowledge of the exact geometric location of the constituents. Generally, this information is

unavailable; in addition, the interesting quantity is the average response of the inhomogeneous medium to external fields, not the local response. Fortunately, so long as the scale on which measurements are made (the wavelength) is large compared to the scale of the fluctuations of the dielectric function (the particle size), the inhomogeneous medium appears to be uniform in its response to external fields and can thus be described by an effective dielectric function, $\varepsilon_{eff}(\omega)$ and permeability $\mu_{eff}(\omega)$. The problem with which theories of inhomogeneous media are confronted, therefore, is in its most general terms the following: given an inhomogeneous medium that has a well-defined local dielectric function $\varepsilon(\vec{r},\omega)$ and permeability $\mu(\vec{r},\omega)$, how can the effective response functions of the entire medium be determined?

4. The effective medium

Historically, the problem of calculating ε_{eff} and μ_{eff} has been addressed from two rather different points of view. The first is a molecular field model originally developed by Clausius, Mossotti, Lorentz, and Lorenz to calculate the local field in a crystal and later applied to the optical properties of an inhomogeneous medium by Garnett (1904, 1906). Garnett's papers were about the colors of stained glasses containing metallic inclusions. Because his full name was James Clark Maxwell Garnett, this model has become known as the Maxwell-Garnett theory (MGT). The second point of view is a symmetrical effective medium approach, initially developed by Bruggeman (1935) and rediscovered by Landauer (1952). The application of this model to optical properties were first suggested by Springett (1973) and by Stroud (1975). This model is generally called the effective medium approximation (EMA), although both it and the MGT are in fact effective medium theories. Each provides an expression for the dielectric function of a homogeneous medium which has properties effectively identical to those of the

inhomogeneous medium.

Each theory (and most subsequent developments) begins with a major simplification. The local dielectric function $\varepsilon(\vec{r},\omega)$ of the inhomogeneous medium is assumed to take on a limited number of discrete values (typically two) rather than being allowed to vary over a continuous range. This simplification corresponds to the example already discussed: the system is a disordered composite, a random mixture of many grains each of which by itself has spatially uniform properties. The composite is characterized by specifying the volume fraction, dielectric function, shape, and size of each grain type. Each grain is then taken to be a polarizable entity, with electric (and magnetic) dipole moment induced by electric (and magnetic) fields from external sources as well as from the fields of the polarized grains in the outside medium.

The principal difference between the MGT and the EMA is the way in which the medium surrounding the grain under consideration is treated. This difference is illustrated in Fig. 2. In the MGT it is assumed that the medium surrounding the grains is one of the constituents of the mixture (for example, the one with the largest volume fraction) while in the EMA it is assumed that the surrounding medium is characterized by the effective properties of the inhomogeneous medium.

B. Response of a single grain.

1. Quasistatic model: Electric dipole moment

The initial step in the solution for the effective properties of an inhomogeneous medium is to find the electromagnetic fields inside and outside of a single particle when that particle is subjected to a plane wave field. For simplicity we will assume for the moment that all particles are spherical, deferring until a later section the discussion of the response of ellipsoidal and cylindrical particles. In the long-wavelength limit, $c/\omega >> a$, the applied fields appear to be spatially uniform and to have $e^{-i\omega t}$ time dependence. The particle in this quasistatic limit has only dipole moments; these moments are time varying so that electric current flows. The electromagnetic power dissipation is proportional to the integral of $\vec{J}\cdot\vec{E}$ thoughout the volume of the particle.

The electric dipole moment is

$$\vec{p} = \Omega \gamma_e \vec{E}_o e^{-i\omega t} \tag{25}$$

where Ω is the volume and γ_e is the electric polarizability per unit volume of the particle, given by the solution to the static boundary value problem of a dielectric sphere in a uniform far field (Jackson, 1975):

$$\gamma_e = \frac{3\epsilon_o}{4\pi} \frac{(\epsilon_p - \epsilon_o)}{(\epsilon_p + 2\epsilon_o)} \tag{26}$$

In Eq. (26) ϵ_p is the complex dielectric function of the particle and ϵ_o is the complex dielectric function of the medium outside the particle. The electric field outside the particle is that of a dipole with

moment $\vec{p}$. Inside, the electric field is

$$\vec{E}_p = \frac{3\varepsilon_o}{\varepsilon_p + 2\varepsilon_o} \vec{E}_o e^{-i\omega t} \tag{27}$$

Note that this field is uniform and parallel to the external field. The difference between $\vec{E}_o$ and $\vec{E}_p$ is called the depolarizing field.

2. Eddy currents: Magnetic dipole moment

Although it may seem that Eqs. (25)-(27) would specify fully the response of the particle to the applied plane waves, it turns out that in the far infrared frequency region magnetic dipole (or eddy current) behavior is often even more important. This effect, which causes the medium to have a nonzero magnetization even though the constituents are nonmagnetic, has been discussed by Tanner, Sievers, and Buhrman (1975), Stroud and Pan (1978), and Russell, Garland and Tanner (1981). The magnetic dipole moment is proportional to the magnetic field strength of the far infrared radiation,

$$\vec{m} = \Omega \gamma_m \vec{H}_o e^{-i\omega t} \tag{28}$$

where γ_m is the magnetic polarizability per unit volume. When vacuum surrounds the particle, this quantity is given by the solution to the boundary value problem of a conducting sphere in a spatially uniform but time varying magnetic field (Ford and Werner, 1973):

$$\gamma_m = \frac{3}{8\pi} \frac{j_2(ka)}{j_o(ka)} \tag{29}$$

In Eq. (29) $k = (\omega/c)\sqrt{\varepsilon_p}$ is the wave vector of light travelling in an infinite medium of dielectric function ε_p. The functions

$$j_0(x) = \frac{\sin x}{x}$$

and

$$j_2(x) = \frac{3\sin x - 3x\cos x - x^2 \sin x}{x^3}$$

are spherical Bessel functions. On substitution, the magnetic polarizibility becomes (Landau and Lifshitz, 1960):

$$\gamma_m = \frac{3}{8\pi}\left[\frac{3}{(ka)^2} - 1 - \frac{3}{(ka)}\cot(ka)\right] \tag{30}$$

At low frequencies, Eq. (30) reduces to a simple expression for the polarizability:

$$\gamma_m = \frac{1}{40\pi} k^2 a^2 = \frac{1}{40\pi}\frac{\omega^2}{c^2} a^2 \varepsilon_{1p} + i\,\frac{1}{10}\,\frac{\omega}{c^2} a^2 \sigma_{1p} \tag{31}$$

The low frequency limit here differs from the long wavelength ($\omega a/c \ll 1$) limit. The low frequency limit is reached only when $ka = \sqrt{\varepsilon_p}\,\omega a/c \ll 1$. Because the far infrared dielectric function can be very large, a particle may be in the long wavelength limit but not in the low frequency limit. (Note that the low frequency limit is essentially identical to requiring that $a \ll \delta$, where δ is the electromagnetic skin depth.)

Although the currents inside the particle are not uniform (at low frequencies they correspond to those of a uniformly charged sphere rotating with angular velocity ω) the fields outside are those of a magnetic dipole of moment $\vec{m}$. This equivalence leads one to define a pseudo-permeability μ for the particle. The motivation for the definition is that eddy current effects

have caused the particle to have a definite dipole moment, $\vec{m}$, and this moment is equivalent to that of a sphere with permeability μ_p in a uniform external field. The permeability,

$$\mu_p = 1 + \frac{4\pi\gamma_m}{1 - \frac{4\pi}{3}\gamma_m} \tag{32}$$

is a complex quantity because ϵ_p and hence γ_m are complex. The imaginary part of the permeability will govern losses in the particle. Note that at low frequencies

$$\mu_p = 1 + \frac{1}{10} k^2 a^2 \tag{33}$$

3. Mie theory.

A rigorous solution for the fields inside and outside of a spherical particle subjected to plane wave irradiation was first given by Mie (1908) and by Debye (1909). As described by van de Hulst (1981) and by Born and Wolf (1975), this solution to Maxwell's equations (or, what is equivalent, the vector wave equations for $\vec{E}$ and $\vec{B}$) for the case of plane waves incident on a sphere of arbitrary size and complex dielectric function gives exactly the fields inside and outside the sphere. The solution is obtained in terms of a pair of series expansions for the fields in spherical Bessel functions and Legendre polynomials--essentially, a multipole expansion. The arguments of the Bessel functions are $ka = \sqrt{\epsilon_p}\omega a/c$ and $k_o a = \sqrt{\epsilon_o}\omega a/c$ where ϵ_o is the dielectric function of the medium surrounding the sphere. This expansion yields the cross section C_e for extinction (extinction = scattering plus absorption; in the far infrared, it is mostly absorption) which is related to the real part of the forward-scattering amplitude function S(0) by

$$C_e = \frac{4\pi c^2}{\omega^2} N_o \mathrm{Re}[S(0)] \tag{34}$$

where $N_o = \sqrt{\varepsilon_o}$. S(0) is in turn given by the series

$$S(0) = \frac{1}{2} \sum_{n=1}^{\infty} (2n + 1)(a_n + b_n) \tag{35}$$

The terms a_n and b_n appearing in Eq. (35) are called the Mie coefficients. The a_n are known as the electric partial waves or TM waves while the b_n are called the magnetic partial waves or TE waves. These quantities are given by the following expressions:

$$a_n = \frac{N_o \psi_n'(N_p x)\psi_n(N_o x) - N_p \psi_n(N_p x)\psi_n'(N_o x)}{N_o \psi_n'(N_p x)[\psi_n(N_o x) + i\chi_n(N_o x)] - N_p \psi_n(N_p x)[\psi_n'(N_o x) + i\chi_n'(N_o x)]} \tag{36}$$

$$b_n = \frac{N_p \psi_n'(N_p x)\psi_n(N_o x) - N_o \psi_n(N_p x)\psi_n'(N_o x)}{N_o \psi_n'(N_p x)[\psi_n(N_o x) + i\chi_n(N_o x)] - N_p \psi_n(N_p x)[\psi_n'(N_o x) + i\chi_n'(N_o x)]}$$

In these expressions, $N_p = \sqrt{\varepsilon_p}$ is the complex refractive index of the particle and $x = \omega a/c$ is a reduced particle radius. The functions ψ_n and χ_n are Riccatti-Bessel functions (with the prime denoting a derivative), which are defined in terms of the ordinary spherical Bessel functions to be:

$$\psi_n(z) = z j_n(z) \qquad \psi_n'(z) = j_n(z) + z \frac{dj_n(z)}{dz}$$

$$\chi_n(z) = z n_n(z) \qquad \chi_n'(z) = n_n(z) + z \frac{dj_n(z)}{dz}$$

If n=1 (dipole terms),

$$\psi_1(z) = \frac{\sin z}{z} - \cos z \qquad \psi_1'(z) = -\frac{\sin z}{z^2} + \frac{\cos z}{z} + \sin z$$

$$\chi_1(z) = -\frac{\cos z}{z} - \sin z \qquad \chi_1'(z) = \frac{\cos z}{z^2} + \frac{\sin z}{z} - \cos z$$

When the external wavelength is long, or the particle size is small, so that $\omega a/c \ll 1$, only these n=1 terms in Eq. (35) remain. This great simplification holds even when $N_p \omega a/c > 1$, because what is important for truncating the series is that the field in the absence of the particle be spatially uniform over the dimensions of the particle. In this limit, those Riccatti-Bessel functions which are functions of $N_o x$ (but not those which are functions of $N_p x$!) may be replaced by their leading terms. After some algebra, the electric partial wave becomes:

$$a_1 = -\frac{2i}{3}\left(N_o \frac{\omega a}{c}\right)^3 \frac{\varepsilon_p - \varepsilon_o + \frac{\varepsilon_o}{2}F(\omega)}{\varepsilon_p + 2\varepsilon_o - F(\omega)} \tag{37}$$

In this expression, $F(\omega)$ is a correction to the quasi-static limit of section III-B-1, above,

$$F(\omega) = \frac{(3-y^2)\tan y - 3y}{\tan y - y}$$

with $y = N_p \omega a/c$

The Mie expression for the electric polarizability is then

$$\gamma_e = \frac{9i}{8\pi}\left(\frac{c}{N_o \omega a}\right)^3 a_1$$

where a_1 is given by Eq. (37) so that

$$\gamma_e = \frac{3\epsilon_o}{4\pi} \frac{\epsilon_p - \epsilon_o + \frac{\epsilon_o}{2}F(\omega)}{\epsilon_p + 2\epsilon_o - \epsilon_o F(\omega)} \tag{38}$$

The magnetic partial wave is

$$b_1 = \frac{i}{3}\left(N_o \frac{\omega a}{c}\right)^3 \left[1 + \frac{3c}{N_p \omega a}\cot\left(N_p \frac{\omega a}{c}\right) - 3\left(\frac{c}{N_p \omega a}\right)^2 - \frac{1}{15}\left(N_o \frac{\omega a}{c}\right)^2\right] \tag{39}$$

If $N_o << N_p$, as has been assumed here, the magnetic polarizability

$$\gamma_m = \frac{9i}{8\pi}\left(\frac{c}{\omega N_o a}\right)^3 b_1$$

is the same as given in Eqs. (29) and (30).

The only difference between the Mie series expressions for the far-infrared electromagnetic response of small particles and the simpler models given earlier in this section is the inclusion of the function $F(\omega)$ in the electric dipole term. For $N_p \omega a/c << 1$, this quantity becomes $F(\omega) \simeq \epsilon_p \omega^2 a^2/5c^2$ and may be neglected completely with respect to ϵ_p. Numerical calculations show that this quantity becomes significant only for particle sizes above 10 μm; it is never as important as the magnetic dipole term for the far infrared absorption.

C. Effective medium theories.

1. Average fields

We will define the effective dielectric constant and permeability of the inhomogeneous medium in terms of volume-averaged fields, $\langle\vec{E}\rangle$ and $\langle\vec{H}\rangle$, and responses $\langle\vec{D}\rangle$ and $\langle\vec{B}\rangle$. (It is also possible to work with the volume averaged dipole moments per unit volume, $\langle\vec{P}\rangle$ and $\langle\vec{M}\rangle$, the choice being entirely a matter of individual preference.) If f_i is the volume fraction of the i^{th} component of the medium, then the average electric field is,

$$\langle\vec{E}\rangle = \Sigma f_i \vec{E}_i \tag{40}$$

with analogous definitions for $\langle\vec{D}\rangle$, $\langle\vec{B}\rangle$, and $\langle\vec{H}\rangle$.

For simplicity we will assume a two component composite and label these constituents type a and type b materials. If f is the volume fraction of type a, then (1-f) will be the volume fraction of type b, so that the average fields are:

$$\begin{aligned}\langle\vec{E}\rangle &= f\vec{E}_a + (1-f)\vec{E}_b \\ \langle\vec{D}\rangle &= f\varepsilon_a\vec{E}_a + (1-f)\varepsilon_b\vec{E}_b\end{aligned} \tag{41}$$

and

$$\begin{aligned}\langle\vec{H}\rangle &= f\vec{H}_a + (1-f)\vec{H}_b \\ \langle\vec{B}\rangle &= f\mu_a\vec{H}_a + (1-f)\mu_b\vec{H}_b\end{aligned} \tag{42}$$

where we have used the local relationships $\vec{D}_i=\varepsilon_i\vec{E}_i$ and $\vec{B}_i=\mu_i\vec{H}_i$. The effective dielectric function and permeability are defined in terms of the average fields:

$$\langle \vec{D} \rangle = \varepsilon_{eff} \langle \vec{E} \rangle \tag{43}$$

$$\langle \vec{B} \rangle = \mu_{eff} \langle \vec{H} \rangle \tag{44}$$

When we write Eqs. (43) and (44), we take the point of view that the interesting property of the medium is the average response to external fields; the external fields are just $\langle \vec{E} \rangle$ and $\langle \vec{H} \rangle$ while $\langle \vec{D} \rangle$ and $\langle \vec{B} \rangle$ are the responses to those fields. (Note that by our definition of the complex dielectric function, Eq. (1), we have included the current density $\langle \vec{J} \rangle$ in $\langle \vec{D} \rangle$.)

2. Maxwell-Garnett dielectric function.

The Maxwell-Garnett theory is implicitly a model for a dilute system. According to the MGT, a single grain of dielectric function ε_a is assumed to lie at the center of a cavity (the Lorentz cavity) carved out of the interior of the inhomogeneous medium. All other type a grains are excluded from this cavity, whose remaining space is assumed to be filled with a medium with dielectric function ε_b. Thus the local field at the grain is the superposition of the uniform applied field and the uniform field from the charge located on the cavity surface. (As discussed by Landauer (1978) in his review of inhomogeneous materials, one way to exclude other grains from the cavity is to cause the cavity tightly to jacket the grain. A more common approach is to assume that the dipolar fields from those neighboring grains which are inside a large cavity sum to zero in the vicinity of the central grain.) With this assumption, the electric field inside the grain is uniform and found by substitution of $\varepsilon_p = \varepsilon_a$ and $\varepsilon_o = \varepsilon_b$ into Eq. (27):

$$\vec{E}_a = \frac{3\varepsilon_b}{\varepsilon_a + 2\varepsilon_b} \vec{E}_b e^{-i\omega t} \tag{45}$$

Combining Eqs. (41), (42), and (45), gives, after some algebra, the Maxwell-Garnett expression for ϵ_{eff} which we label ϵ_{MGT}:

$$\epsilon_{MGT} = \epsilon_b + \epsilon_b \frac{3f(\epsilon_a-\epsilon_b)}{(1-f)(\epsilon_a-\epsilon_b) + 3\epsilon_b} \tag{46}$$

Eq. (46) illustrates two properties which are characteristic of the MGT approach to inhomogeneous media. First, the equation is inherently asymmetric in its treatment of the two constituents: different values are obtained for ϵ_{MGT} depending on whether, for example, we regard the composite as consisting of metal grains embedded in insulator or the other way around. Second, the equation gives a smooth variation of ϵ_{MGT} with volume fraction, from ϵ_b when f=0 to ϵ_a when f=1. That real physical systems do not always behave in this fashion may be seen by considering the low-frequency behavior of an inhomogeneous medium for which $\epsilon_a=1$ and $\epsilon_b=4\pi i\sigma_b/\omega$, i.e., material a is vacuum and material b is a metal. At f=0 the MGT conductivity is just σ_b. As f increases, holes appear in the medium and the effective conductivity will decrease. According to the MGT, the conductivity will remain finite all the way to f=1, when no conducting component remains. In reality, however, the medium is likely to stop conducting at a lower value of f, when the nonconducting regions occupy enough space to block current flow through the sample. This "percolation threshold" is not predicted by the MGT; it is, in fact, specifically excluded by the assumption that the embedded grains do not contact one another. In applications of the MGT the asymmetry and the absence of a percolation transition can be handled in an ad hoc fashion by assuming that as the volume fraction of one constituent increases from zero to one its role changes from that of inclusion to that of host.

Despite its shortcomings, the MGT is generally believed to work

reasonably well in dilute mixtures, where the grains of the minority constituent are well separated. More generally, Hashin and Shtrikman (1962) have shown that the MGT expression, Eq. (46), in its zero-frequency limit represents bounds to the actual conductivity of a two-component heterogeneous medium, an upper bound if $\sigma_a<\sigma_b$ and a lower bound if $\sigma_b<\sigma_a$.

The MGT approach to the properties of inhomogeneous media has been rediscovered and elaborated numerous times over the past 80 years, including work by Doyle (1958), Galeener (1971, 1976), Genzel and Martin (1972), Barker (1973), Weaver et al (1973), Cohen et al (1973), Abeles et al (1975), Granqvist and Hunderi (1977a, 1977b) and Lamb et al (1980). As an example, let us consider the case of small metal particles embedded in a medium with dielectric constant $\epsilon_b=1$. For the metal we assume a simple Drude dielectric function, Eq. (14) with $\epsilon_\infty=1$:

$$\epsilon_a = 1 - \frac{\omega_p^2}{\omega^2+i\omega/\tau} \tag{47}$$

Under these assumptions, the MGT dielectric function becomes

$$\epsilon_{MGT} = 1 + \frac{f\omega_p^2}{\omega_o^2-\omega^2- i\omega/\tau} \tag{48}$$

The effective dielectric function will exhibit a resonant absorption when the frequency of the light equals the Maxwell-Garnett resonant frequency, ω_o.

$$\omega_o = \omega_p \sqrt{(1-f)/3} \tag{49}$$

This resonance arises physically from the fact that the Drude dielectric function of a metal, Eq. (47), is negative below the plasma frequency and can

thus cancel in the electric polarizability, Eq. (26), the positive dielectric constant of the surrounding medium. More sophisticated models, in which the outside medium has dielectric constant ε_b and the metal has a core contribution ε_∞ in its dielectric function, become algebraically more complex but retain the Lorentzian form of Eq. (48). The resonance frequency is shifted in this more general case to

$$\omega_o = \omega_p \sqrt{\frac{(1-f)}{(1-f)\varepsilon_\infty + (2+f)\varepsilon_b}} \tag{50}$$

3. Maxwell-Garnett permeability.

The permeability of a inhomogeneous medium containing grains that have a net magnetic polarizability may be calculated in a way completely analogous to that used to calculate the dielectric function. The permeability is identical in form to Eq. (46),

$$\mu_{MGT} = 1 + \frac{3f(\mu_a - 1)}{(1-f)(\mu_a - 1) + 3} \tag{51}$$

except that we have set the permeability of the insulator equal to unity. Eq. (51) is an interesting result: Although containing no magnetically polarizable substances, an inhomogeneous medium in an external magnetic field possesses a net magnetization. This magnetization results from the eddy currents circulating around metallic inclusions in the medium.

4. Mie expressions for the dielectric function.

The Mie theory is mainly concerned with the properties of a single particle, as described in section III-B-3. For a medium containing n particles per unit volume, the absorption coefficient is related to the cross section for extinction by

$$\alpha = nC_e \tag{52}$$

Eq. (52) contains two implicit assumptions (first, that only single scattering events occur, i.e. that light which is scattered out of the beam by one particle is not subsequently scattered back into the beam by an encounter with a second particle, and second, that no interference occurs in the light scattered by various particles) which restrict it to the case of a random medium of very low density. The complex dielectric function of this medium is given by

$$\epsilon = \epsilon_b + i\epsilon_b \frac{3fc^3}{\omega^3 a^3} S(0) \tag{53}$$

where ϵ_b is the dielectric function of the medium surrounding the particles and we have substituted $f = \frac{4\pi}{3} a^3 n$. Eq. (53) is equivalent to the Maxwell-Garnett dielectric function in the small volume fraction, long-wavelength limit.

5. The effective medium approximation.

The second major approach to the theory of inhomogeneous media, due to Bruggeman (1935), is generally called the effective medium approximation (EMA). In this discussion we will again restrict ourselves to a two-component medium made up of spherical grains. The first component has dielectric function ϵ_a and is present with volume fraction f while the second has ϵ_b and the remaining volume fraction, (1-f).

In contrast to the MGT, the EMA has the attractive feature of treating all constituents of the medium in an equivalent way. It achieves this symmetry by regarding an individual grain (which may be either type of material) as being embedded in an otherwise homogeneous "effective" medium

which is assumed to possess the average properties of the medium. When placed in an external field, the grain in question will be polarized; the field inside is given by Eq. (27), with ϵ_o equal to the effective dielectric function ϵ_{EMA}

$$\vec{E}_p = \frac{3\epsilon_{EMA}}{\epsilon_p + 2\epsilon_{EMA}} \vec{E}_{eff} e^{-i\omega t} \tag{54}$$

where $\vec{E}_{eff}$ is the effective field in the surrounding medium. This field is chosen in a self-consistent way so that the electric field in the medium, when summed over all the grains in the medium, equals $\vec{E}_{eff}$. This self-consistency condition may be incorporated into the theory in a number of ways; the simplest is to set $\vec{E}_{eff}$ equal to the definition of the average field, Eq. (41),

$$\vec{E}_{eff} = f\vec{E}_a + (1-f)\vec{E}_b \tag{55}$$

and then substitute Eq. (54) evaluated for the fields inside the two kinds of grains. After a little algebra, this procedure yields a quadratic equation for ϵ_{EMA}, conventionally written as

$$f \frac{\epsilon_a - \epsilon_{EMA}}{\epsilon_a + 2\epsilon_{EMA}} + (1-f) \frac{\epsilon_b - \epsilon_{EMA}}{\epsilon_b + 2\epsilon_{EMA}} = 0 \tag{56}$$

This quadratic equation may also be obtained by using $\vec{D}_{eff} = \epsilon_{EMA} \vec{E}_{eff}$, with $\vec{D}_{eff} = \langle \vec{D} \rangle$, Eq. (41). The solution to Eq. (56) is

$$\epsilon_{EMA} = \frac{B}{4} \pm \frac{1}{4} \sqrt{B^2 + 8\epsilon_a \epsilon_b} \tag{57}$$

where

$$B = \epsilon_a(3f-1) + \epsilon_b(2-3f)$$

and where the sign of the square root is chosen such that $\mathrm{Im}(\epsilon_{EMA})\geq 0$.

The EMA differs from the MGT in two important ways. First, the equations treat each of the constituents of the medium on an equal basis. The EMA is thus a symmetric theory and is not restricted to a particular range of concentrations. Second, the EMA predicts a metal-insulator transition at a critical volume fraction (for spherical grains) of 1/3. To demonstrate this second point, we assume that the imaginary part of the complex dielectric function dominates the real part as $\omega \to 0$, so that $\epsilon_a \simeq 4\pi i\sigma_{1a}/\omega \gg 1$. If, in addition, $\sigma_{1b}=0$, Eq. (53) may be solved to find

$$\sigma_{1EMA} = \begin{cases} 0 & f<1/3 \\ \frac{3f-1}{2}\sigma_{1a} & f>1/3 \end{cases} \qquad (58)$$

The EMA may readily be extended to systems more complicated than the one considered here. Some of these generalizations will be discussed in subsequent sections of this paper. For metal-insulator composites, with low metal volume fraction, the theory gives a broad absorption peak centered near the Maxwell-Garnett resonance frequency.

6. Effective medium permeability.

The analogy between dielectric function and permeability continues in the case of the EMA. The permeability thus is the solution (with positive imaginary part) to

$$f\,\frac{\mu_a-\mu_{EMA}}{\mu_a+2\mu_{EMA}} + (1-f)\,\frac{1-\mu_{EMA}}{1+2\mu_{EMA}} = 0 \qquad (59)$$

where the insulator has $\mu_b=1$.

IV. Discussion of the theory

A. Numerical examples.

In this section we show the results of model calculations using the two-component MGT and EMA of the previous sections. We have taken the metallic portion of the composite to have a Drude dielectric function, Eq. (14), and the insulating portion to have a real, constant dielectric function, typically $\epsilon_i=4$.

Fig. 3 shows the MGT (left panel) and the EMA (right panel) frequency-dependent conductivity over the entire frequency range from dc to ω_p for metal volume fractions of 0.1, 0.3, 0.6, and 0.7. The MGT was inverted for this last concentration; ie, the metal was taken as host and the insulator as inclusion. Relatively short mean free paths (about 30 Å) were taken in calculating these plots; this choice leads to a broad MGT resonance. The width of the EMA resonance is intrinsic to the theory.

There are several important points to make about this figure. First, there is no dc conductivity in the MGT when the metal is taken as inclusion; there is always a finite dc conductivity when the metal is host. In constrast, the symmetric EMA has a insulator-conductor transition when the metal volume fraction reaches 1/3, the critical concentration for percolation. Second, although both models have a broad resonance centered near the MGT resonant frequency (given by Eq. (50)), this resonance has greater width in the EMA. The low frequency edge of the EMA resonance moves to zero frequency at the percolation transition (Stroud, 1979); this effect is seen in the curve for the f=0.3 sample in Fig 3. Third, (although this point is hard to see from Fig. 3) for small concentrations, the MGT and the EMA give nearly identical results for the low-frequency conductivity.

Fig. 4 shows the electric dipole contribution to the far-infrared absorption (using either the MGT or the EMA) for an f=0.01 concentration of metal in insulator. Curves are shown for three particle radii, a=10, 100 and 1000 Å. These curves were calculated using Eq. (46) for the MGT dielectric function, Eq. (10) (with μ=1) for the absorption coefficient, and taking a model in which the electronic mean free path of the metal (Eq. 13) was dominated by surface scattering, so that ℓ=a. Note that the strength of the absorption goes as 1/a, that the overall magnitude of the absorption is very small, and that the absorption coefficient is quadratic in frequency over the entire range. Fig. 5 shows the magnetic dipole contribution to the absorption coefficient (using either the MGT or the EMA) for a f=0.01 concentration of metal in insulator. Curves are shown for radii of a=100, 300, and 1000 Å. (The curve for a=10 Å could not be plotted on this scale so we have included a=300 Å instead.) These curves were calculated using Eq. (29) for the magnetic polarizability, Eq. (32) for the permeability, Eq. (51) for the MGT permeability, and Eq. (10) (with ε=4.0) for the absorption coefficient. We again have put ℓ=a in the metal dielectric function. Note that the strength of the absorption increases rapidly as the radius increases (it goes as a^3 at low frequencies) and that, although the absorption coefficient increases quadratically at low frequencies and for small sizes, it is tending to saturate at higher frequencies for larger sizes. The magnitude of the absorption coefficient is substantially larger than in the electric dipole case. The combined absorption is not really distinguishable from this eddy current term.

The saturation of the absorption coefficient at high frequencies is a result of the skin effect. As the size or conductivity of the particle increases ($ka \approx a/\delta$ is the important parameter) the eddy currents flowing near

the surface screen the interior of the particle from the external fields. Consequently, the volume in which currents flow is reduced along with the absorption. This effect is clearly seen in Fig. 6, where the calculated magnetic dipole contribution to the absorption coefficient of 1 μm (10,000 Å) radii particles is plotted for three values of the dc conductivity of the particles: 10^5, 10^6, and 10^7 $\Omega^{-1}cm^{-1}$. (10^6 $\Omega^{-1}cm^{-1}$ corresponds to a resistivity of 1 μΩ-cm.) In this size regime, the absorption actually decreases as the particle is made more conducting (except at the very lowest frequencies) because of the dominance of the skin effect. Fig. 7 shows the size dependence of the absorption coefficient at a single frequency (70 cm^{-1}) as a function of radius, again for three conductivity values. The arrows show the radius for which $a=\delta$. The tendency is for the absorption initially to increase with size and then, once the radius is a little larger than the skin depth, to decrease.

B. Expansion at small volume fraction and low frequency

In this section we discuss the predictions of effective medium theories for a composite medium made up from metal (represented by subscript a) and insulator (represented by subscript b). We will assume that three conditions hold. First, we will make the metal volume fraction be small (in comparison both to the insulator volume fraction and to the critical volume fraction for percolation): $f<<1$. In this regime, the EMA and MGT results for the effective response functions are numerically the same. Second we will assume that we are in the low frequency regime for the metal, $\omega<<1/\tau$, so that the metal conductivity is close to the dc value. On account of this limit, it is also true that $|\varepsilon_a|>>|\varepsilon_b|$, i.e., the metal dieletric function is much larger than that of the insulator. Finally, we will assume that the frequency is sufficiently small that the electromagnetic skin depth is large compared to the particle radius: $\delta>>a$.

To obtain our small-concentration, low-frequency limit for the dielectric function we expand Eq. (46) to first order in f and assume that $\mathrm{Re}(\varepsilon_b)>>\mathrm{Im}(\varepsilon_b)$. Then,

$$\varepsilon_{MGT} = \varepsilon_b(1+3f)+i9f\varepsilon_{1b}^2\frac{\varepsilon_{2a}}{\varepsilon_{1a}^2+\varepsilon_{2a}^2} \qquad (60)$$

(Note: $\varepsilon_{2a} = \omega\sigma_{1a}/4\pi$.) The low-frequency-limit equations for the magnetic polarizability of a conducting sphere and the pseudo-permeability of that sphere are given in Eqs. (31) and (33). From Eq. (33) we see that the real part of $\mu\approx 1$ while the imaginary part is small compared to one. Thus, the expansion of Eq. (51) for the effective permeability gives a simple result:

$$\mu_{MGT} = 1+3f + ifIm(\mu_a) = 1+3f + if\frac{2\pi\omega a^2}{5c^2}\sigma_{a1}^2 \qquad (61)$$

The absorption coefficient is, from Eq. (10),

$$\alpha_{MGT} = f\frac{\omega^2}{c^2}\sqrt{\varepsilon_{1b}}\left[\frac{36\pi c\varepsilon_{1b}\sigma_{1a}}{\omega^2\varepsilon_{1a}^2 + 16\pi^2\sigma_{1a}^2} + \frac{2\pi}{5c}a^2\sigma_{1a}\right] + \alpha_b(1+3f) \qquad (62)$$

where $\alpha_b = \frac{2\omega}{c}Im\sqrt{\varepsilon_b}$ is the absorption coefficient of the host. The first term in the brackets in Eq. (62) arises from electric dipole absorption while the second term is due to magnetic dipole absorption. Note that the absorption by the host is enhanced by the presence of the small particles (Simanek, 1977).

The absorption mechanisms all act in parallel in the low concentration limit. As a final simplification, we assume that the host is non-absorbing (α_b=0) and that the metal dielectric function has an imaginary part much larger than its real part. (So that we may neglect $\omega\varepsilon_{1a}$ with respect to $4\pi\sigma_{1a}$.) The absorption coefficient becomes:

$$\alpha_{MGT} = f\frac{\omega^2}{c^2}\sqrt{\varepsilon_{1b}}\left[\frac{9c\,\varepsilon_{1b}}{4\pi\sigma_{1a}} + \frac{2\pi}{5c}a^2\sigma_{1a}\right] \qquad (63)$$

We will compare the results of this model to experiment in subsequent sections of this review. To simplify this comparison, we write

$$\alpha_{MGT} = (K_e + K_m)f\nu^2 \qquad (64)$$

where $\nu=\omega/2\pi c$ is measured in cm^{-1}. The strength of the absorption is governed by the magnitudes of K_e and K_m, which contain all of the material-dependent parameters:

$$K_e = \frac{3\pi\ \varepsilon_{1b}^{3/2}}{10(\sigma_{1a}/30c)}$$

$$K_m = 48\pi^3 a^2 (\varepsilon_{1b})^{1/2} (\sigma_{1a}/30c) \qquad (65)$$

Eq. (65) has been written with the term $\sigma_{1a}/30c$ because the conductivity in $\Omega^{-1}cm^{-1}$ is found by dividing the conductivity in esu (dimensionally in sec^{-1}) by 30c. Thus $\sigma(esu)/30c = \sigma(\Omega^{-1}cm^{-1})$. K_e and K_m both have dimensions of cm.

Note that $K_e \approx 1/\sigma_{1a}$ while $K_m \approx \sigma_{1a}a^2$. Thus, the electric dipole absorption should dominate in very small, poorly conducting particles, while the magnetic dipole absorption would be important in large, highly conducting particles. The two terms are equal when

$$a = \frac{\sqrt{\varepsilon_{1b}}}{4\pi\sqrt{10}(\sigma_{1a}/30c)} \qquad (66)$$

If $\sigma_{1a}/30c = 10^5\Omega^{-1}cm^{-1}$ and $\varepsilon_{1b} = 4$, the equality occurs at a = 50 Å.

C. Other shapes, other constituents, other sizes.

In the preceding parts of this section, we have chosen to work out the effective medium theories for a two-component mixture of identical size spherical particles, because these conditions greatly simplify the algebra. Now, we sketch the modifications to these theories when each of the conditions is relaxed.

1. Ellipsoidal particles.

The dipole moment of an ellipsoid is generally oriented at an angle to the applied external field, so that the polarizability is a tensor quantity,

$$\vec{p} = \Omega \overleftrightarrow{\gamma}_e \cdot \vec{E}_o e^{-i\omega t} \tag{67}$$

with the principal axes of the tensor corresponding to the principal axes of the ellipsoid. Without introducing additional complications we can also assume a tensor dielectric function for the particle, $\overleftrightarrow{\varepsilon}$, so long as the principal axes of the dielectric tensor are aligned with the principal axes of the ellipsoid. Then, the electrostatic boundary value problem (Landau and Lifshitz, 1960) of this ellipsoid in an uniform external field gives an equation similar to Eq. (27) for the field inside a single grain, except that now there are three terms

$$\vec{E}_p = \sum_{j=1}^{3} \frac{\varepsilon_o (\hat{x}_j \cdot \hat{e}) \hat{x}_j}{g_j (\varepsilon_p)_j + (1-g_j)\varepsilon_o} E_o e^{-i\omega t} \tag{68}$$

where the sum runs over the three axes of the ellipsoid, $(\varepsilon_p)_j$ is a component of the dielectric tensor, and ε_o is assumed isotropic. The three vectors $\hat{x}_j$ are unit vectors in a coordinate system aligned with the ellipsoid axes

and $\hat{e}$ is a unit vector in the direction of the external field. The quantities g_j appearing in Eq. (68) are the three depolarization factors of the ellipsoid (Landau and Lifshitz, 1960, Kittel, 1976). The g_j, which are determined by the shape of the ellipsoid, relate the inside electric field along a principal axis of the ellipsoid to the component of dipole moment per unit volume vector along that axis:

$$(E_p)_j = -4\pi g_j P_j$$

The values for g_j vary from nearly zero (for field along the length of a needle) to nearly one (for a field normal to the surface of a flat disc); for a sphere g=1/3. The depolarization factors always add to one:

$$\sum_{j=1}^{3} g_j = 1$$

Along the figure axis (or axis of revolution) of a spheroid the depolarization factor is in general given by

$$g_c = \frac{1-e_c^2}{e_c^2}\left[\frac{1}{e_c}\tanh^{-1}(e_c) - 1\right] \qquad (69)$$

where e_c is an eccentricity for the spheroid

$$e_c = \sqrt{1 - \frac{a^2}{c^2}}$$

c is the figure axis length, and a is the transverse axis length. If c<a (an oblate spheroid), e_c is imaginary. In this case, Eq. (69) may be rewritten (Granqvist and Hunderi, 1977a):

$$g_o = \frac{1 - e_o^2}{e_o^2}\left[1 - \frac{1}{e_o}\tan^{-1}(e_o)\right]$$

with $e_o = \sqrt{a^2/c^2 - 1} = |e_c|$. Finally, the depolarization factor for prolate spheroids is often given as

$$g_p = \frac{1 - e_o^2}{e_o^2}\left[\frac{1}{2e_c}\ln\left(\frac{1 + e_c}{1 - e_c}\right) - 1\right]$$

which is equivalent to Eq. (69).

2. Dielectric function for oriented ellipsoids

An artificial but useful model occurs when we assume that the ellipsoids are oriented parallel to the applied external field. Then, only a single term remains in Eq. (68)

$$\vec{E}_p = \frac{\varepsilon_o}{g\,\varepsilon_p + (1-g)\varepsilon_o}E_o e^{-i\omega t} \tag{70}$$

The MGT and EMA dielectric functions are calculated as was done for spherical particles. The MGT equation becomes

$$\varepsilon_{MGT} = \varepsilon_b + \varepsilon_b \frac{f(\varepsilon_a - \varepsilon_b)}{g(1-f)(\varepsilon_a - \varepsilon_b) + \varepsilon_b} \tag{71}$$

while the EMA dielectric function is the solution (with positive imaginary part) to

$$f\frac{\varepsilon_a - \varepsilon_{EMA}}{g\varepsilon_a + (1-g)\varepsilon_{EMA}} + (1-f)\frac{\varepsilon_b - \varepsilon_{EMA}}{g\varepsilon_b + (1-g)\varepsilon_{EMA}} = 0 \tag{72}$$

The change in the shape of the particles affects the concentration

at which percolation occurs within the EMA. We take $\epsilon_a = 4\pi i\sigma_{1a}/\omega$ and $\epsilon_b = 1$, and find that as $\omega \to 0$,

$$\sigma = \begin{cases} 0 & f \leq g \\ \frac{f-g}{1-g}\sigma_{1a} & f > g \end{cases} \tag{73}$$

so that $g = f_c$, the critical concentration for percolation! That f_c was 1/3 for the EMA in earlier parts of this review (Eq. 58) is a consequence of our having assumed spherical particles.

3. Dielectric function for randomly oriented ellipsoids.

The derivation of the MGT for the case of randomly oriented ellipsoids begins by writing the volume-averaged electric field and displacement vectors in the medium as

$$\langle \vec{E} \rangle = (1-f)\vec{E}_b + \frac{f}{N}\sum_{n=1}^{N}(\vec{E}_a)_n$$

$$\langle D \rangle = \epsilon_b(1-f)\vec{E}_b + \frac{f}{N}\sum_{n=1}^{N}(\vec{D}_a)_n \tag{74}$$

where $\vec{E}_b$ is the electric field in the host (with isotropic dielectric function ϵ_b) and the sum runs over all of the N grains in the medium. The displacement vector inside a particular grain is the dot product of the dielectric tensor of the grain and the field inside the grain

$$\vec{D}_a = \sum_{j=1}^{3}(\epsilon_a)_j(\vec{E}_a \cdot \hat{x}_j)\hat{x}_j$$

On account of the ellipsoidal shape of the particles, both sums in Eq. (74) contain terms with some components parallel and others perpendicular

to the applied field. However the transverse components must sum to zero because by assumption the average electric field in the inhomogeneous medium is parallel to the applied field. We enforce this condition by taking the dot product of both sides of Eq. (74) with $\hat{e}$, define the MGT dielectric function by $\varepsilon_{MGT}\langle\vec{E}\rangle = \langle\vec{D}\rangle$, and use Eq. (68) for the relation between the field inside a grain (with dielectric tensor $\overleftrightarrow{\varepsilon}_a$) and the external field. Then

$$\varepsilon_{MGT} = \frac{(1-f)\varepsilon_b + \frac{f}{N}\varepsilon_b \sum_{n=1}^{N}\sum_{j=1}^{3} \frac{(\varepsilon_j)_j (\hat{e}\cdot\hat{x}_j)^2_n}{g_j(\varepsilon_a)_j + (1-g_j)\varepsilon_b}}{(1-f) + \frac{f}{N}\varepsilon_b \sum_{n=1}^{N}\sum_{j=1}^{3} \frac{(\hat{e}\cdot\hat{x}_j)^2_n}{g_j(\varepsilon_a)_j + (1-g_o)\varepsilon_b}} \tag{75}$$

If we interchange the order of summation in this equation, the sum over particles becomes an orientational average of $\cos^2\Theta$:

$$\frac{1}{N}\sum_{n=1}^{N}(\hat{e}\cdot\hat{x}_j)^2_n = \frac{1}{N}\sum_{n=1}^{N}(\cos^2\Theta_j)_n = \frac{1}{4\pi}\int_{4\pi} d\Omega \cos^2\Theta = \frac{1}{3}$$

and the MGT dielectric function for randomly oriented ellipsoids is (Sen and Tanner, 1982).

$$\varepsilon_{MGT} = \varepsilon_b + \varepsilon_b \frac{f\sum_{j=1}^{3} \frac{(\varepsilon_a)_j - \varepsilon_b}{g_j(\varepsilon_a)_j + (1-g)_j\varepsilon_b}}{3(1-f) + f\varepsilon_b \sum_{j=1}^{3} \frac{1}{g_j(\varepsilon_a)_j + (1-g_j)\varepsilon_b}} \tag{76}$$

which reduces to Eq. (46) if $g_1 = g_2 = g_3 = 1/3$.

As we know, the EMA does not identify either component as the host

material. For self-consistency, the average field in the composite is equal to the effective field felt by each grain

$$\langle \vec{E} \rangle = \vec{E}_{eff} = \frac{f}{N_a} \sum_{n=1}^{N_a} (\vec{E}_a)_n + \frac{(1-f)}{N_a} \sum_{n=1}^{N_b} (E_b)_n \tag{77}$$

where the sums run over all the N_a type a grains and the N_b type b grains. The field inside each grain is given by Eq. (68) with the dielectric function of the medium outside the grain being ϵ_{eff}, the effective dielectric function of the composite. As in the MGT, we also require that the components perpendicular to the average field sum to zero and equate the sum over particles to an angular average of $\cos^2\theta$. The EMA dielectric function is the solution (with positive imaginary part) to the sixth-order equation

$$f \sum_{j=1}^{3} \frac{g_j[(\epsilon_a)_j - \epsilon_{EMA}]}{g_j(\epsilon_a)_j + (1-g_j)\epsilon_{EMA}} + (1-f) \sum_{j=1}^{3} \frac{g_j[(\epsilon_b)_j - \epsilon_{EMA}]}{g_j(\epsilon_b)_j + (1-g_j)\epsilon_{EMA}} = 0 \tag{78}$$

4. Many constitutents

The extension of the MGT or the EMA to media containing three or more constituents (with spherical shape) is relatively straightforward. For the MGT, the volume-averaged fields are

$$\begin{aligned} \langle \vec{E} \rangle &= f_H \vec{E}_H + \sum_{i=1}^{N-1} \frac{3f_i \epsilon_H}{\epsilon_i + 2\epsilon_H} \vec{E}_H \\ \langle \vec{D} \rangle &= f_H \epsilon_H \vec{E}_H + \sum_{i=1}^{N-1} \frac{3f_i \epsilon_H \epsilon_i}{\epsilon_i + 2\epsilon_H} \vec{E}_H \end{aligned} \tag{79}$$

where f_H, ϵ_H, $\vec{E}_H$ are respectively the volume fraction, dielectric function, and electric field in that component which is identified as host; f_i is the

volume fraction and ε_i the dielectric function for the ith one of the N-1 other components. We have used Eq. (27) for the field inside a grain in terms of the outside field. Finally, we invoke a condition on the volume fractions,

$$1-f_H = \sum_{i=1}^{N-1} fi$$

and the MGT dielectric function is

$$\varepsilon_{MGT} = 1 + \frac{3 \sum_{i=1}^{N-1} \frac{f_i\,(\varepsilon_i-\varepsilon_H)}{\varepsilon_i + 2\varepsilon_H}}{1 - \sum_{i=1}^{N-1} \frac{f_i(\varepsilon_i - \varepsilon_H)}{\varepsilon_i + 2\varepsilon_H}} \tag{80}$$

The EMA does not identify a host, so that the average (or effective) field in an N-component medium is

$$\langle \vec{E} \rangle = \sum_{i=1}^{N} \frac{3f_i\,\varepsilon_{EMA}}{\varepsilon_i + 2\varepsilon_{EMA}} \vec{E}_{eff} = \vec{E}_{eff} \tag{81}$$

with the condition

$$\sum_{i=1}^{N} f_i = 1$$

so that the EMA dielectric function is the solution to

$$0 = \sum_{i=1}^{N} f_i \frac{\varepsilon_i - \varepsilon_{EMA}}{\varepsilon_i + 2\varepsilon_{EMA}} \tag{82}$$

Eq. (82) is a N-order polynomial in ε_{EMA}.

5. Size distribution

Up to this point, we have assumed that all of the grains in the inhomogeneous medium were of a single size whereas in real materials there is an unavoidable variation in the sizes of the grains. Because the particle size enters the dielectric function (through the mean free path) as well as the magnetic polarizability, it is important to account for size variations. Sizes are most easily included in our model of a two-component medium by assigning to each size of the a-type grains a volume fraction

$$f_{aj} = f_a P_{aj} \tag{83}$$

where P_{aj} is the probability of finding a particle with radius x_j; ie, P_{aj} is the jth column in the particle size histogram. Clearly,

$$\sum_j P_{aj} = 1$$

so that f_a is the total volume fraction of the a-type mateial. The MGT and EMA response functions resemble those derived for a multiple-component composite medium in the preceeding section, except that the sum now runs over the size histogram rather than the kinds of particles.

We could also assume a continuous probability distribution for the particle size, $P_j = P(x)dx$, and convert the sum into an integral. The EMA dielectric function for a two-component mixture of spherical grains is then the solution to

$$f\int_0^\infty P_a(x)\,\frac{\varepsilon_a(x) - \varepsilon_{EMA}}{\varepsilon_a(x) + 2\varepsilon_{EMA}}dx + (1-f)\int_0^\infty P_b(x)\,\frac{\varepsilon_b(x) - \varepsilon_{EMA}}{\varepsilon_b(x) + 2\varepsilon_{EMA}}dx = 0 \tag{84}$$

where $P_a(x)$ is the probability distribution of sizes x for the type a material and $P_b(x)$ is for type b.

In contrast, the MGT assumption that type b is host permits only type a to have any size variation, and

$$\varepsilon_{MGT} = \varepsilon_b + \varepsilon_b \frac{3f \int_0^\infty P(x) \frac{\varepsilon_a(x) - \varepsilon_b}{\varepsilon_a(x) + 2\varepsilon_b} dx}{1 - f \int_0^\infty P(x) \frac{\varepsilon_a(x) - \varepsilon_b}{\varepsilon_a(x) + 2\varepsilon_b}} . \qquad (85)$$

Eq. (85) reduces to Eq. (46) for a delta function size distribution.

D. Modern theories of small particle composites.

In this section we outline recent theories for composite systems and small particles. Topics addressed include new effective medium theories, percolation theory, and quantum-mechanical calculations of mean free paths in small particles.

1. Effective medium theories.

Stroud (1975) presented a generalized effective medium theory in which he solved formally the self-consistent (EMA) and non-self-consistent (MGT) models for inhomogeneous media using a Green function approach. In addition to obtaining formulas equivalent to Eqs. (46) and (56), he worked out the conductivity of a polycrystalline sample of an uniaxial material and showed that the EMA and MGT are respectively analogues of the coherent-potential approximation and average-t-matrix approximation of alloy theory. In a subsequent paper, Stroud and Pan (1978) discussed electromagnetic wave propagation in an inhomogeneous medium. They derived an equivalent of the effective medium approximation for the case of Mie scattering within an inhomogeneous medium. The self-consistency condition (the equivalent of our Eq. 55) for this dynamic effective medium theory is

$$\sum_i S_i(0) = \langle S(0) \rangle = 0 \tag{86}$$

where the sum runs over all the grains in the medium, the brackets denote a volume average, and the function S(0) is the forward scattered amplitude. We have given an Eq. for S(0) in Eq. (35). For a two-component medium of spherical particles, Eq. (86) reduces to

$$fS_a(0) + (1-f)S_b(0) = 0 \tag{87}$$

When only electric and magnetic dipole terms are kept in (87) the absorption is equivalent to our EMA expressions for the dielectric function and permeability. Recently, Chylek and Srivastava (1983) have extended this model to include the effects of size distributions.

In 1979, Stroud derived a number of sum rules for composite systems. In particular, he showed that the f-sum rule (Eq. 12) carries over

$$\int_0^\infty \sigma_1(\omega')d\omega' \approx f \frac{\pi}{2} \frac{ne^2}{m} \qquad (88)$$

He also showed that the low-frequency edge of the "impurity band" in $\sigma_1(\omega)$ (the EMA equivalent of the Maxwell-Garnett resonance) drops to zero as $f \to fc$ and then moves back to finite frequencies at higher concentrations, leaving a pole at dc behind. This effect can be seen in the EMA conductivity of Fig. 3. Fig. 8 shows the concentration dependence of several characteristic frequencies in $\sigma_1(\omega)$ and the loss function, $\mathrm{Im}(-1/\varepsilon)$. The shift of the low-frequency edge of the conductivity to zero frequency implies that the concentration dependence of the far infrared absorption near percolation should be stronger than linear. Calculations by Russell et al (1981) show that this conjecture is true within the EMA.

Webman, Cohen, and Jortner (1977) also derived the EMA equation for the dielectric function from a scattering-theory viewpoint. They further showed that similar behavior for the dielectric function could be obtained from a random cubic resistor lattice except that the resistor lattice had a smaller value of the percolation threshold ($f_c \approx 0.15$).

Wood and Ashcroft (1977) and Lamb, Wood, and Ashcroft (1980) have investigated the application of the EMA to optical properties. The effects of electrically insulating coatings surrounding each of the metallic grains were

examined; in this case the EMA prediction for the dielectric function becomes equal to the MGT dielectric function. This result is not unexpected because, with every metal particle coated with insulator, the metal particles cannot contact each other; this no-contact rule is invoked from the start by the MGT. This effect is illustrated by Fig. 9.

Sheng (1980a and 1980b) has also considered effects of inhomogeneities within the particles themselves. In one case, he considered the inhomogeneous medium to consist both of insulator-coated metal and metal-coated insulator particles with the probability of finding a particular structure determined by the metal volume fraction. In particular, the probability of finding insulator-coated metal grains, determined by the free volume available to the grain center inside the spherical region, is

$$p = \frac{(1-f^{1/3})^3}{(1-f^{1/3})^3+[1-(1-f)^{1/3}]^3} \tag{89}$$

where f is as always the metal volume fraction. (Note that our notation differs from that of Sheng.) This probability is large when $f<0.4$ and is very small when $f>0.6$. An effective medium approach to the properties of a mixture of these coated particles leads to an increase of the critical concentration for percolation to $f_c \approx 0.5$. This sort of consideration justifies the often used MGT procedure of assuming that as the volume fraction of a constituent increases, its role becomes that of host when $f \approx 0.5$. In the second case, Sheng considered the individual grains to consist of two hemispheres stuck together; the probability that either hemisphere was formed from a particular substance was equal to the volume fraction of that substance in the medium. The EMA was then used to calculate the effective properties of a collection of these grains. At intermediate concentrations this assumption led to a

substantial amount of interfacial contact between the individual constituents of the medium. In contrast, the only interfaces in the ordinary EMA are those between a particular grain and the surrounding effective medium. Both of these models sharpen up the small-particle resonance compared with the EMA, making the dielectric function at optical frequencies resemble the MGT dielectric function yet retaining a dc percolation transition. At low frequencies, however, the predictions of these models resemble closely the EMA, as long as comparisons are not made at concentrations where one model is above the percolation point and the other below.

2. Percolation theory.

Percolation theory addresses the properties of inhomogeneous materials by investigating an ordered lattice in which each site (or bond) is occupied with probability p or vacant with probability (1-p) and in which adjacent occupied sites (or bonds) are regarded as being electrically connected. The probability p in this model plays the role of volume fraction for a continuous medium. A computer is used to generate the lattices and to solve Kirchoff's laws for the conductivity of the lattice as a function of the occupation probability, the dimensionality, the nature of the interconnection, and the type of lattice employed.

Percolation theories always give a percolation transition, but the critical probability varies from as low as 0.2 to as high as 0.7 depending on the coordination number and dimensionality. Scher and Zallen (1970) and Powell (1979) have argued, however, that when the amount of space that can be filled by spheres (of equal size) in a particular lattice is taken into account, the critical volume fraction in three dimensions is always in the range $0.16<f_c<0.18$, a value which is close to experiment (Grannan et al, 1981). The electrical resistance of a percolating system has been considered

by a number of authors (among them Kirkpatrick, 1971, 1976 and 1977, Last and Thouless, 1971, Ambegaokar et al, 1973, Watson and Leath, 1974, Webman et al, 1975, and Levinshtein et al, 1976). Straley (1976, 1977a, and 1977b) has stressed the relation of the percolation transition to a second-order thermodynamic phase transition and has constructed a scaling theory of the transition. The main prediction of this idea, which has also been studied by Stinchcombe and Watson (1976), Efros and Shklovskii (1976), Harris and Fisch (1977), and Bergman and Imry (1977), is that many properties of the inhomogeneous medium obey power-law dependences on the quantity $(p-p_c)$. For instance, the conductivity of a lattice, σ_e, goes to zero at p_c according to

$$\sigma_e = \sigma_a(p-p_c)^t \qquad p>p_c \tag{90}$$

where σ_a is the conductivity of the resistors, while the static dielectric constant ε_e diverges below p_c as

$$\varepsilon_e = \varepsilon_b(p_c-p)^{-s} \qquad p<p_c \tag{91}$$

where ε_b is the dielectric constant of the insulating links. According to the scaling theory, quantities such as the percolation threshold and the prefactors in Eqs. (90) and (91) may vary from system to system depending upon the details of material and sample preparation, but the exponents s and t are universal; they depend only on the dimensionality. In three dimensions $t\approx1.7$ and $s=0.6$ (Straley, 1978). The latter estimate in particular is in remarkably good agreement with experiment (Grannan et al, 1981). Note that both scaling exponents differ from those of the EMA, for which $s=t=1$ (Pan et al., 1976).

Only recently has the frequency dependence of the conductivity been discussed. According to the EMA, the low-frequency conductivity varies as ω^2 for $f<<f_c$ and as $\sqrt{\omega}$ for $f>f_c$. Bergman and Imry (1977) have suggested that the conductivity at $p=p_c$ obeys

$$\sigma_e \propto \omega^{\beta} \tag{92}$$

with $\beta=0.73$. Similarly, Stroud and Bergman (1982) found that

$$\sigma_e \propto \omega^{t/(t+s)} \tag{93}$$

The exponent $t/(t+s)\approx 0.75$. More recently, Wilkinson et al. (1983) obtained that at low frequencies and for $p<p_c$

$$\sigma_e \propto \omega^2 (p_c - p)^{t/t+s} \tag{94}$$

3. Mean free path and non-local effects.

There is a basic contradiction in the way that we have been characterizing the properties of an individual grain. We have assumed up to this point that the grain is described by a local dielectric response function, $\varepsilon(\omega)$, yet that the mean free path can be equal to the particle radius. Clearly, with this long a free path, the current density at a point within the particle will be determined not only by the electric field at that point, but also by the value of the field at neighboring points; a non-local dielectric function should be used. This point was discussed by Trodahl (1979) with respect to eddy-current absorption. He found that non-local effects were relatively minor, reducing the magnetic dipole moment and the

absorption coefficient by a small amount,

$$\alpha_{n\ell} = \frac{5}{8}\,\alpha_{\ell} \tag{95}$$

where the subscript 'nℓ' stands for non-local and 'ℓ' for local. A more detailed theory was made recently by Mal'shukov (1982). He pointed out that for a small particle there are really two distinct relaxation rates, which may have rather different values. The first applies to the momentum of the electrons and the second to the angular momentum. The momentum relaxation time τ_p enters into the electric dipole absorption whereas the angular momentum relaxation time τ_m governs the magnetic dipole absorption. Physically, the difference occurs because the electric currents that give rise to the electric dipole moment travel across chords of the sphere and always intersect the surface, while the currents associated with the magnetic dipole moment circulate around the axis of the sphere in a tangential direction. If we define τ_b to be the bulk relaxation time (determined by collisions with phonons, impurities, etc.) and τ_c to be the classical results for the mean time between collisions with the surface,

$$\tau_c = \frac{a}{v_F} \tag{96}$$

then Mal'shukov's theory gives

$$\tau_p^{-1} = \tau_c^{-1}\left[\frac{4}{9} + \frac{1}{6}\ln(2\omega_p\tau_c)\right] + \tau_b^{-1} \tag{97}$$

and

$$\tau_m^{-1} = \frac{8}{5}\tau_c^{-1}(1-P) + \tau_b^{-1} \qquad (98)$$

where P is the probability that the surface scattering is specular. These two relaxation times enter the Drude dielectric function of the metal, which is in turn used to find the electric and magnetic dipole contributions to the absorption coefficient. Note that in the case of diffuse surface scattering (P=0 in Eq. 98) Mal'shukov's result for the magnetic dipole absorption is identical with that of Trohdal.

A somewhat different approach was taken by Kawataba and Kubo (1966) and by Wood and Ashcroft (1982). These authors made a quantum-mechanical calculation of the dielectric response of a small particle using linear response theory and the random phase approximation. We will discuss quantum size effects (i.e., the quantization of the electronic energy levels in a small particle by the surface of the particle) in a later part of this review. One result of both calculations, however, was that the small particle resonance has the same width as predicted by the classical theory using a local dielectric function and τ_c.

Penn and Rendell (1981, 1982) have investigated the properties of small particles also within the random phase approximation. The particle was characterized by the Lindhard dielectric function. The presence of the particle surface greatly enhances the cross section for the electron-hole pair production. This enhancement occurs because interactions with the surface can soak up momentum, so that the momentum of an electron-hole pair produced by photon absorption need not be zero, as it is in a bulk metal. (Another way of stating this idea is that the wave vector $\vec{k}$ is no longer a good quantum number for the electronic states in the particle.) The result of their calculation is again equivalent to the Mie (or Maxwell-Garnett) classical theory if the

mean free path is taken as the particle radius.

We close this section by noting that the optical measurements of Doyle (1958) and the electron energy-loss studies by Batson (1980) provide experimental support for the use of the particle radius as the mean free path. Thus, although our use of a local dielectric function and our assumption that the mean free path is equal to the radius are inconsistent in a strict sense, they give results that are in accord with more sophisticated theories.

V. Experiments on normal-metal and insulator composites

Despite the wide variety of inhomogeneous systems that exist, relatively few attempts have been made to correlate the effective dielectric function of these systems with the properties of their constituents. In our opinion, there are two reasons for this lack of information on what is obviously an important problem. First, the interesting features of the effective dielectric function occur over a range of frequencies which extends from d.c. through the visible spectrum, so that a comprehensive experimental study requires elaborate laboratory facilities. Second, despite the large number of inhomogeneous materials, few of them can be sufficiently well characterized to make such an investigation worthwhile. It is important to have not only an accurate measure of the size and concentration of the inhomogeneities, but also to be certain that the effective dielectric function of the material being studied is governed only by the dielectric function of the constituent particles and not by other physical processes. For example, there is a large literature devoted to the physics of hopping conduction in semiconductors (see Bottger and Bryskin, 1976, for a review). The onset of hopping conduction in many ways resembles the percolation transition; however, because the hopping process depends on tunneling probabilities and activation energies in addition to conductivities, these semiconducting materials are not suitable candidates for studying the properties of inhomogeneous materials.

A. Near infrared and visible studies

1. Very dilute systems

For materials that are essentially homogeneous except for occasional small grains ($f < 0.01$), it may be reasonably assumed that the grains have a very small probability of coming into contact with one another. In this regime, the MGT and the EMA yield quite similar expressions for the effective dielectric function and appear to describe reasonably well the available experimental data.

Optical transmission measurements on dielectrics containing small numbers of conducting particles have been made by Doyle (1958), Doremus (1964), Kreibig and Fragstein (1969), Jain and Arora (1974, 1975), and Ganiere, Recheiner, and Smithard (1975). The metal particles in these samples were generally grown as precipitates by means of irradatiation or thermal treatment processes. Because of the in situ particle growth, not a great deal was known about the size distribution, crystallinity, or conductivity of the metal particles except that they were approximately spherical with dimensions ranging from 10-100Å. In all cases a relatively narrow peak in the optical absorption was observed at a frequency below the plasma frequency of the bulk metal. Although the peak was referred to by several names in the original works, it appears to be simply a consequence of the Maxwell-Garnett resonance discussed in section III-C-2. When the MGT was used to calculate the absorption coefficient, the center frequency of the resonance in all cases was accurately predicted (to within ten percent), although the width of the resonance was always substantially larger than expected. It is possible that the concentration of particles in some of the samples was too great to preclude particle-particle interactions, so that the EMA (which predicts a broadened resonance in such situations) would have yielded better results.

Similar considerations have been reported by Galeener (1971) for another interesting type of very dilute system. In this case the background medium, amorphous germanium, was conducting while the inhomogeneities were of the form of non-conducting cracks within the germanium. The MGT equations for this situation also preduct a Maxwell-Garnett resonance, often called a "void" resonance. Structure in the optical constants near 8eV was attributed to this phenomenon.

When the volume fraction of inhomogeneities exceeds a few percent in a heterogeneous material, the interactions between grains become significant and actual physical contact between grains of the minority constituent becomes likely. We consider separately three types of materials that have been used to study the influence of these effects on the average dielectric function: discontinuous films, granular metals, and gas evaporated particles.

2. Discontinuous films

In the initial stages of evaporated metal film growth it is common to have isolated metallic islands form on the substrate. These islands are 20-300Å in diameter - depending on the conditions of preparation. They grow in size and number as metal atoms are deposited and eventually coalesce into a continuous film. In the island growth phase, the films consist of small isolated grains of metal affixed to the substrate surface. The optical properties of these discontinuous films have been measured by Sennett and Scott (1950), Doremus (1966), Yoshida, Yamaguchi and Kinbara (1971, 1972), Hetrick and Lambe (1975), Truong and Scott (1976), and Norrman, Andersson and Granqvist (1977, 1978), who studied samples made of gold, silver, indium and aluminum deposited onto glass. The frequency range investigated was limited by the transparency of the glass to the narrow range between the near infrared and the near ultraviolet. In all cases, a relatively broad absorption peak

was observed at a frequency below the plasma frequency of the bulk metal. Although the experiments were analyzed by means of the MGT, the agreement with theory was not particularly strong. The width of the resonance was again substantially greater than calculated from using the bulk optical constants of the metal, and the measured and effective film thicknesses -- obtained by matching the theoretical and measured intensity of transmitted light -- were in disagreement by a factor of two or more.

The difficulty in accounting theoretically for the measured properties of discontinuous films probably results from their complexity. Electron microscope photographs of typical specimens show that the islands take on a variety of shapes, each of which has a characteristic depolarization factor. Furthermore, the presence of the substrate seriously perturbs the induced dipole fields in the vicinity of each conducting grain. The influence of the substrate is most easily seen when considering the frequency of the optical resonance; in fact, some workers have found that better agreement with experiment is obtained by using the dielectric constant of the substrate in calculations rather than the dielectric constant of the vacuum (or air) which actually fills the space between the islands. Finally, the two dimensional character of the films also poses particular difficulties. The averaging procedures in both the MGT and the EMA assume implicitly that a given particle has neighbors located randomly in three dimensions.

3. Granular metal films

There has been a considerable amount of research on the properties of thin films formed by simultaneously sputtering insulating and conducting particles onto a glass substrate. These ceramic-metal (cermet) films are particularly interesting because the concentration of metal particles may be made to vary over the entire range from $0 \leq f \leq 1$. The experiments performed

by the RCA group on these materials represent, to our knowledge, the first attempt to investigate systematically the entire range of concentrations on a single class of materials and, in addition, to compare the optical properties of these materials with the measured d.c. electrical conductivities.

The d.c. properties of cermet films have been studied by Abeles, Pinch, and Gittleman (1975), and by Abeles and Gittleman (1976) who have found that the metal-insulator transition occurs abruptly at a metal concentration of $f \approx 0.6$ rather than the lower concentration of $f \approx 1/3$ predicted by the EMA. The abruptness of the transition appears to result from a peculiarity of the growth phase that prevents the metal particles from contacting each other at concentrations below the transition. In other words, these films do not form the labyrinthine interpenetrating structure of conducting and non-conducting filaments which a strictly random two component system would exhibit over a wide range of concentrations. Because of this feature of the cermets, the MGT, which neglects interactions between particles, may be used with a degree of confidence at higher concentrations than would ordinarily be possible.

Cohen et. al. (1973) have applied the MGT to their measurements of the optical transmission of Au-SiO_2 and Ag-SiO_2 cermet films between near infrared and near ultraviolet frequencies. The convention adopted by these workers was to regard films having a metal concentration $f < 0.6$ as consisting of ellipsoidal metal grains embedded in a dielectric medium, while for $f > 0.6$ the reverse assumption was used. Using this procedure, the MGT was found to agree relatively well with their experimental results. In particular, they found that at low concentrations their samples had low optical absorption in the infrared with a broad absorption peak in the visible. The absorption peak became larger and shifted to lower frequencies as the volume fraction of metal

was increased up to the metal-insulator transition. Above this transition the films exhibited the strong frequency-dependent absorption characteristic of the bulk metal in the infrared, while the absorption peak, which is not a characteristic of the bulk metal, persisted in the visible spectrum to quite high concentrations.

In a comparison of their data for a Ag-SiO_2 cermet film with the predictions of both the MGT and the EMA, Gittleman and Abeles (1977) found that the MGT appeared to give better results. Although the MGT overestimated the strength and the sharpness of the absorption peak in the visible, it otherwise showed good qualitative agreement with measurements. The EMA, on the other hand, had already predicted a metal-insulator transition for this sample and therefore gave a qualitatively incorrect frequency dependence for the optical absorption over the entire frequency range.

4. Gas evaporated particles

If a metal is evaporated in the presence of an inert gas at low pressure, the metallic atoms coalesce into small particles while in the gas. By choosing properly the type of gas -- typically argon, helium or nitrogen -- and the pressure of the gas, the radii of the particles can be made to vary between 10Å - 1000Å. The particles produced in this way have nearly ideal characteristics: they are spherical, crystalline and, for a given gas pressure, almost uniform in size (Granqvist and Buhrman, 1976).

The substance formed by depositing the gas evaporated particles onto a surface is generally called a "smoke" or "black" and has very interesting properties. The density of a smoke as deposited is very low ($f < .01$), with the majority of the material consisting of empty spaces between particles. The particles themselves are able to enclose these large empty regions by forming long chainlike structures with each other. In other words, even

though the volume fraction of metal in the smoke is quite small, there is an extremely high probability of contact between metal particles. Smokes can be easily prepared with a thickness of several microns, so the chainlike structure are clearly three dimensional. Smokes prepared in an ultrapure inert gas atmosphere are often found to be conducting. The reverse is true, however, when a small amount of oxygen is present in the atmosphere. Although it is reasonable to speculate that the presence of oxygen coats each metal particle with a non-conducting oxide layer, the real explanation may be more complicated since even gold particles - which do not readily form oxides - exhibit this property.

Almost all optical measurements in the near infrared to near ultraviolet spectral region have been made on gold smokes, which were prepared both in pure inert atmospheres and in the presence of oxygen. The early experiments were done by Harris and coworkers were reviewed in section II of this review. More recent studies of gold smokes were made by McKenzie (1976) who found a direct correlation between the d.c. conductivity of the gold smokes and the measured optical properties. He further determined that Mie theory (essentially the MGT) could account reasonably well for the oxygen-prepared insulating smokes, but that it failed to account for the properties of the conducting smokes.

The optical absorption of dilute non-conducting gold smokes near the Maxwell-Garnett resonance has also been studied extensively by Granqvist and Hunderi (1976, 1977a). Their work is particularly interesting because they were able to analyze their data successfully using two different approaches. In their first approach, the MGT was invoked under the assumption that the gold particles in the smoke deposit were spherical, with a depolarization factor of 1/3. In order to fit the theory to their data, the thickness of the

sample and the plasma frequency of the gold were treated as adjustable parameters. Their results, which are reminiscent of those found for discontinuous films where a similar procedure was used, required a depressed plasma frequency and an effective film thickness equal to twice the measured value. The second model used by Granqvist and Hunderi was physically more appealing in that the bulk value of the plasma frquency and the measured film thickness were used. In order to account for the elongated structures observed in their samples by electron microscopy, a set of effective depolarization factors was introduced into the MGT formalism.

B. Far infrared studies

Of all the types of inhomogeneous materials, normal-metal/insulator mixtures have been the most studied in the far infrared. The reason for this emphasis is the simplicity of the system: The far-infrared dielectric functions and conductivities of metals and insulators differ greatly and are often nearly frequency independent. Such systems can be in the form of metal smokes, which consist of nearly spherical particles with controllable sizes. (One less desirable aspect is the affinity of the small metal particles to form long chains or clusters, which makes the materials non-random unless special care is taken in sample preparation.) The insulating component in early experiment was just the voids between the metallic grains; later an alkali-halide host was used.

Inhomogeneous mixtures other than metal-insulator mixtures are certainly feasible and in some cases are actually finding applciations as far-infrared filters. Black polyethylene, one of the most commonly used far-infrared filters, is actually a composite of carbon particles embedded in a polyethylene host. Other filters have been produced using mixtures of glass particles in teflon and alkalai-halide powders in polyethylene (Yoshinaga et al., 1960). To date, however, the design of such filters is not due to a quantitative theoretical understanding but more a matter of trial and error.

1. Unsupported smokes

In section II we discussed some of the earlier experiments on gold smokes. These measurements constitute the first work on metal-insulator mixtures with voids between the grains playing the role of the insulator. The possibility for observing size-quantization effects led to more recent interest in small particle composites. Tanner et. al. (1975) measured the far-infrared properties of Cu, Al, Sn, and Pb small particles. The metal

particles were produced by noble gas evaporation (with some oxygen), or by a colloidal technique. The small particle powders, clamped between spaced sheets of polyethylene, had metallic volume fractions less than 0.1 with most between 0.02 and 0.04. Therefore, these samples of unsupported metal particles were mostly voids and in the dielectric (non-conducting) regime. The experimentally measured quantity, the absorption coefficient, was found to increase as ω^n with $1<n<2$. Comparisons were made with the predictions of both quantum mechanical (Gor'kov and Eliashberg 1965) and MGT (Garnett, 1903, 1905) models. In most cases, particularly for the larger particles, the absorption was much greater than predicted by the theories. Fig. 10 shows the absorption coefficient of two Al samples, with median radii of 190 and 200 Å (diameters of 375 and 400 Å). The solid line is a calculation from the quantum-mechanical theory (Gor'kov and Eliashberg, 1965), although the classical theory (including eddy currents) would have given about the same absorption coefficient.

Granqvist et. al. (1976) measured the far-infrared absorption in unsupported aluminum small metal particles (diameters < 100Å). The results of these measurements are shown in Fig. 11. The absorption followed

$$\alpha(\nu) = C_{exp}\nu^2 \qquad (99)$$

where C_{exp} was frequency independent. Both classical (MGT) and quantum mechanical theories predict this behavior; however, Granqvist et. al. found that $C_{exp} >> C_{theory}$ for either classical (MGT) or quantum mechanical theories. Additionally, the absorption was found to increase with particle size, contrary to the quantum theory and electric-dipole absorption but in reasonable agreement with the classical theory when magnetic dipole effects

were included. The majority of the recent studies of composite systems has focused on resolving this anomaly.

2. Metal-particle/insulator composites

Russell et. al. (1981) measured the absorption by 1 μm diameter Pd particles embedded in KCl. There were several reasons for this choice of sample. An undesirable aspect of the unsupported small metal particle samples is the lack of control over the metallic concentration. Also, as already mentioned, the inert gas evaporated small particles tend to form long chain-like clusters, a factor which can not be theoretically treated in a simple way. The small particles of Pd used by Russell et. al. were prepared by a chemical precipitation process. The mean particle size was quite large (1 μm), to avoid any quantum effects associated with extremely small sizes. Instead of studying the as-prepared material, the metal particles were mixed with powdered KCl, an insulating material which is transparent for $\omega<100$ cm^{-1}. Known volumes of metal and insulator were mixed and compacted into a solid wafer to make samples with filling fractions between 0.001 and 0.1.

The results of these measurements showed an absorption for $f < 0.1$ which was quadratic at low frequencies ($\omega<30$ cm^{-1}) and tended to saturate at higher frequencies.This behavior is shown in Fig. 12. The saturation was interpreted as due to the skin effect becoming important at these frequencies, ie in terms of magnetic dipole (eddy current) effects. The magnetic dipole absorption gave the correct shape for the absorption, but the magnitude was a factor of ten too small. An important result of these measurements, illustrated in Fig. 13, was the linear dependence on metallic concentration for all but the highest concentration samples, in agreement with both the EMA and MGT in the low concentration limit. The sample with $f\simeq0.1$ was not in the

low concentration limit and followed the expectations of the EMA more closely than these of the MGT.

Measurements were made by Carr et al. (1981) on particles made from Ag, Pd, Au, and Al whose sizes (150-700 Å radius) were smaller than those of Russell et al. The metal particles were made by the gas evaporation technique and were dispersed in an insulating host. As in all previous studies, the absorption was much larger than theoretical predictions. Fig. 14 shows the absorption coefficent of Pd and Ag particles in powdered Al_2O_3. The solid lines are fits to

$$\alpha = Kf\nu^2$$

with the coefficient K (in cm) given in the figure. As in the case of larger Pd particles, the absorption initially increases as the square of the frequency but at higher frequencies it tends to saturate.

Fig. 15 shows data for 450 Å radius Al particles. The frequency dependence was quadratic all the way up to 90 cm^{-1}, where the KCl begins to absorb. The magnitude of the absorption, while somewhat smaller (with $K \approx 0.2$ cm), is still about a factor of ten larger than theory. One unusual result for some of the Al samples was the concentration dependence of the absorption, which was found to increase as f^2 rather than linearly in f. In our more recent measurements, however, the absorption is found to be linear in concentration over $0.001 < f < 0.032$ (Kim and Tanner, 1984). The earlier results may have been caused by faulty sample-preparation procedures. The magnitude of the absorption coefficient for the more recent measurements is very close to that shown in Fig. 15.

Carr et al. also measured the static dielectric constant of their

composite samples by analysis of the interference fringes caused by multiple internal reflections between the surfaces of their samples. The result of this measurement, shown in Fig. 16, was that the dielectric constant is enchanced by the addition of the metal particles, in agreement with the much more accurate audio-frequency measurements of Grannan et al. (1981).

3. Other systems

Finally, infrared absorption in doped semiconductors was also successfully analyzed using the MGT by Barker (1973). He assumed that the introduction of a donor or acceptor into a polar semiconductor changed the dielectric function of the semiconductor in a small spherical volume centered on the impurity site. These small polarizable particles embedded in the host semiconductor produced an absorption resonance just below the longitudinal optical phonon frequencies. This effect is just a Maxwell-Garnett-like resonance in the composite dielectric function where the longitudinal optical phonon frequency takes the place of the plasma frequency in the theory of metal particles.

VI. Superconductivity

Superconductivity, a phenomenon with typical energies in the far infrared, has been studied for many years in this spectral region. In this part of our review we will discuss recent studies of inhomogeneous superconductors. To provide background, the next section describes the far infrared behavior of homogeneous bulk and thin film superconductors. Only after ordinary superconductors have been introduced will we continue to a detailed discussion of results for granular superconductors.

A. Homogeneous superconductors

The dynamic properties of superconductivity stem from the existence of an energy gap 2Δ. The gap is the minimum energy necessary to produce an excitation, i.e. to break apart a pair. In the Bardeen-Cooper-Schrieffer (BCS) theory this energy at 0 K is given by

$$2\Delta=3.53k_bT_c \qquad (100)$$

where k_b is Boltzmann's constant and T_c is the superconducting transition temperature. Actual superconductors do not adhere rigidly to this relation; in particular, the so-called "strong coupling" superconductors may have $2\Delta\approx 5kT_c$. However, in most cases the gaps are clustered near the BCS value; for Sn with T_c=3.7 K, Eq. (100) implies a gap energy of 11 meV, corresponding to a frequency of 9 cm^{-1} and close to the experimental value. It is thus clear that far infrared photons are excellent probes for superconducting phenomena.

1. The frequency-dependent conductivity of a superconductor

This qualitative insight into the importance of the energy gap can be supported by detailed calculation. The convention is to use the complex optical conductivity,

$$\sigma(\vec{q},\omega) = \sigma_1(\vec{q},\omega) + i\,\sigma_2(\vec{q},\omega) \tag{101}$$

rather than the dielectric function to describe the optical response. One can readily convert between conductivity and dielectric function using Eq. 20.

Mattis and Bardeen (1958) have calculated $\sigma_s(\vec{q},\omega)$, the full wavevector and frequency dependent conductivity within the BCS framework. They then simplified matters by assuming that the normal state metallic properties were either in the extreme dirty limit, where the electronic mean free path is much smaller than the scale of spatial variation of the electromagnetic wave, or the extreme anomalous limit, where the opposite is true. It is an interesting and very simplifying result that in both of these limits the ratio $\sigma_s(\vec{q},\omega)/\sigma_n(\vec{q},\omega)$ (σ_n is the normal state conductivity) is the same and independent of $\vec{q}$. The results are for $0<\hbar\omega<2\Delta$

$$\frac{\sigma_{1s}}{\sigma_n} = \frac{2}{\hbar\omega}\int_{\Delta}^{\infty} dE\ \left[f(E)-f(E+\hbar\omega)\right] \frac{E^2+\Delta^2+\hbar\omega E}{(E^2-\Delta^2)^{1/2}\left[(E+\hbar\omega)^2-\Delta^2\right]^{1/2}} \tag{102a}$$

$$\frac{\sigma_{2s}}{\sigma_n} = \frac{1}{\hbar\omega}\int_{\Delta-\hbar\omega}^{-\Delta} dE \left[1-2f(E+\hbar\omega)\right] \frac{E^2+\Delta^2+\hbar\omega E}{(\Delta^2-E^2)^{1/2}\left[(E+\hbar\omega)^2-\Delta^2\right]^{1/2}} \tag{102b}$$

while for $\hbar\omega>2\Delta$

$$\frac{\sigma_{1s}}{\sigma_n} = \frac{2}{\hbar\omega}\int_{\Delta}^{\infty} dE\ \left[f(E)-f(E+\hbar\omega)\right] \frac{E^2+\Delta^2+\hbar\omega E}{(E^2-\Delta^2)^{1/2}\left[(E+\hbar\omega)^2-\Delta^2\right]^{1/2}}$$
$$+ \frac{1}{\hbar\omega}\int_{\Delta-\hbar\omega}^{-\Delta} dE \left[1-2f(E+\hbar\omega)\right] \frac{E^2+\Delta^2+\hbar\omega E}{(E^2-\Delta^2)^{1/2}\left[(E+\hbar\omega)^2-\Delta^2\right]^{1/2}} \tag{103a}$$

$$\frac{\sigma_{2s}}{\sigma_n} = \frac{1}{\hbar\omega}\int_{-\Delta}^{\Delta} dE\ \left[1-2f(E+\hbar\omega)\right] \frac{E^2+\Delta^2+\hbar\omega E}{(\Delta^2-E^2)^{1/2}\left[(E+\hbar\omega)^2-\Delta^2\right]^{1/2}} \tag{103b}$$

In these equations, the zero of energy is taken as the Fermi energy and

$$f(E) = \frac{1}{1+e^{-E/k_bT}}$$

is the Fermi function. The results of a calculation of σ_{1s}/σ_n and σ_{2s}/σ_n at 0 K with $2\Delta=9$ cm^{-1} are shown in Fig. 17.

The physical interpretation of these results is direct if one recalls that the power absorbed by a metal is proportional to σ_1. Photon energies below the gap cannot dissociate Cooper pairs so both σ_{1s} and the absorption are zero. Absorption begins at $\hbar\omega=2\Delta$ and smoothly approaches the normal state value.

2. Thin superconducting films

Many studies have dealt with thin superconducting films, which for mechanical strength are usually mounted on substrates. In films for which the thickness d is comparable to the skin depth δ_c, transmission measurements become possible. In the case when $d<<\delta_c$, simple expressions relating the optical conductivity to the transmission and reflection can be found. These expressions, due originally to Tinkham (1958), are

$$T = 4n/[(n+1+y_1)^2+y_2^2] \qquad (105)$$

for the transmission and

$$R = [(n-1+y_1)^2+y_2^2]/[(n+1+y_1)^2+y_2^2] \qquad (106)$$

for the reflection. Here n is the refactive index of the substrate, $y_1+iy_2=(4\pi/c)\sigma d$, and $4\pi/c=Z_o$, the impedance of free space, which in practical units is 377 Ω. Effects due to multiple internal reflections and absorption within the substrate have been omitted here for simplicity.

Eqs. (105) and (106) may be used in two ways. When both $T(\omega)$ and $R(\omega)$ can be measured with sufficient accuracy, the equations can be inverted to yield the microscopic quantities σ_1 and σ_2 for comparison with theory. The first such analysis was made by Palmer and Tinkham (1967) who found good agreement between experiment and theory for Pb films. Recent measurements by Karecki et al. (1983) on NbN are shown in Fig. 18. The results for σ_1 agree with Mattis-Bardeen theory, as does the shape but not the magnitude of σ_2. This latter discrepancy is due to strong coupling or scattering time effects. The Leplae (1983) theory, an extension of the Mattis-Bardeen result to be discussed below, gives an improved fit as shown.

It is not always possible to measure T and R with adequate accuracy, especially as the reflectance generally undergoes only a small change between superconducting and normal states. In that case Eq. (105) can predict the transmission, given the correctness of the model for σ_s and the availability of other parameters. One striking feature in the ratio of T_s (the superconducting state transmission) to T_n (the normal state transmission) is an unmistakable peak which occurs near the gap frequency. This peak is seen in Fig. 19 which shows T_s/T_n for an amorphous film of NbN.

3. Deviations from Mattis-Bardeen prediction

In many cases, the extreme dirty limit is unnecessarily confining,

as it implies that $\omega\tau=0$. In some superconductors, $\omega\tau$ may be of the order of unity in the far-infrared. An extension of Mattis-Bardeen theory which does not assume either of the extreme dirty or the extreme anomalous limit has been provided by Leplae (1983), who writes σ_{1s} in a form which incorporates the normal state conductivity. At $T=0$, $\sigma_{1s}=0$ for $\hbar\omega<2\Delta$, while for $\hbar\omega>2\Delta$

$$\sigma_{1s}(\omega) = \frac{1}{2\hbar\omega} \int_{\Delta}^{\hbar\omega-\Delta} \{[g(E,E')-1]\sigma_{1n}(|\varepsilon'|-|\varepsilon|)+[g(E,E')+1]\sigma_{1n}(|\varepsilon'|+|\varepsilon|)\}\, dE \tag{107}$$

where

$$g(E,E') = (EE'-\Delta^2)/|\varepsilon\varepsilon'-\Delta^2|$$

$$\varepsilon = (E^2-\Delta^2)^{1/2}$$

$$\varepsilon' = (E'^2-\Delta^2)^{1/2}, \quad E'=\hbar\omega-E$$

The Kramers-Kronig relation (Eq. 11) then gives σ_{2s}

$$\sigma_{2s}(\omega) = \frac{2\omega}{\pi} P \int_0^{\infty} \frac{\sigma_{1s}(\omega')}{\omega^2-\omega'^2}\, d\omega' + \frac{2A}{\pi\omega} \tag{108}$$

and A is determined by the conductivity sum rule, $A = \int_0^{\infty} d\omega' \left[\sigma_{1n}-\sigma_{1s}\right]$. In this development, if σ_n is inserted as the constant σ_o, the Mattis-Bardeen dirty limit is derived. For $\sigma_n(\omega)=\sigma_o/(1-i\omega\tau)$, the Drude form, a modified $\sigma_{1s}(\omega)$ is obtained with τ as a new parameter.

Besides omitting the scattering time effects described above, the Mattis-Bardeen calculation is not adequate for describing the strong-coupling

superconductors such as lead. Nam's theory (1968) provides very good results for members of this class of superconductor, though its application can be quite involved. The dominant effect of strong coupling is a uniform decrease in σ_{2s}. Fortunately, this same behavior is found from the Leplae forumation for $\omega\tau<1$. Therefore, reasonable fits to experimental results for strong-coupled materials can be obtained with its use, though the interpretation τ of in this case is not so clear. As examples, we show in Figs. 18 and 19 the improvement over Mattis-Bardeen theory when the Leplae theory is used to fit data for homogeneous NbN.

To add the complexities of full strong-coupling analysis to the intracacies of a granular system and geometry would give a very difficult situation. Because the Leplae extension of the MB theory gives a satisfactory means of fitting homogeneous superconducting behavior, it serves as an adequate starting model for the analysis of granular systems.

B. Theories for inhomogeneous superconductors

A discussed in the previous section, a qualitative change occurs in the far-infrared properties of a metal when it goes from the normal to the superconducting state. Comparable changes should occur in the far-infrared response of an inhomogeneous material as its metallic constituent becomes superconducting. The far-infrared properties of an inhomogeneous superconductor should be described by the model appropriate to the system in its normal state (the EMA, for instance) with the substitution of the dielectric function of a bulk superconductor for the dielectric function of the metallic constituent. This approach seems reasonable as long as the superconducting component can be expected to possess bulk characteristics.

One immediately obvious difference that can be incorporated into the model is a change in the relaxation time τ, as discussed in section IV-D-4. This change affects both the normal and superconducting state response. Because $\omega\tau \to 0$ as the grain size shrinks, the response of highly granular superconductors should approach more closely the Mattis-Bardeen dirty limit results. However, in contrast to the normal state, two additional length scales are associated with superconductivity: the coherence length, ξ, and the penetration depth, λ. The dynamics of a superconductor are modified when any of its dimensions is smaller than either of these quantities.

1. Small dimensions

The intrinsic Pippard coherence length, ξ_o, for a superconductor is usually derived within the framework of the BCS theory. We will present only a qualitative derivation for ξ_o in order to gain some physical insight into this length scale. The BCS theory shows that the superconducting state differs from the normal state only for those electrons lying within approximately $k_b T_c$ of the Fermi energy, implying that the many-particle

wavefunction of the superconducting state is formed with eigenfunctions whose energy spread is of the order

$$\Delta E \approx k_B T_c \tag{109}$$

and whose momentum spread is

$$\Delta p \approx \frac{k_B T_c}{v_F} \tag{110}$$

The uncertainty relation now sets a lower limit on spatial variations in the superconducting state

$$\xi_o \approx \frac{h}{\Delta p} \approx \frac{h v_F}{k T_c} \tag{111}$$

Note that a second coherence length occurs in the Ginzberg-Landau phenomenological theory, which is valid near T_c. This approach gives a temperature dependent coherence length

$$\xi(T) \approx \xi(0) \sqrt{\frac{T_c}{T_c - T}} \tag{112}$$

where except for factors O(1), $\xi(0)=\xi_o$. Typical values for ξ_o range from 50 to 50,000 Å, depending on the material.

The other length scale, originally from the London theory for superfluids, is the penetration death λ. This parameter describes the depth to which external fields penetrate before being completely screened by the superconducting electrons. It too is a temperature dependent quantity, diverging as T increases toward T_c. Typical values at T=0 are on the order of

1,000 Å, with little dependence on material.

These lengths play qualitatively different roles in the properties of small superconducting samples. On the one hand, when the dimensions of a sample decrease below the penetration depth, an external field is no longer completely screened from the interior of the superconductor. On the other hand, as the dimensions decrease to less than the coherence length, thermodynamic fluctuations become increasingly important. Fluctuations, and their effects, are greatest near the transition temperature. The effect of fluctuations on the optical conductivity has been calculated by a number of workers (Schmid, 1968, Schmidt, 1968 and 1970, Eilenberger, 1970, Bray and Rickayzen, 1972, and Tanner, 1973) by use of a time-dependent generalization of the Ginzberg-Landau equations. The fluctuation conductivities are maximum near T_c, are inversely proportional to a characteristic length scale (the thickness of a film in 2-d, the volume in 0-d), and follow a $1/\omega$ frequency dependence. Because most experimental studies of granular systems have used thin (2-d) films containing small (0-d) grains, fluctuations may considerably alter the optical properties from the Mattis-Bardeen bulk values, especially near T_c.

2. Effective medium theories for superconducting-particle composites.

Most experiments have used granular superconductors mixed with an insulator, frequently the superconductor's native oxide. We will therefore consider superconductor-insulator mixtures first. Furthermore, most composite samples have been dilute, with $f \ll f_c$. Because the MGT and EMA yield identical results in this limit, we will employ the simpler MGT, whose dielectric function is given in Eq. (46) while the permeability is given by combining Eqs. (29), (32), and (51).

Replacing the dielectric function of a normal metal with that of a superconductor (ignoring fluctuations) gives the results for the absorption coefficient of the composite shown in Fig. 20. The normal state absorption is also shown. Parameters appropriate for 250 Å radius Sn grains in KCl were chosen. For this case, the eddy current term dominates the electric dipole term. The superconducting state composite absorption is predicted to be zero below the gap, the same as in the bulk case. The absorption coefficient above the gap increases roughly as $(\omega - 2\Delta)^2$, rising nearly parallel to the normal state result. In the case of extremely small grains, the electric dipole term becomes appreciable; Fig. 21 shows the absorption coefficient for electric dipole absorption only. We again use parameters for Sn in KCl, but with a grain radius of 25 Å. Now, in contrast to the normal state, the superconducting state result reveals an electric dipole absorption with a shape different from the magnetic dipole absorption. This difference arises from the sensitivity of the electric dipole term to the imaginary part of the conductivity, σ_{2s}.

It is important to note that the low-frequency, dilute limit expression for the absorption coefficient of ordinary metal particles, Eq. (63), is not valid when $\sigma_2 \approx \sigma_1$ as occurs in superconductors. The appropriate expression valid for superconductors is Eq. (62), which we write here in terms of σ_1 and σ_2

$$\alpha_s = f \frac{\omega^2}{c^2} \sqrt{\epsilon_{1i}} \left[\frac{9c\epsilon_{1i}\,\sigma_{1s}}{4\pi(\sigma_{1s}^2+\sigma_{2s}^2)} + \frac{2\pi a^2 \sigma_{1s}}{5c} \right] \tag{113}$$

The change in the absorption coefficient due to the superconducting transition, $\Delta\alpha \equiv \alpha_s - \alpha_n$, can be calculated for either electric or magnetic dipole absorption. Starting with Eq. (113), which can be written

$$\alpha_s = f^2\nu^2 \left[C_E \frac{\sigma_{1s}}{\sigma_{1s}^2+\sigma_{2s}^2} + C_M\sigma_{1s}\right] = \alpha_{sE}+\alpha_{sN} \tag{114}$$

where $C_E = 9\pi c\epsilon_{1i}^{3/2}$ and $C_M = 8\pi^3\,\epsilon_{1i}^{1/2}/5c$ and $\nu = \omega/2\pi c$ is the frequency in cm^{-1}. Considering electric dipole alone, one obtains

$$\Delta\alpha_E = C_E f\nu^2\left(\frac{1}{\sigma_n}\right)\left[\frac{\sigma_{1s}/\sigma_n}{(\sigma_{1s}/\sigma_n)^2 + (\sigma_{2s}/\sigma_n)^2} - 1\right] \tag{115}$$

while for the magnetic dipole case,

$$\Delta\alpha_M = C_M f\nu^2\sigma_n\left(\frac{\sigma_{1s}}{\sigma_n} - 1\right) \tag{116}$$

Calculations for these two cases are shown in Fig. 22. The electric dipole case has $\Delta\alpha_E>0$ when the frequency is a little larger than 2Δ. The magnetic dipole case has the opposite behavior. However, for grains larger than 50 Å the magnetic dipole term is expected to be larger so that the absorption coefficient in the superconducting state is predicted to be smaller than in the normal state. Grain size distributions have little effect on the normal state properties because both electric and magnetic dipole absorption follow ν^2. The superconducting state is more complicated because these absorptions become quite different and may actually compete. This competition would be a problem when the mean grain size falls in the region of crossover from electric to magnetic dipole domination, about 50 Å.

3. Thin granular films

The fraction of area occupied by metal in a 2-d granular metal film is typically large, on the order of 50% or higher. Therefore these systems are not in the dilute limit, so that simple expressions for the effective

response are not available. In fact the initial premise of effective medium theories, that each grain is immersed in a uniform effective field, becomes questionable not only because of the dipolar fields from neighboring grains but also due to the presence of a substrate. Still, we may expect to determine at least qualitative behaviors and note the success of effective medium theories in explaining normal state properties at near infrared and optical frequencies (see section V-A-2 and V-A-3). The metal grain shape in many granular films is not spherical but instead more of an oblate spheroid (pancake). This shape leads to a change in the depolarization factor for the grain, which, in the EMA, causes the dc percolation concentration to move from 1/3 to around 1/2. Other results for the effective theories show the same general trends as found for the 3-d case.

4. Superconducting/normal-metal composites.

Recently, Garner and Stroud (1983) used the EMA to calculate the optical conductivity for a superconductor-normal metal mixture. As might be expected, the presence of the normal component gives a non-zero conductivity even at frequencies less than the bulk energy gap of the superconductor. Especially striking behavior occurs near the percolation concentration where the EMA predicts a very large conductivity for $\omega < 2\Delta$. This effect can be understood qualitatively as follows: for frequencies well below the gap, a superconductor better screens applied fields than does a normal metal. Therefore, the field outside an inclusion increases when the inclusion becomes superconducting. An absorptive component adjacent to the superconductor "sees" more field and absorbs more energy. The absorption can be affected by increasing the volume fraction of superconductor (which improves the screening) or by increasing the amount of normal metal (which provides more absorptive material). Of course there is a trade-off between the two effects

with the maximum absorption, perhaps not surprisingly, occurring at the percolation concentration.

The MGT also can be applied to this system; the results reflect the asymmetry between the host and inclusion. The case of normal metal host and superconducting inclusions gives results qualitatively similar to the EMA results. On the other hand, for a superconductor host and normal metal inclusion, the large real conductivity for $\omega<2\Delta$ is not observed, because the superconductor tends to exclude the fields from the normal inclusions.

Lastly, mixtures of two differing superconductors can be considered. Above the gap for both superconductors, the material appears metallic with a conductivity representing an average of the two components. For $\omega<2\Delta_{min}$, ($2\Delta_{min}$ is the smaller of the two gaps) the real conductivity is zero. In the intermediate region, the material appears as a mixture of superconductor and normal metal for which large values for σ_1 can occur near percolation.

C. Experimental studies of inhomogeneous superconductors.

As of the present, only a few far-infrared experiments have been performed on inhomogeneous superconductors. These experiments investigated composites of superconducting small particles with insulating grains and granular superconducting films.

1. Superconducting small particles.

Free standing (unsupported) granular tin "smoke" was investigated by Tanner et al (1975). Sn is a superconductor with T_c = 3.7 K and 2Δ = 11.3 meV = 9 cm^{-1}. The smoke, which consisted of small metal grains and voids, was produced by a standard inert gas evaporation technique. Some oxygen was included in the gas to produce a thin oxide layer on the grains. The method produced single crystal grains with mean radius near 70 Å. The smoke was collected from the evaporator and placed between spaced sheets of polyethylene for far-infrared studies. The volume fraction was about 0.018, a typical value for small metal particle smokes produced by evaporation. As noted in Sec. V, the metal particles tend to form an open network of chain-like structures, most likely due to Van der Waals attractive forces between the particles. A combination of lamellar grating interferometer and a ^{3}He cooled bolometer allowed transmission measurements to below 4 cm^{-1}. From these data, the absorption coefficient was computed.

The normal state absorption at T=4.2 K was surprisingly large and increased as ω^2, as described in Sec. V. Transmission measurements for temperatures below 3.7 K were expected to show the effects of superconductivity. In particular, the absorption coefficient was expected to vanish below 9 cm^{-1} because $\sigma_{1s}(\omega)=0$ when $\omega<2\Delta$. However, no change was observed even for temperatures well below the bulk transition temperature ($T_c \approx 3.7$ K). Because the grain size was significantly less than the

coherence length (ξ_o=2300 Å for Sn), this result could be due to fluctuations, which are significant in zero-dimensional grains for temperatures even far below T_c and provide for absorption at low frequencies. A second explanation however, is that in the vicinity of 2Δ both normal and superconducting absorptions were nearly zero for these samples. Hence, any change due to the superconductivity may have gone unnoticed.

Systems of small Sn or Pb particles embedded in KCl were investigated by Carr et al. (1979, 1983). The far-infrared spectrometer consisted of a lamellar grating interferometer and low temperature bolometer. To manufacture these samples, a mixture of metal smoke, produced by inert gas-evaporation and finely ground (a≈10 μm) KCl were compressed into a solid wafer. The compression took place in an evacuated press at a pressure of 10 kbar, sufficient to make the KCl flow. The resulting composite wafer was extracted from the press, reground and re-pressed several times in an effort to improve uniformity. Unfortunately, it was difficult to determine if this technique was entirely successful.

Sn samples which had average particle radii in the 50 to 300 Å range were studied. Fig. 23 shows the absorption coefficient of two composite samples. The normal state absorption is large and increases as ν^2. The superconducting state absorption coefficient is notably different from the normal state result. The differences between superconducting and normal state absorption are shown more clearly in Fig. 24. At frequencies well below 2Δ, the superconducting state absorption is less than for the normal state (though not always zero), while for frequencies at and above the gap, the superconducting absorption is typically 50% larger than the normal state absorption. Similar results for small Pb particles in KCl were observed, although the absorption below the gap was much closer to zero, while the

absorption increase above the gap was smaller than for the Sn.

The non-zero value of σ_{1s} below the gap for Sn particles can be understood by invoking fluctuations effects. Although the grain size was comparable for both the Sn and Pb composites, fluctuations will be more prominent for the Sn due to the larger size for the clean-limit coherence length (2300 Å for Sn, 1000 Å for Pb). This difference may explain why the absorption below the gap was closer to zero for the Pb composites.

The absorption increase above the gap is not so easily reconciled with theoretical predictions. The results shown in Fig. 22 should be compared with the predictions of Figs. 20 and 21. It is also worth summarizing the theoretical predictions and the experimental results for the normal state absorption. Although the theoretical magnitude is not correct to explain the normal state absorption, the magnetic dipole term is closer in magnitude and is also in better agreement with the grain size and frequency dependence of the absorption than the electric dipole term. The results for the superconducting state agree with neither term (magnetic nor electric dipole), although there is some resemblance to the electric dipole term. An adequate explanation for this peculiar effect is still not available. One clue may come from the dependence of the superconducting absorption increase on the amount of oxide on the grains of tin. During the smoke evaporation process, a controlled amount of oxygen was admitted into the bell-jar in order to improve electrical isolation between the grains. Those smokes made with a relatively large amount of oxygen displayed a reddish-brown color, rather than the typical black. This color change was attributed to a thick oxide layer on the surface of each grain. Composites made with such smoke had a smaller absorption increase in the superconducting state, as compared to the composites made from less oxidized black smokes, suggesting that interactions

between the grains may play an important role.

2. Granular films.

The far infrared properties of thin granular superconducting films have been investigated by Carr et al., (1983) Perkowitz (1982) and Karecki et al (1983). Muller and Pomerantz (1981) and Pomerantz and Muller (1981) have investigated such films in the microwave region. Granular superconducting films differ from the composites described above not only in their intrinsically 2-d nature, but also in the close proximity of their grains to one another. This proximity makes the sheet resistance, or resistance per square,

$$R_{\square} = 1/\sigma_1 d \qquad (117)$$

the most useful characterizing quantity for granular films.

Granular films are typically produced by some form of vacuum deposition, such as evaporation, rf sputtering, e-beam deposition and ion beam deposition. In most cases, the material "beads up" as it is deposited onto the substrate. The degree of granularity can often be affected by changes in substrate temperature, evaporation rate, and the residual pressure of inert gas or inert gas/oxygen mixture.

Muller and Pomerantz (1981) made cavity shift and loss measurements of granular Al films (30-50 Å diameter grains separated by Al_2O_3) at 9.4 GHz (0.3 cm^{-1}), a frequency lower than the zero temperature energy gap of Al (about 2 cm^{-1}). The films were flash evaporated onto glass substrates and had dc sheet resistances in the range of 100-1000 ohm/$\square$. During the transition to superconductivity, the cavity resonance frequency shifted by an amount proportional to σ_{2s} whereas the loss was proportional to σ_{1s}. This shift and

the loss were measured as a function of temperature (see Fig. 25). As the temperature was reduced, the film became superconducting and the frequency shift saturated. The loss (which depends on σ_{ls}) typically decreased but did not become zero. In one sample, the loss initially increased as the temperature passed through T_c for the grains. The loss which remained after the frequency shift had saturated was attributed to normal conducting regions between many of the superconducting grains. Even though a connected superconducting path across the sample existed, ac fields would still be sensitive to the presence of any remaining normal regions. The temporary increase in the loss with decreasing temperature may have been due to the overall change in the sample's impedance. The absorption by a thin metallic film on a substrate does not always increase monotonically with the sheet conductance. These data were interpreted in terms of fluctuation effects.

Granular Pb films, with $R_\square$ in the range 10-1000 ohm/□, have been investigated between 5 and 40 cm^{-1} by Carr et al. (1983). These films were formed by ion beam deposition of Pb onto sapphire substrates. A layer of SiO_2 was deposited on top to improve the stability of the Pb against oxidation in the atmosphere. The grains observed by a scanning electron microscope were irregular in shape and about 1000 Å in size. The less granular samples (having large, extended grains with poorly defined voids between them) had values for $R_\square < 50$ Ω/□ while the more granular ones (consisting of smaller isolated grains) had $R_\square > 500$ Ω/□ .

The dc transport properties were studied to provide additional characterizing information. The resistive transitions were typical of granular superconducting films; the resistance did not abruptly disappear at the bulk T_c, but instead gradually approached zero at some lower temperature. The I-V properties below T_c revealed reduced critical currents

and voltage steps. These steps are characteristic of Josephson devices, providing evidence that the superconducting coupling between the grains was weak.

The measured quantities were the normal state transmission and the superconducting to normal state transmission ratio (T_s/T_n). For the films with $R_\square$ < 50 Ω/□ , normal state transmissions were frequency independent, consistent with the Drude model for metals with $\omega\tau<<1$. The superconducting to normal state transmission ratios had a peak near 2Δ (22 cm^{-1} for Pb), consistent with the results from the Mattis-Bardeen calculation that were shown in Fig. 19, although the measured peak was often not as high as the predicted one. In contrast, as shown in Fig. 26 the films with $R_\square$ > 50 Ω/□ had normal state transmissions which decreased with increasing frequency. This decrease implies that the optical conductivity increases with frequency, a behavior inconsistent with the Drude model. The measured transmission ratios, T_s/T_n, were very surprising. Several are shown in Fig. 27. The usual peak near 2Δ was found to be severely suppressed and shifted to higher frequencies. At and below the gap, the ratio became less than one, suggesting that the superconducting state absorption was actually greater than the normal absorption (assuming a value for σ_{2s} no larger than for the bulk case). Because the Mattis-Bardeen calculation predicts zero absorption below the gap, it is incapable of describing these results.

Granular NbN has been investigated by Perkowitz (1980) and by Karecki et al. (1983). Granular NbN sample preparation differs from most techniques in that it begins by making a uniform polycrystalline layer of NbN by reactive sputter deposition. Afterwards, an electrochemical etching process converts NbN at crystal boundaries into oxides of Nb, principally Nb_2O_5. The crystalline grains become electrically isolated from one another,

producing a high resistivity mixture of NbN and insulator. NbN is a strong coupled superconductor with $T_c \approx 14$ K and $2\Delta(0) = 35$ cm^{-1}.

Perkowitz (1980) measured the transmission properties of NbN using a far-infrared laser. Two samples were investigated, one homogeneous with $R_\square$= 78 Ω/□ and one highly granular with $R_\square$= 21000 Ω/□ . The grains were determined from TEM photographs to be about 80 Å across and 30 Å in thickness. The laser technique gave the transmission as a function of temperature for a particular laser frequency. These results were then compared to the temperature dependent calculation of Mattis and Bardeen. For laser frequencies greater than the gap, $\hbar\omega > 2\Delta$, reasonable agreement between theory and experiment was achieved. At lower frequencies, however, the fits were not satisfactory, especially near T_c, where the transmission was too low. Including the contribution to the conductivity from fluctuations immensely improved the fit for the highly granular sample. As described earlier, fluctuations increase the conductivity at low frequencies and for temperatures near T_c. This increase in conductivity would cause the transmission to decrease, as observed.

In the work of Karecki et al (1983), four films of granular NbN were studied, including the highly granular film investigated by Perkowitz discussed above. These films were all deposited under similar conditions to produce comparable crystallite sizes. However, each was anodized for a differing amounts of time yielding samples with $R_\square$'s of 206, 313, 715 and 21000 Ω/□ . The resistive transitions and I-V properties were similar to those found by Carr et al (1983).

A Michelson type interferometer with a low temperature bolometer was used to measure both the transmission and reflection for each film. From these measurements, the real part (and in many cases the imaginary part) of

the optical conductivity was determined for direct comparison with the theory. The less granular films ($R_\square$ = 206 Ω/□ and 313 Ω/□) had frequency independent transmissions consistent with the Drude model for $\omega\tau=0$. Measurements in the superconductive state gave values for σ_{1s}/σ_n and σ_{2s}/σ_n which followed the calculation of Mattis and Bardeen. The more granular samples ($R_\square$ = 715 Ω/□ and 21000 Ω/□) had normal state transmissions which decreased with frequency, inconsistent with the Drude model. In the superconducting state, the real part of the optical conductivity, σ_{1s}, was no longer zero below the bulk gap frequency. This result is shown in Fig. 28. In particular, the optical conductivity for the sample with the largest T_N was actually larger in the superconducting state than in the normal state for frequencies below the gap.

The results for the optical conductivity for highly granular NbN can be compared to the EMA or MGT calculations discussed in sections VI-B-3 and VI-B-4. The mixture of superconducting NbN grains with insulating Nb_2O_5 suggests using a S-I mixture, but neither theory for these two constituents gives absorption (non-zero σ_{1s}) below the gap. However, comparison with the EMA results for S-N mixtures shows some qualitative agreement. Actually, it may turn out that the experimental system is better described as a S-N mixture whose normal component is only weakly conducting, leading to tunneling or hopping between the grains. The conductivity ratios computed from the EMA show the large low frequency increase even for a weakly conducting normal component, as long as the system is close enough to the percolation concentration. Similar results apply to the MGT for a normal metal host with superconducting inclusions except that the large low frequency absorption occurs only for superconducting volume fractions near unity.

VII. Discussion of the anomalies.

A number of ideas that have been advanced to explain the anomalous far infrared absorption in small metal particles will be discussed in this section. These ideas include the influence of oxide coatings on the particles, the role of interactions and clustering, interparticle hopping, and quantum size effects.

A. Oxides

Simanek (1977) proposed that the far infrared absorption takes place in an amorphous oxide layer coating the particles. In his model these coated particles are stuck together to form needlelike structures. He calculated first the dielectric function of the needles using the MGT for spherical metal particles embedded in an oxide host material. Next, he used what is essentially the MGT for infinite cylinders ($g=0$) embedded in a medium with dielectric constant $\varepsilon=1$ to find the absorption coefficient due to the needles. These calculations were compared to the measurements of Granqvist et al (1976). Two factors in Simanek's model enhance the far infrared absorption. First, the presence of the metal particles in the oxide magnifies the absorption by the oxide (see Eq. 62). Second, the aggregation of the particles into cylinders (having $g=0$) increases the electric field inside the oxide and hence the absorption. The calculated absorption was further increased by the assumption that the volume fraction of oxide plus metal in the composite material was larger than the metal volume fraction (ie, that the oxide does not grow at the expense of the metal constituent). He found that the absorption coefficient is

$$\alpha_{ox} = K_{ox} f \nu^2 \qquad (118)$$

where $K_{ox} \approx 4 \times 10^{-2}$. This value would be reduced to $K_{ox} = 1.5 \times 10^{-2}$ if one assumes that the specified metal volume fraction of the sample includes both the metallic particles and the metal-oxide coating. Because the volume fraction is determined in most samples by weighing the particles, this second assumption is probably the more reasonable one. (For further discussion of this point, see Carr et al, 1981.)

A number of difficulties with Simanek's model have been pointed out by Russell et al (1981), Carr et al (1981) and Sen and Tanner (1982). First, many samples have absorption coefficients that exceed the predictions of this model by a factor of ten to thirty. Second, oxides themselves do not show such a high far infrared absorption. Third, unoxidized small particles (Au and Pd) also show a high far infrared absorption. Fourth, because each metal particle is assumed to be coated with an insulator, the composite would never become conducting, even if the volume fraction and geometry allowed percolation. If conduction eventually did occur, the transition would be expected to occur at a relatively high value of metal volume fraction, as happens for example in the case of the cermets (where the metal grains are coated with insulator and the transition occurs at volume fractions exceeding 0.5).

In an extension of Simanek's model that overcomes the last objection, Ruppin (1979) used the EMA to describe the individual clusters, so that the clusters became conducting when the volume fraction of metal in them exceeded 1/3. He found an absorption that was larger than that of Simanek, but the frequency dependence was too strong; the absorption coefficient went as ν^3 rather than ν^2.

B. Interactions and clustering.

Although the role of the oxide was the principal focus of Simanek and Ruppin, clustering played an important role in their models. The effects of clustering were considered in some detail by Sen and Tanner (1982). Both needle-shaped and spherical clusters were investigated; the effects of conducting (ie, absorbing) coatings surrounding the individual particles were also discussed. Sen and Tanner found that if the individual small particles were first coated with a poorly conducting ($\sigma \approx 10\ \Omega\text{-cm}^{-1}$) layer and then organized into needle-shaped clusters there could be a high far infrared absorption but with a $\nu^{1/2}$ rather than ν^2 frequency dependence. None of the parameters tried could cause the model simultaneously to give the correct frequency dependence and the observed magnitude of the absorption coefficient.

Clusters of particles made from ionic compounds were considered from a lattice dynamics point of view by Clippe et al (1976). This model was extended by Ausloos and Clippe (1978), and has been used by Ausloos (1979), Gerardy and Ausloos (1979, 1982a, and 1982b), and Clippe and Ausloos (1982). Clusters containing as many as 21 grains have been worked out. The central result is that interactions among neighboring particles shift the surface phonon peak (the equivalent of the MGT resonance in a metal sphere) from the frequency at which it occurs in the isolated grain, with the direction and amount of the shift determined by the geometry of the cluster. The lowest resonance frequencies were at approximately $0.5\omega_{MGT}$ in long chains of particles while the highest were at approximately $2\omega_{MGT}$ for large clusters with cubic symmetry. On the basis of this calculation, a composite containing many different kinds of clusters would be expected to have a much broader MGT resonance than one with isolated particles. This result suggest that the broad resonance predicted by the EMA may result from the effective medium

surrounding each grain playing the role of the neighboring grains in a cluster.

The reason that clustering affects the effective response of the medium is that the dipolar field from neighbors can make the external field at a particle differ from the average field. To estimate the distance necessary for this effect to be important, we consider the interactions of two spherical grains separated by a distance d in the direction of the average field, $\vec{E}_o$. In the presence of a field, each particle acquires a dipole moment which, according to Eq. (25) is

$$\vec{p} = \Omega\gamma_e \vec{E}_{ext} \tag{119}$$

where Ω is the particle volume and $\vec{E}_{ext}$ is the total electric field applied to the particle. This field is the sum of the average field and the field from the neighboring particle

$$\vec{E}_{ext} = \vec{E}_o + \frac{2\vec{p}}{d^3} \tag{120}$$

The dipole moment of the particle is thus given by

$$\vec{p} = \frac{\Omega\gamma_e}{1 - 2\gamma_e \frac{\Omega}{d^3}} \vec{E}_o \tag{121}$$

Dipolar coupling may be ignored as long as the second term in the denominator of Eq. (121) is not important, ie as long as

$$d >> \left(\frac{8\pi}{3} \gamma_e\right)^{1/3} a \tag{122}$$

where a is the particle radius. According to Eq. (26),

$$\gamma_e < \frac{3}{4\pi} \varepsilon_o$$

so that our criterion becomes

$$d \gg (2\varepsilon_o)^{1/3} a \tag{123}$$

This criterion does not necessarily limit us to low volume fractions. For example, suppose that the particles are arranged on a simple cubic lattice with lattic constant d (an unrealistic model). The volume fraction is $f=4\pi a^3/3d^3$ and our requirement is

$$f \ll \frac{4\pi}{6\varepsilon_o} \approx 0.5 \tag{124}$$

with $\varepsilon_o \approx 4.8$.

C. Hopping conduction

The treatment of metal-insulator mixtures using effective field theories given in section III presumed that the insulator had zero conductivity. If the insulating layer between two conductors is very narrow, electrons may tunnel between the grains; this tunneling constitutes an additional conduction mechanism that is not included in the classical model. The effects of tunneling are most noticable just below percolation, where the electrons are normally localized to a particular conductor. The process of electron transfer from one localized state to another is termed hopping.

Much of the formalism on hopping has been developed to model conduction in amorphous and doped semiconductors. In these systems, electron localization is due to disorder, rather than the grain boundaries found in granular metals. Hopping transport in such systems has been considered by Scher and Lax (1973) using a model based upon a random walk on a lattice, which they showed to be approximately equivalent to a random walk between random sites once the averaging over the sites is carried out. More recently, Odagaki and Lax (1981) and Odagaki, Lax and Puri (1983) have combined the random walk model with the coherent potential approximation (CPA) and the bond-percolation model to give expressions for the conductivity as a function of frequency. For low frequencies, they find a conductivity which typically increases as a power of ω. For instance, on a 2-d square lattice, the real part of the conductivity initially increases as ω^2 for $p<p_c$, where p is the average probability that a given bond exists and $p_c=1/2$. For $p>p_c$, the real conductivity initially increases as ω. In either case, the conductivity rapidly approaches a constant for higher frequencies, becoming indistinguishable from bulk conduction mechanisms. Results for other dimensions are similar.

In granular metals, the hopping probability can not be treated as entirely random because there is a minimum threshold energy for the process. The hopping process requires the removal of an electron from a neutral grain, leaving it in a charged state. By considering the charged grain and the surrounding polarizable medium as a capacitor, Sheng (1973), Abeles (1975) and Chui (1981) have shown that the minimum energy required for the hopping process should be

$$E_o = \frac{e^2}{\epsilon_1(0)a}$$

where e is the electronic charge, a is the grain radius, and $\varepsilon_1(0)$ is the static dielectric constant of the medium. This energy may be available as heat (thermally activated hopping) or from external illumination (photon assisted hopping). Besides the charging energy requirements, the hopping conduction process also depends on the distance between grains and the electron density of states on the grains, the latter possibly influenced by size quantization effects in very small grains.

Much of the evidence for hopping is due to temperature dependent dc conductivity measurements on granular metal films by Sheng (1973), Abeles (1975), Chui (1981) and Sichel (1982). Granular films with metallic concentration below percolation ($p<p_c=1/2$), show a negative temperature coefficient of resistivity. Detailed analysis has revealed that the majority of data for the conductivity follows

$$\sigma = \sigma_o \exp(-A/T^{\alpha})$$

with α close to 1/2.

Calculations for the temperature dependent conductivity are usually based on a bond percolation model. The distribution of grain sizes and inter-grain distances in these granular films gives a distribution of hopping probabilities, and likewise, inter-grain conductances. The system's conductivity can then be determined by finding the critical percolation conductivity, as developed by Ambegaokar et al. (1971). This method has been used by Simanek (1981) and Sheng and Kalfter (1983), resulting in temperature dependent conductivities of the form observed in the experiments. Additionally, Sheng has found that the exponent, α, can vary from 1/4 to near

1, depending on the distribution of grain sizes, with $\alpha=1/2$ holding over a large temperature range if one chooses distributions similar to those found in actual samples.

There are, at present, no specific treatments on hopping as applied to the far-infrared properties of mixtures containing small metal particles. The effect of charging energy has not been incorporated into any calculations which yield frequency dependent conductivities. It is not even clear whether hopping is an important mechanism in the far-infrared, compared to single grain conduction mechanisms. Still, several qualitative features can be expected. First, one would expect hopping to be unimportant in mixtures for which the metallic concentrations are well above p_c, due to a lack of localized electrons and the dominance of normal conduction processes. At the other end of the scale, samples with very low concentrations have large average distances between grains, which make the hopping process unlikely. One therefore expects hopping to be most important for metallic concentrations near p_c where one has a large number of isolated grains (or grain clusters) in reasonable proximity to one another. Second, one should expect a conductivity which initially increases with frequency as ω^s with $2<s<1/2$ (as found from considerations of random hopping). Whether or not hopping conduction is ever comparable in size to single grain conduction remains to be answered.

D. Quantum size effects.

The conduction electrons in a bulk metal have an electronic spectrum which is for all practical purposes a continuum. This continuous range of energies is responsible for the ordinary electrical properties of metals. The wave functions of the conduction electrons are usually thought of as completely delocalized, extending throughout the metal. In contrast, the energy spectrum of a single atom consists of discrete, well-defined levels.

The wave functions of the electrons in the atom are, of course, localized in the vicinity of the atom. These two views of electronic states are completely different, and the question of crossover from one regime to the other, which should occur for small particles, is a fascinating one.

1. The gap.

The electronic energies of a small particle are neither continuous as they are in a bulk metal nor are they as widely spaced as in an isolated atom. Frohlich (1937) was the first to point out that the presence of the surface leads to energy levels quantized at certain discrete values with no allowed states at intermediate energy values. Thus, there will be an energy gap δ between the highest occupied level and the lowest unoccupied one; the presence of this gap is expected to lead to dramatic effects in the electronic properties of these particles when the energy range investigated is comparable to the gap value.

There are two opinions about the value of the gap. According to one (Kawabata and Kubo, 1966, Wood and Ashcroft, 1982) the states of an electron confined within a small volume are worked out explicity and then these states are filled, beginning with the lowest one and continuing until all the electrons in the particle are used up. The energy difference between the highest occupied and the lowest unoccupied levels is the gap. If the shape of the particle is taken to be spherical, the electronic wave functions are products of spherical harmonics and spherical Bessel functions; for cubical particles, the wave functions are products of sinusoids. As discussed by Wood and Ashcroft, the energy spectrum of a cube and sphere at large values of the quantum numbers (i.e., near the Fermi level) differ only by geometrical factors of order unity and the cubical wave functions are much easier to use. For the cube, the wave functions are

$$\psi = A\sin(k_x x)\sin(k_y y)\sin(k_z z) \tag{125}$$

The boundary conduction that the wave function vanish on the surface of the cube, which has edge L, allows only certain values of the wave vector $\vec{k}$:

$$k_x L = i\pi \qquad k_y L = j\pi \qquad k_z L = \ell\pi \qquad (i,j,\ell) = 1,2,3,\ldots \tag{126}$$

The energy levels are given by

$$E_{\ell np} = \frac{\hbar^2}{2m} k^2 = \frac{\hbar^2\pi^2}{2mL^2}(i^2+j^2+\ell^2) \tag{127}$$

The Fermi energy is determined by the electron <u>density</u> n and not the number of electrons, just as in the usual free electron model (Kittel, 1976)

$$E_F = \frac{h^2}{2m}(3\pi^2 n)^{2/3} \tag{128}$$

The energy of the unoccupied level just above the Fermi level is $E(k_F+\pi/L)$ so that the gap is

$$\delta = E(k_F+\pi/L) - E_F = \left(\frac{2\pi}{Lk_F}\right)E_F \tag{129}$$

(Note that in Eq. 129 we have neglected $\Delta k = \pi/L$ with respect to k_F. Because the particle size, L, is substantially larger than the interatomic spacing, this approximation is justified.) Finally, using $k_F = (3\pi^2 N/L^3)^{1/3}$, the gap becomes

$$\delta = \left(\frac{8\pi}{3N}\right)^{1/3} E_F \tag{130}$$

which is of order of $\delta \approx E_F/N^{1/3}$.

A contrasting view is that of Kubo (1962) and Gor'kov and Eliashberg (1965). These authors argue that the surface of any actual particle will be rough on an atomic scale and that this roughness will lift all of the degeneracies (except for spin) existing in the electronic energy spectrum. The gap will just be the inverse of the single spin density of states, evaluated at the Fermi energy:

$$D(E_F) = \frac{V}{2\pi^2} \left(\frac{2m}{\hbar^2}\right)^{3/2} E_F^{1/2} \tag{131}$$

where V is particle volume. Because the Fermi energy is determined by the electron density, n, rather than the total number of electrons in the particle N, (Eq. 128) this gap is

$$\delta = \frac{2E_F}{3N} \tag{132}$$

There are two important consequences of the assumption that surface roughness lifts all of the degeneracies in the electronic system. First, it is no longer possible to obtain the electronic wave functions as it was for the case of cubes and spheres. Second, small variations in the shape of individual particles making up a composite system will lead to significant differences among the energy levels of these particles. It then becomes necessary to invoke statistical arguments about energy level spacings to determine the properties of the composite. We will return to this second point shortly.

The magnitudes of the gaps predicted by Eqs. (130) and (132) differ by a large amount. Consider a 75 Å radius silver particle, containing 100,000 electrons. The gap predicted by Eq. (130) is 1900 cm^{-1} while that from Eq. (132) is only 0.3 cm^{-1}. Friedel (1977) has argued convincingly for the correctness of the smaller, or Kubo, gap. This argument is similar to Peierls' theorem about the instability of a one dimensional metal towards a lattice distortion, resulting in an insulating state. It goes as follows: Suppose that the highest occupied level is in fact highly degenerate and partially filled. (That it be partially filled is the most likely case; if the number of states having this energy is M, then only 1/M of the time will the level be completely filled.) Now, because the energies and the eigenstates are determined by the boundary conditions, it is possible to lift the degeneracy by an elastic deformation of the particle. In particular, it will be possible to find some deformations which raise the energy of the unoccupied states while lowering the energy of the occupied states, thereby lowering the electronic energy. The cost of breaking the degeneracy is the elastic energy associated with the deformation; however, because the scale of elastic energies (the Debye energy) is always much smaller than that of electronic energies (the Fermi energy), the system will always find it favorable to deform and break the degeneracy.

2. The static dielectric constant.

The static dielectric constant turns out not to depend on the model chosen to find the gap. In the case of a cube with edge L, Wood and Ashcroft (1982) find

$$\varepsilon_1(0) = 1 + \frac{1}{3\pi} k_F a_o \left(\frac{L}{a_o}\right)^2 \qquad (133)$$

while for a sphere (Gor'kov and Eliashberg, 1965; but see also the comment by Strassler, Rice, and Wyder, 1972)

$$\varepsilon_1(0) = 1 + \frac{4}{5\pi} k_F a_o \left(\frac{a}{a_o}\right)^2 \tag{134}$$

The quantity a_o appearing in Eqs. (133) and (134) is the Bohr radius: $a_o=\hbar^2/me^2$. If the cube and sphere have equal volumes (i.e. the same number of electrons) then the dielectric constants are the same to within about 10%.

Eq. (134) may be rewritten as

$$\varepsilon_1(0) = 1 + \frac{1}{5} q_s^2 a^2 \tag{135}$$

where $q_s^2=3\omega_p^2/v_F^2$ is the Thomas-Fermi wave vector. (See Kittel, 1976, p 296.) A comparison of Eq. (135) with the general Thomas-Fermi expression for the zero-frequency, q-dependent dielectric function,

$$\varepsilon_1(q) = 1 + \frac{q_s^2}{q^2} \tag{136}$$

suggests that the dominant wave vector for a small particle is $q \approx \sqrt{5}/a$. (Strassler, Rice, and Wyder (1972) show that the factor of 5 comes from an integral of r^2 over the volume of the sphere.)

3. The frequency-dependent dielectric function.

The presence of a level distribution in a small particle will modify in a significant way the infrared and optical properties of the particle. We would expect optical absorption when the photon energy of the light equals the difference in energy between a filled and an empty level. If the levels were uniformly spaced with separation δ then the absorption spectrum would be a series of sharp peaks, such as occur in the rotation spectrum of a polar

diatomic molecule. However, there are two reasons why this type of spectrum is not observed. First, the samples studied consist of many individual particles with small variations in size and shape, so that there are also variations in level spacing. Second, the gap δ is only the average distance between the levels; the dielectric function depends on the statistical distribution of levels.

Gor'kov and Eliashberg (1965) applied a theory of random matrices due to Dyson (1962) and Mehta and Dyson (1963) to the optical properties of small particles. Readers interested in the subject should also consult the work of Devaty and Sievers (1980), Strassler, Rice and Wyder (1972) and Maksimenko, Simonov, and Lushnikov (1977) for corrections to the original Gor'kov and Eliashberg paper. The review by Perenboom, Wyder, and Meier (1981) gives a good description of this theory. The theory of random matrices, originally developed to investigate excitations in heavy nucleii, uses a statistical description of an ensemble of identical (in size and shape) particles. Because the underlying Hamiltonian must be invariant under particular symmetry operations, a group-theoretical analysis shows that there are only three classes of ensembles: the orthogonal, symplectic and unitary groups. Physically, the orthogonal group corresponds to particles with small spin-orbit coupling (light elements), the sympletic group to those with large spin-orbit coupling (heavy elements), and the unitary group to particles in strong static magnetic field, $\mu_B B >> \delta$.

To determine the frequency-dependent part of the dielectric function, Gor'kov and Eliashberg averaged the electric dipole matrix element over the three ensembles of level distributions. Their result applies to particles where the bulk electronic mean free path is larger than the particle radius. (If the mean free path is short with respect to the particle size,

Maksimenko et al. (1977) show that the classical result is found.) It also is applicable only at low frequencies, $\omega << 1/\tau_c = v_F/a$. The dielectric function is given by:

$$\varepsilon = 1 + \frac{1}{5} q_s^2 a^2 + 4\pi Q A(\omega) \tag{137}$$

where

$$Q = \frac{139}{1200\pi^2 a_o k_F} \tag{138}$$

and where $A(\omega)=A_1(\omega)+iA_2(\omega)$ is a dimensionless quantity which is determined by the particular ensemble chosen. This quantity may be written conveniently as a function of the dimensionless argument

$$z = 2\pi \frac{\omega}{\delta}$$

with ω and δ in the same units. (Note that Gor'kov and Eliashberg and Devaty and Sievers use $\eta = z/2$ as argument of A for the orthagonal and unitary cases.) It is also convenient to write the dielectric function as

$$\varepsilon(\omega) = 1 + \frac{3}{5} \omega_p^2 \tau_c^2 \left[1 + \frac{139}{90} \omega\tau_c \frac{A(z)}{z}\right] \tag{139}$$

where $\tau_c = a/v_F$ is the classical value for the scattering time. The A(z) for the three ensembles are

Orthogonal:

$$A_1^o(z) = 2 - \frac{4}{z}\sin\left(\frac{z}{2}\right) - 2\,Ci\left(\frac{z}{2}\right)\left[\frac{2}{z}\sin\left(\frac{z}{2}\right) - \cos\left(\frac{z}{2}\right)\right] \quad (140a)$$

$$A_2^o(z) = z - \frac{4}{z}\sin^2\left(\frac{z}{2}\right) - 2\left[Si\left(\frac{z}{2}\right) - \frac{\pi}{2}\right]\left[\frac{2}{z}\sin\left(\frac{z}{2}\right) - \cos\left(\frac{z}{2}\right)\right] \quad (140b)$$

Symplectic:

$$A_1^s(z) = 2 - \frac{1}{2z}\sin(2z) - Si(z)\left[\frac{1}{z}\cos(z) + \sin(z)\right] \quad (141a)$$

$$A_2^s(z) = z - \frac{\sin^2(z)}{z} - Si(z)\left[\frac{1}{z}\sin(z) + \cos(z)\right] \quad (141b)$$

Unitary:

$$A_1^u(z) = 2 - \frac{2}{z}\sin(z) \quad (142a)$$

$$A_2^u(z) = z - \frac{4}{z}\sin^2(z) \quad (142b)$$

Here, Si(z) and Ci(z) are the sine and cosine integral functions.

Fig. 29 shows the functions $\frac{A(z)}{z}$, the absorption coeffients, and the derivatives of the absorption coefficient for the three ensembles. In these calculations, the particle dielectric function was evaluated from the quantum mechanical expression, and then the absorption coefficient of a composite was found using the MGT. The quantity x is the particle diameter; the absorption coefficients were calculated using a volume fraction of 0.02 and parameters appropriate to Al. Note that only for the sympletic ensemble are visible oscillations in the absorption coefficient predicted by the theory. As pointed out by Granqvist (1978) and Devaty and Sievers (1980), even these oscillatons are washed out when any distribution in particle size is assumed. This washout occurs because the gap (Eq. 128) is such a strong function of particle radius.

4. Comparison to classical models

Finally, we would like to compare this quantum mechnical theory with the classical expression for the dielectric function. In the limit as $\delta \to 0$ (or as $z \to \infty$), $A(z)/z \to i$, and

$$\varepsilon_1(\omega) \approx 1 + \frac{3}{5}\omega_p^2\tau_c^2 \tag{143a}$$

$$\sigma_1(\omega) \approx \frac{417}{1800\pi}\omega_p^2\omega^2\tau_c^3 \tag{143b}$$

If we use the low-frequency Drude model (Eqs. 18 and 19) the comparison fails. Note that even the sign is wrong for the real part of the dielectric function. The failure occurs because the quantum mechanical theory is in effect a theory for $\varepsilon(q,\omega)$ at a finite wavevector q while the Drude model is a strictly q=0 limit. Starting with the Boltzmann transport equation, Harrison (1979) gives a classical expression for $\varepsilon(q,\omega)$:

$$\varepsilon(q,\omega) = 1 + \frac{3\omega_p^2}{q^2 v_F^2}\left\{1 + \frac{\frac{\omega\tau}{2qv_F}\ln\left(\frac{1 - i\omega\tau + iqv_F\tau}{1 - i\omega\tau - iqv_F\tau}\right)}{i\left[1 + \frac{1}{2qv_F\tau}\ln\left(\frac{1 - i\omega\tau + iqv_F\tau}{1 - i\omega\tau - iqv_F\tau}\right)\right]}\right\} \tag{144}$$

Eq. (144) is valid as long as $q \ll 2k_F$. If $qv_F \ll |\omega + i/\tau|$, the logarithms may be expanded, to find

$$\varepsilon(q,\omega) = 1 - \frac{\omega_p^2}{\omega^2 + i\omega/\tau}\left\{\frac{3\omega\tau(1 - i\omega\tau)^2}{3\omega\tau(1 - i\omega\tau)^2 + (qv_F\tau)^2}\right\} \tag{145}$$

As $q \to 0$, we recover the Drude model (Eq. 14) while as $\omega \to 0$ we obtain the Thomas-Fermi dielectric function (Eq. 136). At this point if we let $\omega \ll 1/\tau$ but keep leading terms in ω, we get

$$\epsilon(q,\omega) = 1 + \frac{3\omega_p^2}{q^2 v_F^2}\left[1 + i\,\frac{3\omega\tau}{(qv_F\tau)^2}\right] \qquad (146)$$

At zero frequency, Eq. (146) is the same as Eq. (136). If, now, we take $q = \sqrt{5}/a$ and $\tau_c = a/v_F$, Eq. (146) becomes

$$\epsilon_1(q,\omega) = 1 + \frac{3}{5}\,\omega_p^2 \tau_c^2 \qquad (147a)$$

$$\sigma_1(q,\omega) = \frac{9}{100\pi}\,\omega_p^2 \omega^2 \tau_c^3 \qquad (147b)$$

Except for numerical factors, Eq. (147) is the same as Eq. (143). Thus, when $\omega >> \delta$, the quantum-mechanical treatment is the same as the classical treatment with $q \approx \sqrt{5}/a$, except that the conductivity is a factor of 2.5 larger.

This comparison with the classical theory suggest that the quantum size theory agrees with classical theory when $\omega >> \delta$, as it should. When $\omega \approx \delta$, the quantum theory predicts a somewhat reduced absorption, as shown by Granqvist et al (1976), and Devaty and Sievers (1980). Thus, the anomalously large far-infrared absorption cannot be explained as due to quantum effects.

5. Observation of quantum size effects

The possibility that quantum size effects might be observed in far infrared experiments is a facinating one. Such an observation would give fundamental information about the crossover of electronic properties from those of a solid to those of an atom or molecule. These observations have eluded experiments for more than twenty years. (See the review by Perenboom, Wyder, and Meier, 1981.) The quantum theory predicts structure in the far infrared absorption by a collection of identical small particles. Because any sample contains particles with varying sizes and shapes, this structure would

become washed out. Most authors (Devaty and Sievers, 1980; Granqvist et al, 1976) have concluded that these effects are not observable by far infrared studies.

There remains one effect, however, that is not washed out so long as the particle size distribution is reasonably narrow. This effect is the gap between the highest occupied level and the lowest unoccupied one. At frequencies smaller than the gap, a particle should not absorb far infrared energy. A collection of particles whose size distribution is relatively narrow should exhibit a threshold for absorption at the gap frequency. The size and shape distribution will blur this threshold a bit, but should not make it disappear entirely. Early experiments (Tanner, Sievers, and Buhrman, 1975) were suggestive that this gap might occur, but to date, no other experiments have proved this issue.

VIII. Another inhomogeneous material: Layered semiconductor systems

Modern semiconductor technology makes heavy use of layered semiconductors in different forms. The most common type is a thin epitaxial film of semiconductor usually a few microns thick, grown on a semiconductor substrate. Many of these structures involve III-V compounds such as InAs on GaAs, AlGaAs on GaAs, and InGaAsP on InP, but combinations like one alloy of PbSnTe on another or even polar-non polar systems like GaAs on Ge have also been fabricated. A second type of system is the so-called "quantum well" or superlattice in which very thin layers of two semiconductors alternate. A prevalent example is AlGaAs alternating with GaAs. All of these structures exhibit a form of spatial inhomogeneity in the direction perpendicular to the surface, because the semiconductor properties change more or less drastically at each interface. This inhomogeneity is better controlled than what we have encountered, for instance, in granular films, because it exists in only one dimension and because the layer-to-layer spacing is fixed and is often very well known. Nevertheless, the existence of boundaries between different materials has a profound effect on the electrical and optical properties of these systems.

In optical terms, a useful way to determine the scale of the inhomogeneity is to compare it to the penetration depth of the radiation. A typical penetration depth for UV-visible radiation in a semiconductor is less than 1 μm, so reflection data taken on an epitaxial layer more than a few microns thick does not sample as far as the first interface. Far infrared radiation, on the other hand, can penetrate tens of microns so that for a typical film it may return information about one or more interfaces. In the remainder of this section we show how this kind of spatial inhomogeneity plays a role in far infrared measurements. A careful analysis of far infrared data

can give useful information about the sample interfaces, although extremely sophisticated analyses have not yet been carried out.

The main features of this one-dimensional spatial variation can easily be included in an optical theory. The basic idea is to represent each layer as a slab of semiconductor having a spatially constant dielectric function and then to assume that the interfaces between layers are perfectly abrupt. The frequency dependence of the dielectric function for both the lattice and free carrier responses of the semiconductor is well known in the far infrared (Perkowitz, 1983, Jensen, 1983). For the j'th layer, the complex dielectric function ε_j determines the complex index of refraction, $N_j = n_j + i\kappa_j = \sqrt{\varepsilon_j}$. As Fig. 30 shows, it is then a straightforward analysis to follow the incident light beam through the sample layer-by-layer and to calculate the effect of each interface as it is encountered. For the calculation of reflectivity, for instance, the amplitude reflection coefficient between the j'th and j+1'th layer is given by

$$r_{j,j+1} = \left(\frac{N_{j+1} - N_j}{N_{j+1} + N_j}\right) \tag{148}$$

A summation over all the layers then yields the net reflection coefficient. Similar methods give the net transmission coefficient. It will be seen that departures of the data from this simple model contain interesting information about spatial variations near the interfaces.

A pioneering effort in layered systems was made by Tennant and Cape (1976) who examined the far infrared reflection of a low carrier density ($\approx 10^{16}/cm^3$), 8 μm-thick film of $Pb_{0.88}Sn_{0.12}Te$ on a high carrier density ($\approx 10^{18}/cm^3$) $Pb_{0.78}Sn_{0.22}Te$ substrate. Their reflection data, given in Fig. 31, shows clearly by the presence of interference fringes the existence of a

definite optical interface within the sample. Further details became apparent when they fitted the data with the abrupt interface model. The figure shows that this procedure did not give a good fit at the higher frequencies. The fit became satisfactory only when the assumption of abrupt change was replaced by a fit that allowed the carrier concentration to vary continuously over the interface region. This variation was modeled by defining many thin slabs to approximate the carrier gradient. Such grading is likely to occur because of carrier diffusion during the growing of the film.

Further evidence of the effect of inhomogeneity in semiconductor structures was obtained by Amirtharaj et al. (1977 and 1979) who examined a 12 μm thick film of InAs grown on a GaAs substrate. As seen in Fig. 32, these data also show interference fringes arising from the InAs film. Again, however, a fit using a two layer-abrupt interface model was unsatisfactory. An acceptable fit could be produced only by including additional spatial variation near the interface. Rather than introduce a graded region as Tennant and Cape had done, a third layer, representing the transition region between the epitaxial layer and the substrate, was included in the fit. The properties of this transition region were varied to provide the best fit and it turned out that a 1 μm thick interface layer composed of the ternary InGaAs vastly improved the fits to both reflection and transmission data. Later measurements (Wagner, 1976) on sister samples using Auger spectroscopy and energy-dispersive x-ray analysis confirmed the existence of such a ternary interface layer and predicted a thickness of about 2 μm, reasonably close to the estimate made using far infrared techniques.

With the addition of this third layer the fit values of lattice and free-carrier parameters in each layer became satisfactorally close to known or measured results. Fig. 32 shows one other factor in the spatial analysis. It

is known that InAs can develop thin surface accumulation layers with high carrier concentrations. The figure illustrates how the addition of a 0.1 μm surface layerw ith 10^{17} cm^{-3} carriers further enhances the fit especially at the highest frequencies. This extension requires several additional fitting parameters and should not be considered definitive without corroborating evidence, but it shows that far infrared data are sensitive to as little as 1000 Å of semiconductor layer.

These analyses and others made by Durschlag and DeTemple (1981) in a superlattice system and by Palik and coworkers (1979) in GaAs systems have all modelled the sample as a stack of layers, each with an appropriate classical bulk dielectric function. This approach is probably inadequate as probe of detailed microscopic behavior at the interface. Two analytical improvements are needed. One is to use a more general solution for Maxwell's equations, such the one developed by Hild and Grofsic (1978), for the case where the optical parameters are spatially varying. The other is to introduce the modifications in the bulk dielectric functions due to such factors as enhanced surface scattering in thin layers, band bending near the interfaces, and modified band structure in the case of the superlattices. Such improved analytic tools combined with infrared and other optical probes like Raman spectroscopy should give exceptionally useful results for layered semiconductors.

IX. Summary

The qualitative the far-infrared properties of inhomogeneous materials are reasonably well understood; they are in agreement with the ideas of the effective medium approximation. The effective complex dielectric function which characterizes these materials depends on the concentrations of the constituents, the properties of the individual constituents, their sizes, and the method of preparation of the sample. Three regimes can be identified: low concentrations, concentrations near the percolation transition, and high concentrations.

At low concentrations of metal in insulator, the dielectric function is mainly real with a real part which is close to that of the insulating constituent. The absorption coefficient (or conductivity) increases as the square of the frequency so long as the particle size is smaller than the electromagnetic skin depth. Near percolation, the real dielectric constant is much larger than that of the insulator; the absorption is also large. Finally, at concentrations well above percolation, the properties resemble those of a dirty or disordered metal.

In contrast to this qualitative understanding, the magnitude of the far-infrared absorption in low-volume-fraction composites ($f < 0.05$) is mysteriously large. The discrepancy between the observed absorption and model calculations which consider only electric dipole absorption (i.e., the dielectric functions of Eqs. 46 or 57) is about a factor of 10^6. When eddy current absorption is included in the model (and when the most favorable parameters are used in the calculation) the discrepancy is a factor of 10 to 100, even though the eddy current absorption correctly predicts the frequency, concentration, and size dependence of the absorption. Note that at small concentrations and low frequencies, both the MGT and the EMA give essentially

identical numerical values for the absorption, so that the anomaly is not dependent upon the effective medium model chosen. Finally, in superconducting samples the frequency dependence of the observed absorption also disagrees with calculations.

In addition to these anomalies, the major unanswered question in this area has to do with quantum size effects. Although there is a general belief that quantum size effects should become important in very small particles, there has been no unambiguous observation of these effects. Thus there is no experimental information about the magnitude of the energy gap or the details of the level distribution in small particles, despite the fundamental importance of these issues.

Acknowledgements

One of us (S.P.) would like to thank Professor V. Jaccarino and the Physics Department, University of California at Santa Barbara, for their generous hospitality during a portion of the writing of this chapter; and acknowledges support from the Office of Naval Research and the U.S. Department of Energy (Contract No. DE-AS05-79ER10436) for some of the work carried out at Emory University.

References

Abeles, B. and J.I. Gittleman, Appl. Opt. 15, 2328 (1976).

Abeles, B., H.L. Pinch, and J.I. Gittleman, Phys. Rev. Lett. 35, 247 (1975).

Abeles, B., P. Sheng, M.D. Coutts, and Y. Arié, Adv. Phys. 24, 407 (1975).

Ambegaokar, V., B.I. Halperin, and J.S. Langer, Phys. Rev. B 4, 2612 (1971).

Ambegaokar, V., S. Cochran, and J. Kurkijarvi, Phys. Rev. B 8, 3682 (1973).

Amirtharaj, P.M. B.L. Bean and S. Perkowitz, J. Opt. Soc. Am. 67, 939 (1977).

Amirtharaj, P.M. and S. Perkowitz, Thin Solid Films 62, 357 (1979).

Ausloos, M. and P. Clippe, Phys. Rev. B 18, 7176 (1978).

Bardeen, J., L.N. Cooper, and J.R. Shrieffer, Phys. Rev. 108, 1175 (1957).

Barker, Jr., A.S., Phys. Rev. B 7, 2507 (1973).

Batson, P.E., Solid State Commun. 34, 477 (1980).

Bergman, D.J. and Y. Imry, Phys. Rev. Lett. 39, 1222 (1977).

Bergman, D.J., Phys Rep. C: Phys. Lett. 32, 377 (1978).

Bergman, D.J., and D. Stroud, Phys. Rev. B 22, 3527 (1980).

Born, M. and E. Wolf, Principles of Optics (Pergamon, Oxford, 1970).

Bottger, H. and V.V. Bryksin, Phys. Stat. Sol. (B) 78, 9 (1976).

Bray, A.J. and B. Rickayzen, J. Phys. F 2, 1114 (1972).

Bruggeman, D.A.G., Ann. Physik (Leipz.) 24, 636 (1935).

Carr, G.L., J.C. Garland, D.B. Tanner, in Inhomogeneous Superconductors-1979, D.U. Gubser, T.L. Francavilla, J.R. Leibowitz, and S.A. Wolf, eds. (AIP, New York, 1980) p. 288.

Carr, G.L., J.C. Garland, and D.B. Tanner, Phys. Rev. Lett. 50, 1607 (1983).

Carr, G.L., R.L. Henry, N.E. Russell, J.C. Garland, and D.B. Tanner, Phys. Rev. B. 24, 777 (1981).

Chantry, G., Submillimetre Spectroscopy (Acadmeic Press, London, 1971).

Chui, T., G. Deutscher, P. Lindenfeld, and W.L. McLean, Phys. Rev. B 23, 6172 (1981).

Chylek, P. and V. Srivastava, Phys. Rev. B 27, 5098 (1983).

Chylek, P., D. Boice, and R.G. Pinnick, Phys. Rev. B 27, 5107 (1983).

Clippe, P. and M. Ausloos, Phys. Stat. Sol. (B) 110, 211 (1982).

Clippe, P., R. Evrard, and A.A. Lucas, Phys. Rev. B 14, 1715 (1976).

Cohen, R.W., G.D. Cody, M.D. Coutts, and B. Abeles, Phys. Rev. B 8, 3689 (1973).

Devaty, R.P. and A.J. Sievers, Phys. Rev. B22, 2123 (1980).

Debye, P., Ann. de Physik 30, 57 (1909).

Doremus, R.H., J. Chem. Phys. 40, 2389 (1964).

Doremus, R.H., J. Appl. Phys. 37, 2775 (1966).

Doyle, W.T., Phys. Rev. 111, 1072 (1958).

Durschlag, M.S. and T.A. DeTemple, Solid State Commun. 40, 307 (1981).

Dyson, F.J, J. Math Phys. 3, 140, 157, 166 (1962).

Efros, A.L. and B.I. Shklovskii, Phys. Stat. Sol. (B) 76, 475 (1976).

Eilenberger, G., J. Phys. 236, 1 (1970).

Ford, G.W. and S.A. Werner, Phys. Rev. B 8, 3702 (1973).

Friedel, J., J. Phys. (Paris) 33, C2-1 (1977).

Frohlich, H., Physica 6, 406 (1937).

Galeener, F.L., Phys. Rev. Lett. 27, 421 (1971); 27, 1716 (1976).

Ganiere, J.-D., R. Rechsteiner, and M.-A, Smithard, Solid State Commun. 16, 113 (1975).

Garnett, J.C.M., Phil. Trans. Roy. Soc. A203, 385 (1904); A205, 237 (1906).

Garner, J. and D. Stroud, Phys. Rev. B (1983).

Genzel, L. and T.P. Martin, Phys. Stat. Sol. (B) 51, 91 (1972).

Genzel, L. and T.P. Martin, Surf. Sci. 34, 33 (1973).

Gerardy, J.M. and M. Ausloos, Phys. Rev. B 22, 4950 (1980).

Gerardy, J.M. and M. Ausloss, Phys. Rev. B 25, 4202 (1982).

Gerardy, J.M. and M. Ausloos, M., Phys. Rev. B 26, 4703 (1982).

Gittleman, J.I. and B. Abeles, Phys. Rev. B 15, 3273 (1977).

Gor'kov, L.P. and G.M. Eliashberg, Sov. Phys. JETP 21, 940 (1965).

Grannan, D.M., J.C. Garland, and D.B. Tanner, Phys. Rev. Lett. 46, 375 (1981).

Granqvist, C.G., R.A. Buhrman, J. Wyns, and A.J. Sievers, Phys. Rev. Lett. 37, 625 (1976).

Granqvist, C.G. and R.A. Buhrman, J. Appl. Phys. 47, 2200 (1976).

Granqvist, C.G. and O. Hunderi, Solid State Commun. 19, 939 (1976).

Granqvist, C.G. and O. Hunderi, Phys. Rev. B 16, 1353 (1977).

Granqvist, C.G. and O. Hunderi, Phys. Rev. B 16, 3513 (1977).

Granqvist, C.G., Z. Physik B 30, 29 (1978).

Harris, A.B. and R. Fisch, Phys. Rev. Lett. 38, 796 (1977).

Harris, L., T.R. McGinnes, and B.M. Siegel, J. Opt. Soc. Am. 38, 582 (1948).

Harris, L. and J.K. Beasley, J. Opt. Soc. Am. 42, 134 (1952).

Harris, L. and A.L. Loeb, J. Opt. Soc. Am. 43, 1114 (1953).

Harris, L. J. Opt. Soc. Am. 51, 80 (1961).

Harrison, W.A., Solid State Theory, (Dover, New York, 1979).

Hashin, Z. and S. Shtrikman, J. Appl. Phys. 33, 3125 (1962).

Hetrick R.E. and J. Lambe, Phys. Rev. B 11, 1273 (1975).

Hild, E. and A. Grofcsik, Infrared Phys. 18, 23 (1978).

Huffman, D.R. (1977).

Hughes, A.E., Contemp. Phys. 12, 257 (1971).

Jackson, J.D., Classical Electrodynamics (Wiley, New York, 1975).

Jain, S.C. and N.D. Arora, Solid Stat Commun. 15, 433 (1974).

Jain, S.C. and N.D. Arora, Solid State Commun. 16, 421 (1975).

Jensen, B., in Infrared and Millimeter Waves, ed. K.J. Button, Vol. 8, pp. 127-171 (Academic Press, New York, 1983).

Karecki, D.R., G.L. Carr, S. Perkowitz, D.U. Gubser, and S.A. Wolf, Phys. Rev. B27, 5460 (1983).

Kawabata, A. and R. Kubo, J. Phys. Soc. Jap. 21, 1765 (1966).

Kim, Y.H. and D.B. Tanner, Bull. Am. Phys. Soc. (1984).

Kirkpatrick, S., Phys. Rev. Lett. 27, 1722 (1971).

Kirkpatrick, S., Rev. Mod. Phys. 45, 574 (1973).

Kirkpatrick, S., Phys. Rev. Lett. 36, 69 (1976).

Kirkpatrick, S., Phys. Rev. B 15, 1533 (1977).

Kittel, C., Introduction to Solid State Physics (Wiley, New York, 1974).

Kreibig, U. and C.V. Fragstein, Z. Physik 224, 307 (1969).

Kubo, R., J. Phys. Soc. Jpn. 17, 975 (1962).

Lamb, W., D.M. Wood, and N.W. Ashcroft, Phys. Rev. B. 21, 2248 (1980).

Landauer, R., J. Appl. Phys. 23, 779 (1952).

Landauer, R., in Electrical Transport and Optical Properties of Inhomogeneous Media, J.C. Garland and D.B. Tanner, eds. (The American Institute of Physics, New York, 1978), p. 1.

Landau, L.D. and E.M. Lifshitz, Electrodynamics of Continuous Media (Pergamon, New York, 1960).

Last, B.J. and D.J. Thouless, Phys. Rev. Lett. 27, 1719 (1971).

Leplae, L., Phys. Rev. B 27, 1911 (1983).

Levinshtein, M.E., B.I. Shklovskii, M.S. Shur, and A.L. Efros, Sov. Phys JETP 42, 197 (1975).

Lushnikov, A.A. and A.J. Simonov, Phys. Lett. 44A, 45 (1973).

Lushnikov, A.A., V.V. Maksimenko, and A.J. Simonov, Z. Physik B 27, 321 (1977).

Maksimenko, V.V., A.J. Simonov, and A.A. Lushnikov, Phys. Stat. Sol. (B) 82, 685 (1977).

Maksimenko, V.V., A.J. Simonov, and A.A. Lushnikov, Phys. Stat. Sol. (B) 83, 377 (1977).

Mal'shukov, A.G., Solid State Commun. 44, 1257 (1982).

Martin, T.P. and L. Genzel, Solid State Commun. 17, 139 (1975).

Martin, T.P. and H. Schaber, Phys. Stat. Sol. (B) 81, K41 (1977).

Martin, T.P., Physics Reports 95, 167 (1983).

Marzke, R.F., Catal. Rev. Sci. Eng. 19, 43 (1979).

Mattis, D.C. and J. Bardeen, Phys. Rev. 111, 412 (1958).

McKenzie, D.R., J. Opt. Soc. Am. 66, 249 (1976).

Mie, G., Ann. d Physik 25, 377 (1908).

Mehta, M.L. and F.J. Dyson, J. Math. Phys. 4, 713 (1963).

Mitra, S.S. and S. Nudelman, Far-Infrared Properties of Solids, (Plenum, New York, 1970).

Möller, K.D. and W.G. Rothschold, Far-Infrared Spectroscopy, (Wiley, New York, 1941).

Muller, K.A., M. Pomerantz, C.M. Knoedler, and D. Abraham, Phys. Rev. Lett. 45, 832 (1980).

Nam, S.B., Phys. Rev. 156, 487 (1967).

Norrman, S., T. Andersson and C.G. Granqvist, Solid State Commun. 23, 261 (1977).

Norrman, S., T. Andersson, C.G. Granqvist, and O. Hunderi, Phys. Rev. V 18, 674 (1978).

Odagaki, T. and M. Lax, Phys. Rev. B 24, 5284 (1981).

Odagaki, T., M. Lax, and A. Puri, Phys. Rev. B 28, 2755 (1983).

Palik, E.D., R.T. Holm and J.W. Gibson, Thin Solid Films 47, 167 (1977).

Palmer, L.H. and M. Tinkham, Phys. Rev. 165, 588 (1968).

Pan, F.P., D. Stroud, and D.B. Tanner, Solid State Commun. 20, 271 (1976).

Peierls, R.E., Quantum Theory of Solids (Clarendon Press, Oxford, 1955), p. 108.

Penn, D.R. and R.W. Rendell, Phys. Rev. Lett. 47, 1067 (1981).

Penn, D.R. and R.W. Rendell, Phys. Rev. B 26, 3047 (1982).

Perenboom, J.A.A.J., P. Wyder, and F. Meier, Physics Reports 78, 173 (1981).

Perkowitz, S., Phys. Rev. B25, 3420 (1982).

Perkowitz, S. in Infrared and Millimeter Waves, ed. K.J. Button, Vol. 8, pp. 71-125 (Academic Press, New York) (1983).

Pomerantz, M. and K.A. Muller, Physica 107B, 325 (1981).

Powell, M.J., Phys. Rev. B 20, 4194 (1979).

Robinson, L.C., Physical Principles of Far-Infrared Radiation, (Academic Press, New York, 1973).

Ruppin, R., Surf. Sci. 34, 20 (1973).

Ruppin, R., Phys. Rev. B 19, 1318 (1979).

Russell, N.E., J.C. Garland, and D.B. Tanner, Phys. Rev. B 23, 632 (1981).

Scher, H. and R. Zallen, J. Chem. Phys. 53, 3759 (1970).

Scher, H. and M. Lax, Phys. Rev. B 7, 4491 (1973), Phys. Rev. B 7, 4502 (1973).

Schmid, A., Z. Phys. 215, 210 (1968); 216, 336 (1968); 232, 442 (1970).

Sen, P.N. and D.B. Tanner, Phys. Rev. B 26, 3582 (1982).

Sennett, R.S. and G.D. Scott, J. Opt. Soc. Am. 40, 203 (1950).

Sheng, P., B. Abeles, and Y. Arie, Phys. Rev. Lett. 31, 44 (1973).

Sheng, P., Phys. Rev. B 22, 6364 (1980).

Sheng, P. and J. Kalfter, Phys. Rev. B 27, 2583 (1983).

Sheng, P., Phys. Rev. Lett. 45, 60 (1980).

Shklovskii, B.I. and A.L. Efros, Sov. Phys.-Usp. 18, 845 (1975).

Sichel, E.K., M. Knowles, M. Rubner, and J. Georger, Jr., Phys. Rev. B 25, 5574 (1982).

Simanek, E., Phys. Rev. Lett. 38, 1162 (1977).

Simanek, E., Sol. St. Comm. 40, 1021 (1981).

Springett, B.E., Phys. Rev. Lett. 31, 1463 (1973).

Stinchcombe, R.B. and B.P. Watson, J. Phys. C: Solid State Phys. 9, 3221 (1976).

Straley, J.P., J. Phys. C: Solid State Phys. 9, 783 (1976).

Straley, J.P, Phys. Rev. B 15, 5733 (1977).

Straley, J.P., J. Phys. C: Solid State Phys. 10, 3009 (1977).

Straley, J.P., in Electrical Transport and Optical Properties of Inhomogeneous Media, J.C. Garland and D.B. Tanner, eds. (The American Institute of Physics, New York, 1978), p. 118.

Strassler, S. and M.J. Rice, Phys. Rev. B 6, 2575 (1972).

Stroud, D., Phys. Rev. B 12, 3368 (1975).

Stroud, D., Phys. Rev. B 19, 1783 (1979).

Stroud, D. and D.J. Bergman, Phys. Rev. B 25, 2061 (1982).

Stroud, D. and F.P. Pan, Phys. Rev. B 17, 1602 (1978).

Tanner, D.B., Phys. Rev. B8, 5045 (1973).

Tanner, D.B., A.J. Sievers, R.A. Buhrman, Phys. Rev. B 11, 1330 (1975).

Tennant, W.E. and J.A. Cape, Phys. Rev. B13, 2540 (1976).

Tinkham, M. and R.E. Glover, III., Phys. Rev. 110, 771 (1958).

Trodahl, H.J., Phys. Rev. B 19, 1316 (1979).

Truong, V.V. and G.D. Scott J. Opt. Soc. Am. 66, 124 (1976).

Van de Hulst, H.C., Light Scattering by Small Particles (Dover, New York, 1981).

Wagner, N.K., Thin Solid Films 38, 353 (1976).

Watson, B.P. and P.L. Leath, Phys. Rev. B 9, 4893 (1974).

Weaver, J.H., R.W. Alexander, L. Teng, R.A. Mann, and R.J. Bell, Phys. Stat. Sol. (a) 20, 321 (1973).

Webman, I. and J. Jortner, Phys. Rev. B 11, 2885 (1975).

Webman, I., J. Jortner and M.H. Cohen, Phys. Rev. B 15, 5712 (1977).

Wilkinson, D., J.S. Langer and P.N. Sen, Phys. Rev. B 28, 1081 (1983).

Wood, D.M. and N.W. Ashcroft, Phil. Mag. 35, 269 (1977).

Wood, D.M. and N.W. Ashcroft, Phys. Rev. B 25, 6255 (1982).

Wooten, F., Optical Properties of Solids (Academic, New York, 1972).

Wyder, P. Infrared Phys. 16, 243 (1976).

Yoshida, S., T. Yamaguchi, and A. Kinbara J. Opt. Soc. Am. 61, 62 (1971).

Yoshida, S., T. Yamaguchi, and A. Kinbara, J. Opt. Soc. Am. 62, 1415 (1972).

Yamada, Y., A. Mitsuishi, and H. Yoshinaga, J. Opt. Soc. Am. 52, 17 (1962).

Zallen, R., ed. by E.W. Montrell and J.L. Lebowitz, North-Holland Publ. Co., 179 (1979).

Figure Captions

Figure 1 Transmission of gold black in the far infrared (from Harris, 1961).

Figure 2 Schematic pictures of the MGT and EMA views of an inhomogeneous medium.

Figure 3 Frequency-dependent conductivity calculated from the Maxwell-Garnett theory (left panel) and the effective medium approximation (right panel).

Figure 4 Electric dipole contribution to the far-infrared absorption coefficent. Curves are shown for three particle sizes, 10, 100, and 1000 Å.

Figure 5 Magnetic dipole contribution to the far-infrared absorption coefficient. Curves are shown for three particle sizes, 100, 300, and 1000 Å.

Figure 6 Magnetic-dipole contribution to the far-infrared absorption coefficient of a f = 0.01 small-particle composite. The particle radius is 1 μm (10,000 Å). Curves are shown for three values of the conductivity.

Figure 7 Magnetic dipole contribution to the 70 cm^{-1} absorption coefficient. Curves are shown for three values of particle conductivity over particle radii from 100 to 10^4 Å. The arrows indicate the value of the skin depth of the metal.

Figure 8 Concentration dependence of characteristic frequencies of a metal-insulator composite. ω_+ and ω_- are the impurity band limits, as calculated in the EMA. Heavy lines at $\omega = 0$ and $\omega = \omega_p$ are the two percolation modes, ω_{imp} and ω_{imp} are the impurity band centroids. Finally, the dashed line denotes the

peak in $-\mathrm{Im}\varepsilon_{\mathrm{eff}}^{-1}(\omega)$, as computed in the EMA. Right-hand scale expresses the correspondence between the frequency and the alternate variable $\varepsilon_m/\varepsilon_i$. (From Stroud, 1979.)

Figure 9 Frequency-dependent conductivity for a coated metal particle according to the EMA. The parameter Q=1-(oxide thickness)/(radius). Thus Q = 1 is for no oxide. Note that $f=0.4 > f_c$. (From Wood and Ashcroft, 1977.)

Figure 10 Measured absorption coefficient for Al smoke versus frequency. The solid line is calculated from the orthogonal ensemble and applied to either specimen. The instrumental resolution is shown. (From Tanner et al., 1975.)

Figure 11 Absorption coefficient of 24 Å radius Al smoke versus frequency. The volume fraction of metal in this unsupported smoke was $f = 0.015$. (From Granqvist et al., 1976.)

Figure 12 Far-infrared absorption coefficient of 1-μm-radius Pd particles in KCl, shown on a log-log scale. Data are shown for Pd volume fractions of 0.003, 0.01, 0.03, and 0.1. (From Russell et al., 1981.)

Figure 13 Far-infrared absorption coefficient divided by the volume fraction for Pd particles in KCl. Data are shown for Pd volume fractions of 0.001, 0.003, 0.01, 0.03, and 0.1. (From Russell et al., 1981.)

Figure 14 Far-infrared absorption coefficient of Pd and Au small particles in an Al_2O_3 host. The absorption by the host has been subtracted from the data. A fit to a quadratic curve is also shown. (From Carr et al., 1981.)

Figure 15 Far-infrared absorption coefficient of 450-Å radius Al particles in KCl. Data are shown for metal volume fractions of 0.003, 0.01, and 0.03. (From Carr et al., 1981.)

Figure 16 Far-infrared dielectric constant of composite samples of Al in KCl, inferred from the period of the internal reflection interference pattern, versus metal volume fraction. (From Carr et al., 1981.)

Figure 17 The real and imaginary parts of the frequency-dependent conductivity of a superconductor.

Figure 18 Experimentally determined real and imaginary parts of the frequency-dependent conductivity of NbN. Dashed line is Mattis-Bardeen theory; solid line is Leplae theory. (From Karecki et al., 1983).

Figure 19 Ratio of superconducting state transmission to normal state transmission for a NbN film. Curve a: fit from Leplae theory. Curves b and c: fits from Mattis-Bardeen theory with two different sets of parameters. (From Karecki et al., 1983.)

Figure 20 MGT prediction for the absorption coefficient of 250 Å Sn small particles in an insulating host. The volume fraction of metal was assumed to be 0.01. Eddy current (magnetic dipole) effects dominate the absorption. The solid line shows the normal-metal absorption whereas the dotted line gives the result when the Sn is superconducting.

Figure 21 MGT prediction for the absoprtion coefficient of Sn small particles at a volume fraction of 0.01 when only electric dipole absorption is included. The particle radius was taken to be 25 Å. The solid (dotted) line shows the normal (superconducting)

state absorption.

Figure 22 Calculated difference between superconducting and normal-state absorption for electic-dipole and magnetic-dipole absorption.

Figure 23 Far-infrared absorption by small Sn particles in KCl. (From Carr et al., 1983.)

Figure 24 Difference between the superconducting and normal-state absorption for Sn small particles in KCl. (From Carr et al., 1983.)

Figure 25 Microwave response of a granular aluminum film. (From Muller and Pomerantz, 1981.)

Figure 26 Far-infrared transmission of granular Pb films at T = 10 K (the normal state).

Figure 27 Ratio of superconducting-state transmission to normal-state transmission for granular Pb films. (From Carr et al., 1983.)

Figure 28 Real part of the frequency-dependent conductivity of a NbN granular film. (From Karecki et al., 1983.)

Figure 29 Upper panels: The function A(z)/Z for the Gor'kov and Eliashberg theory as calculated by Devaty and Sievers (1980). Results are shown for the three ensembles. The solid line shows the real part; the dashed line the imaginary part. Middle Panels: The absorption coefficient predicted by the model. Lower Panels: The frequency derivative of the absorption coefficient.

Figure 30 A schematic layered semiconductor structure showing one or more thin films of different materials grown in sequence on a substrate. The net reflection and transmission coefficient R and T relative to the incident light intensity I_o are calculated by applying appropriate electromagnetic boundary conditions at each interface.

Figure 31 Reflectivity of an 8 μm thick $Pb_{0.88}Sn_{0.12}$ Te film on a substrate of $Pb_{0.78}Sn_{0.22}$ Te. Interference fringes are apparent above 120 cm^{-1}. The fitting curves arise from the following models: curve A, two layer, abrupt interface; curve B, graded interface, linear variation of carrier concentration; and curve C, graded interface exponential variation of carrier concentration. (After Tennant and Cape, 1976).

Figure 32 Reflectivity of a 15 μm thick InAs film on a GaAs substrate. Free carrier effects appear below 50 cm^{-1}; interference fringes are apparent between 50 and 200 cm^{-1}; and lattice modes dominate above 200 cm^{-1}. Curve a: best fit with two layer abrupt interface model. Curve b: best three layer fit with added 1 μm-thick interface layer of InGaAs. Curve c: best four layer fit with added 0.1 μm-thick surface accumulation layer of InAs with 10^{17} carriers/cm^3. (After Amirtharaj and Perkowitz, 1979).

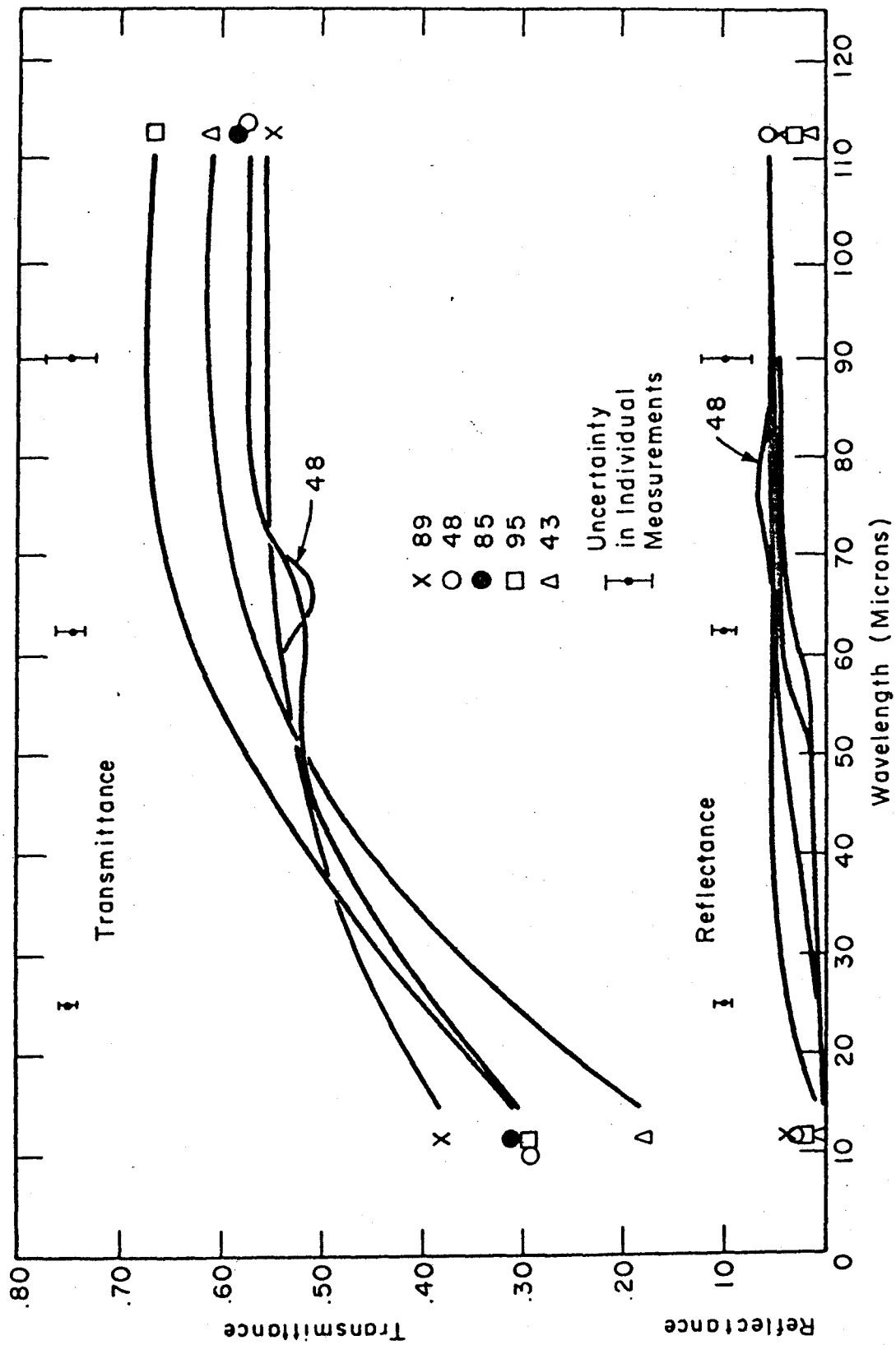
Transmittance
Reflectance
48
48
X 89
○ 48
● 85
□ 95
Δ 43
Uncertainty
in Individual
Measurements
Transmittance
Reflectance
Wavelength (Microns)
.80
.70
.60
.50
.40
.30
.20
10
0
10
20
30
40
50
60
70
80
90
100
110
120

Figure 1

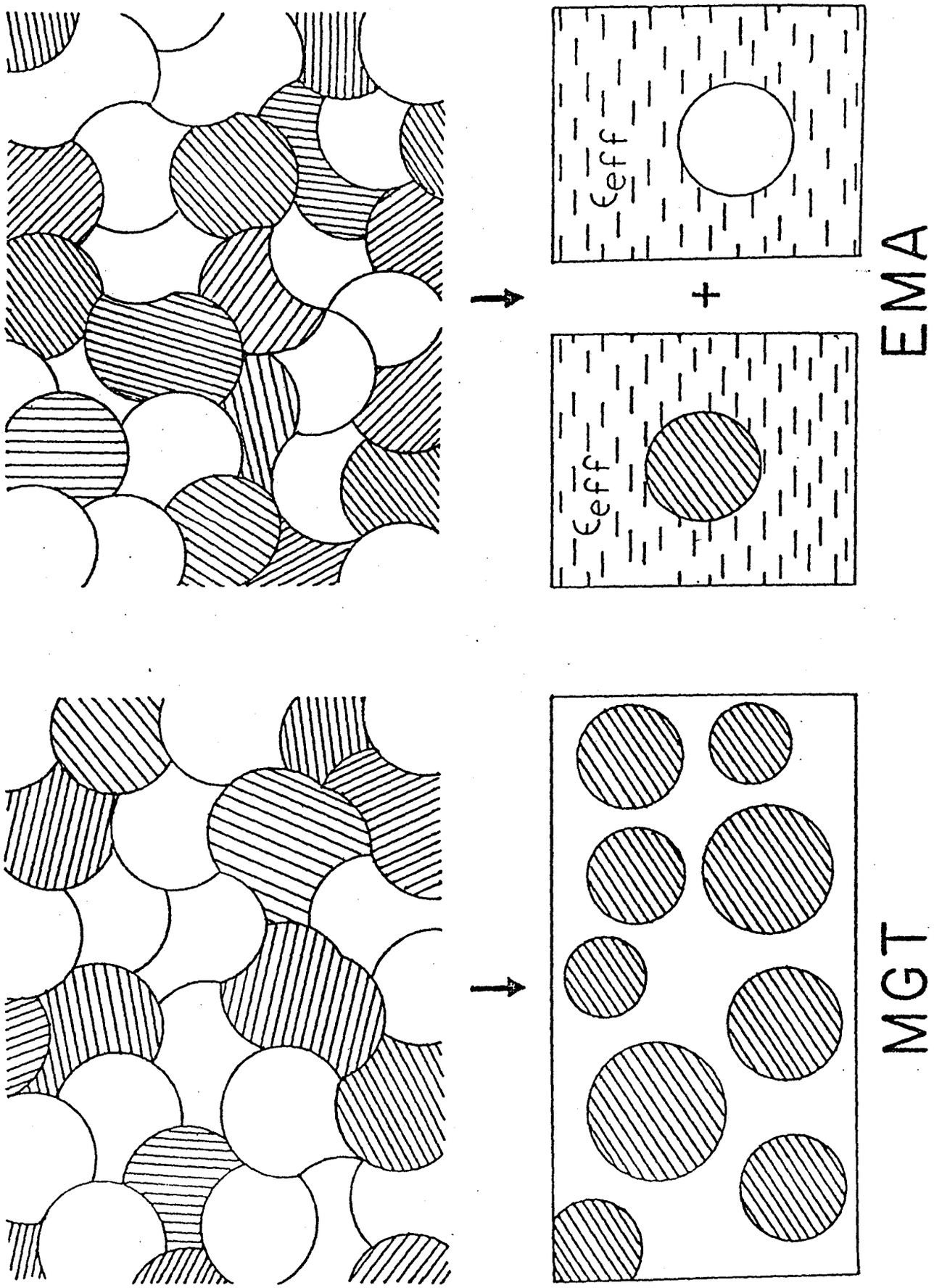

Figure 2

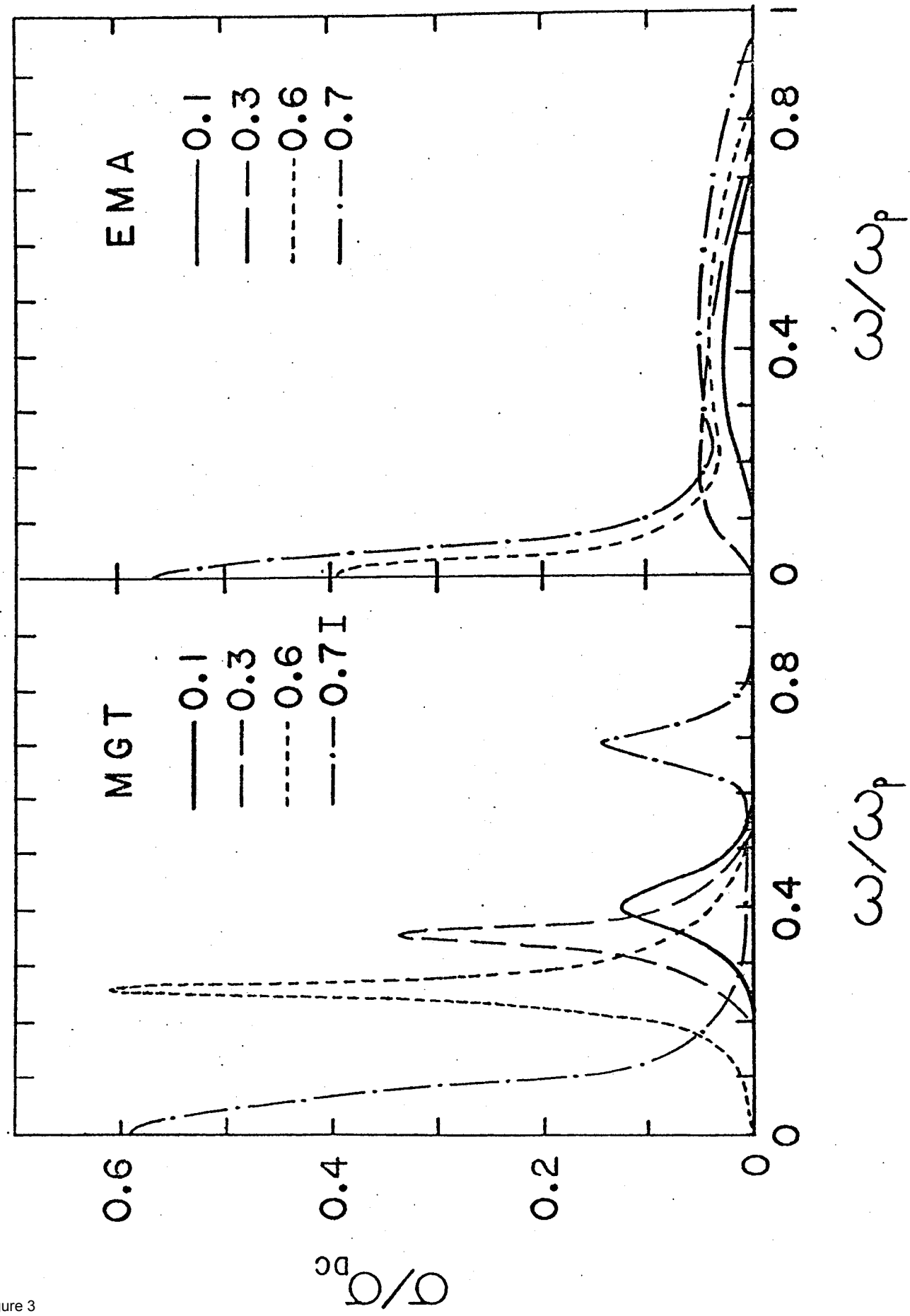

Figure 3

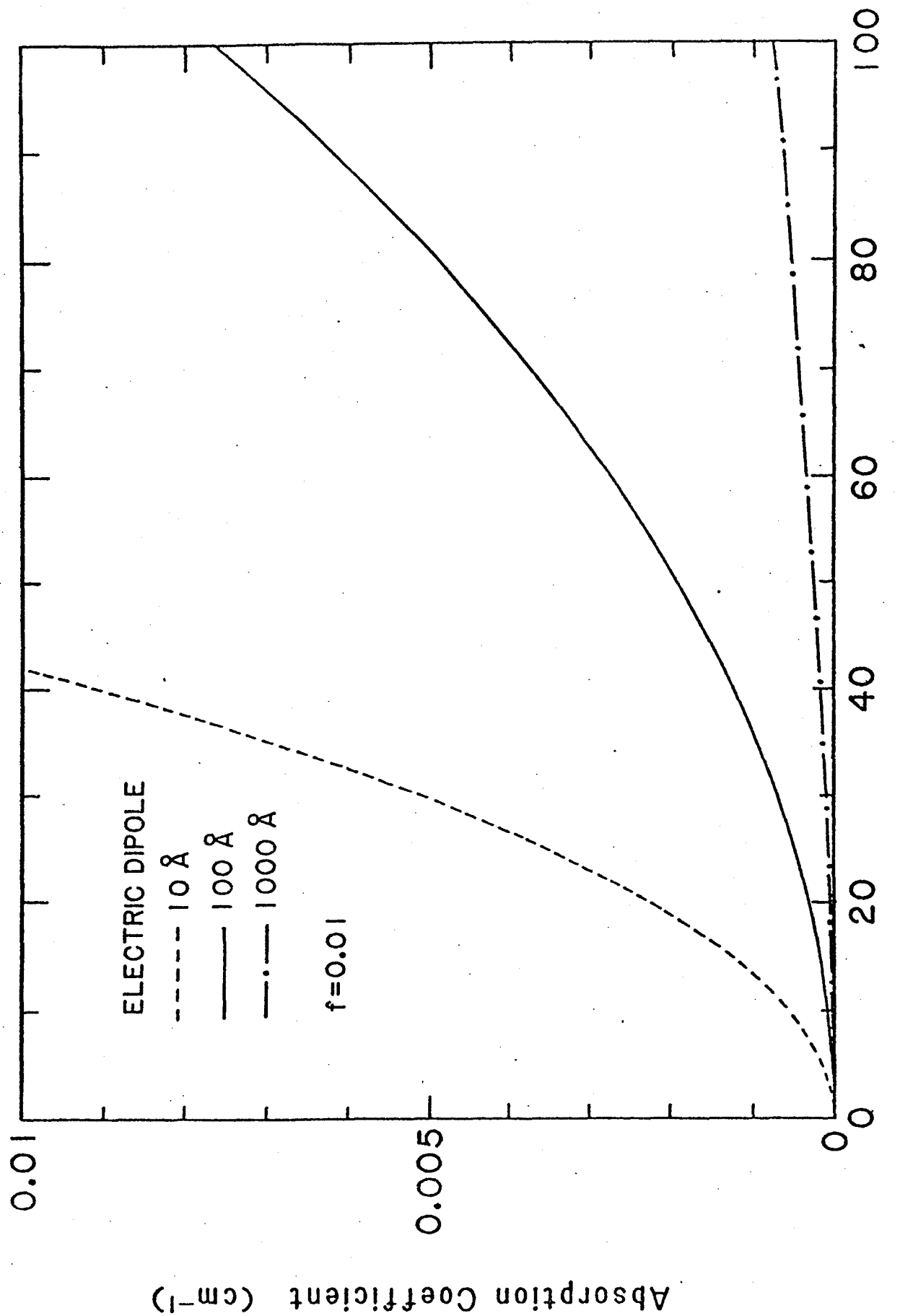
ELECTRIC DIPOLE
10 Å
100 Å
1000 Å
f=0.01
0.01
0.005
0
0
20
40
60
80
100
Absorption Coefficient (cm⁻¹)
Frequency (cm⁻¹)

Figure 4

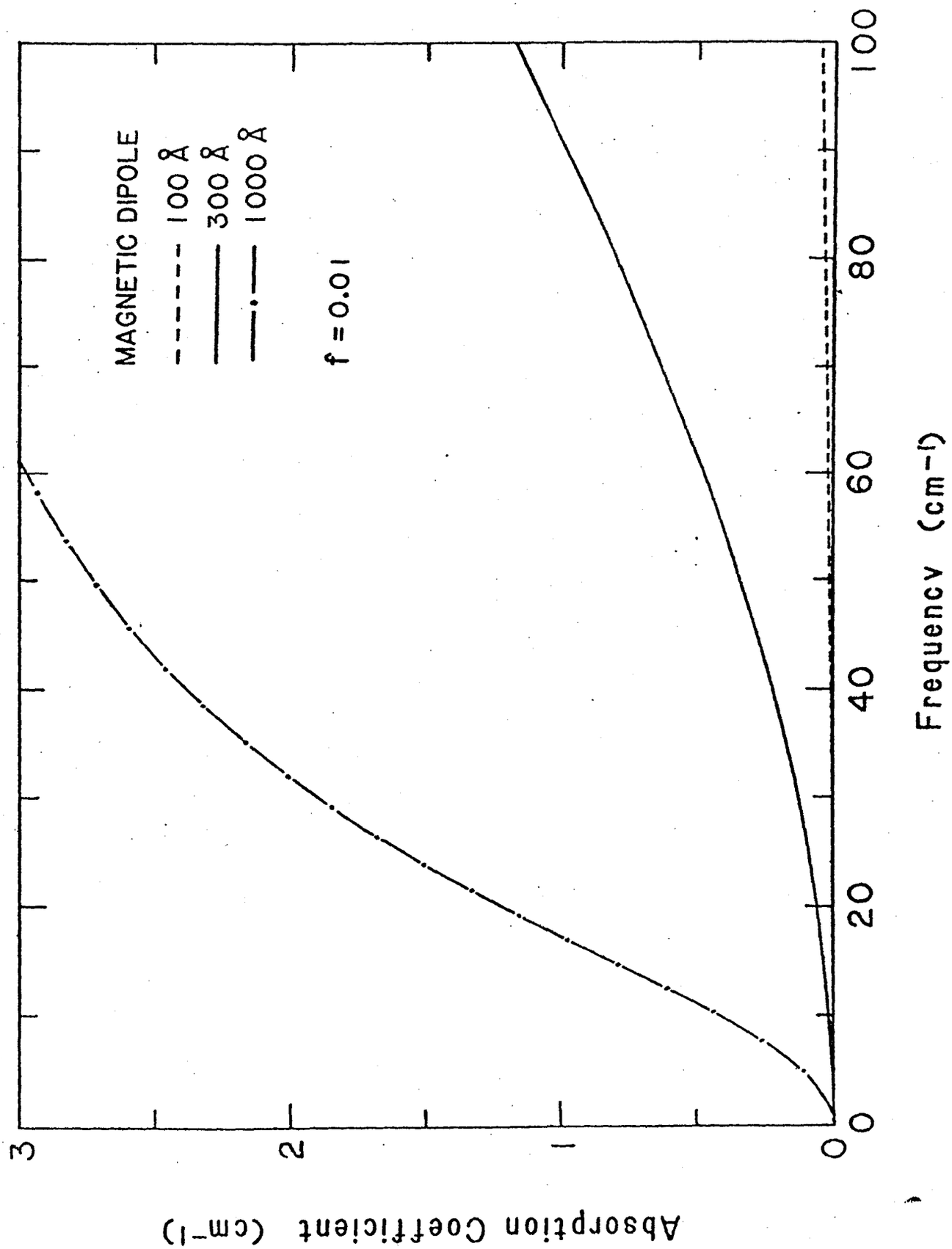
MAGNETIC DIPOLE
100 Å
300 Å
1000 Å
f = 0.01
Absorption Coefficient (cm⁻¹)
Frequency (cm⁻¹)
0
1
2
3
20
40
60
80
100

Figure 5

Fig. 6

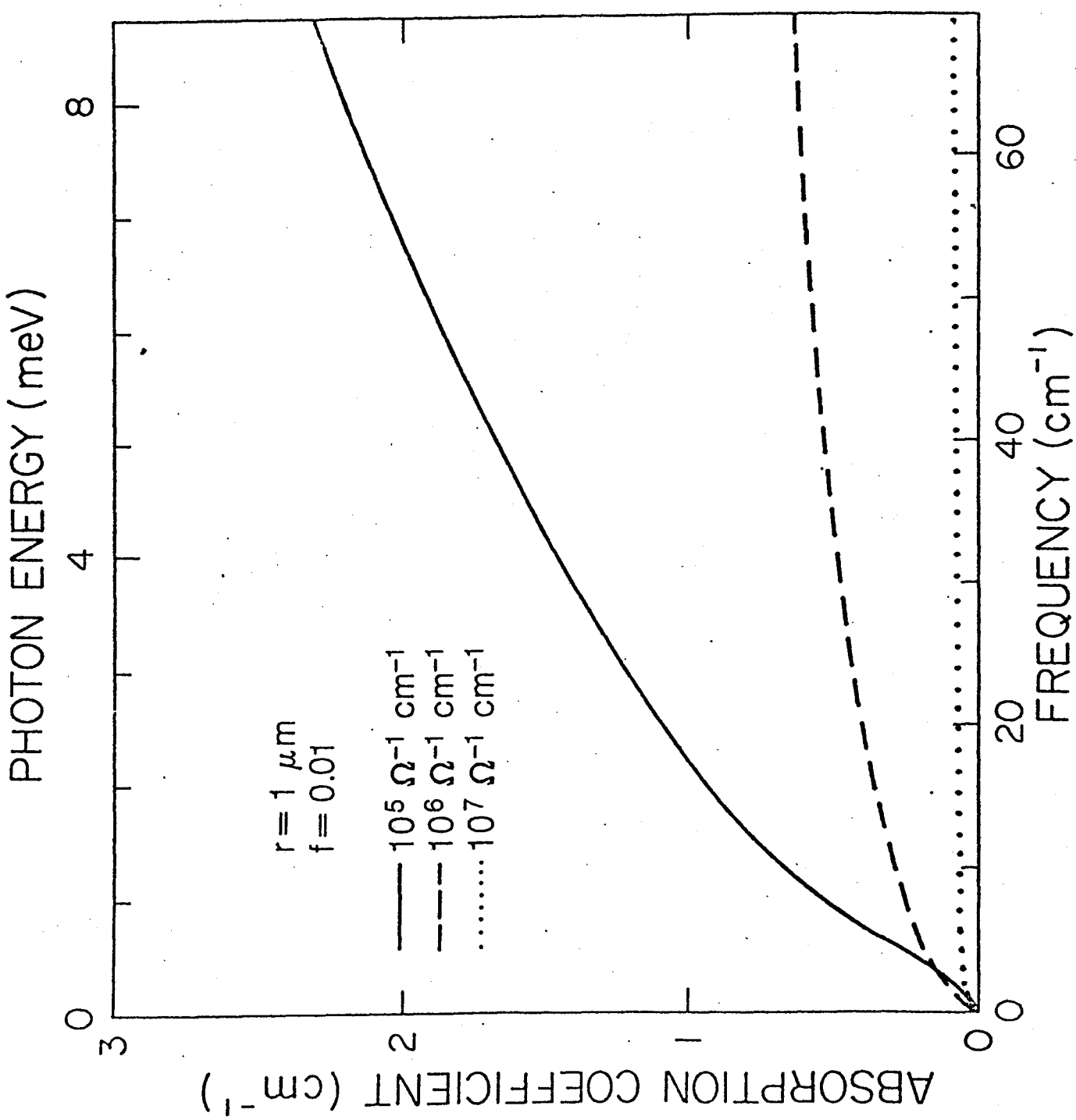

Figure 6

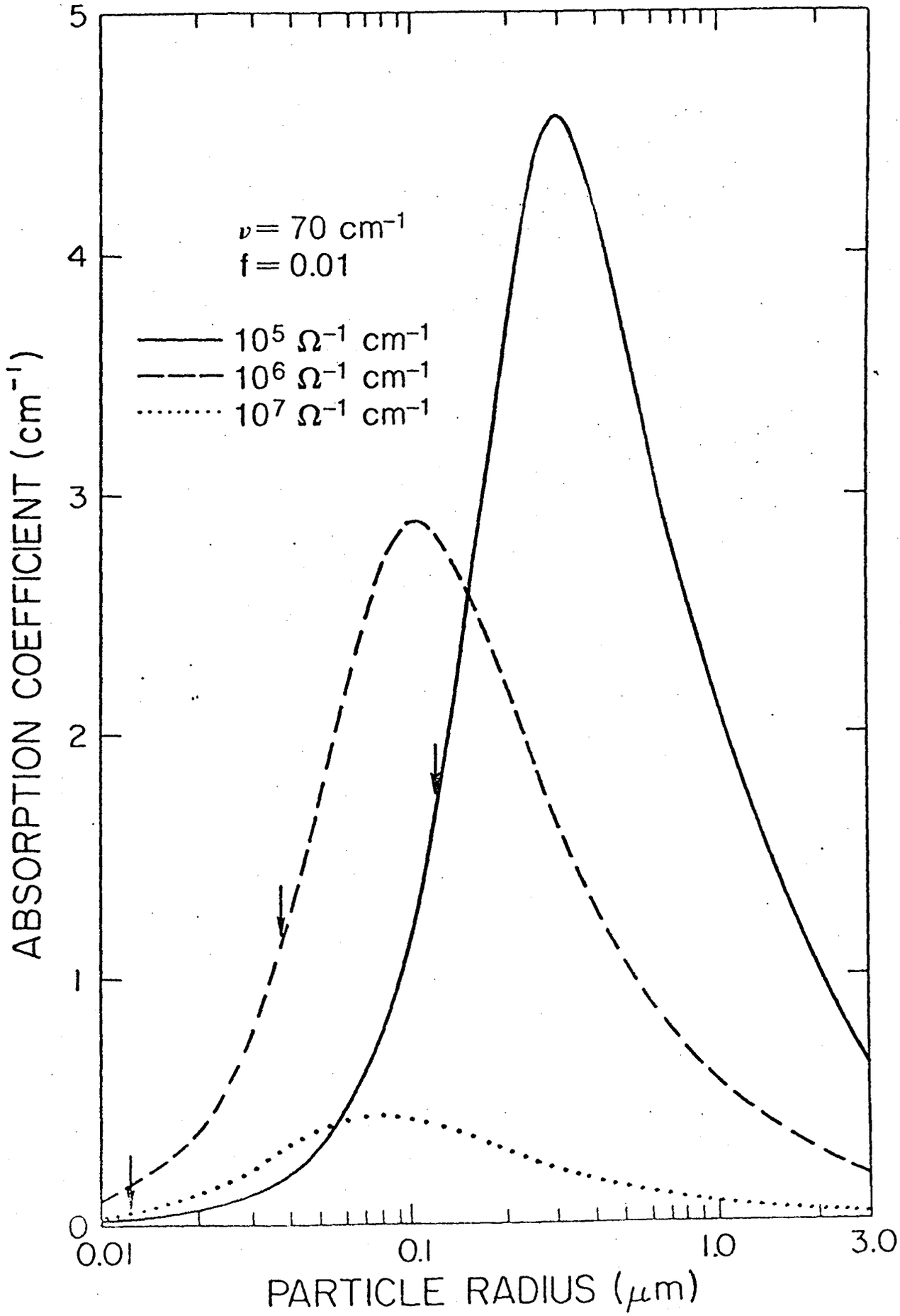
ν = 70 cm⁻¹
f = 0.01
10⁵ Ω⁻¹ cm⁻¹
10⁶ Ω⁻¹ cm⁻¹
10⁷ Ω⁻¹ cm⁻¹
ABSORPTION COEFFICIENT (cm⁻¹)
PARTICLE RADIUS (μm)
0
1
2
3
4
5
0.01
0.1
1.0
3.0

Figure 7

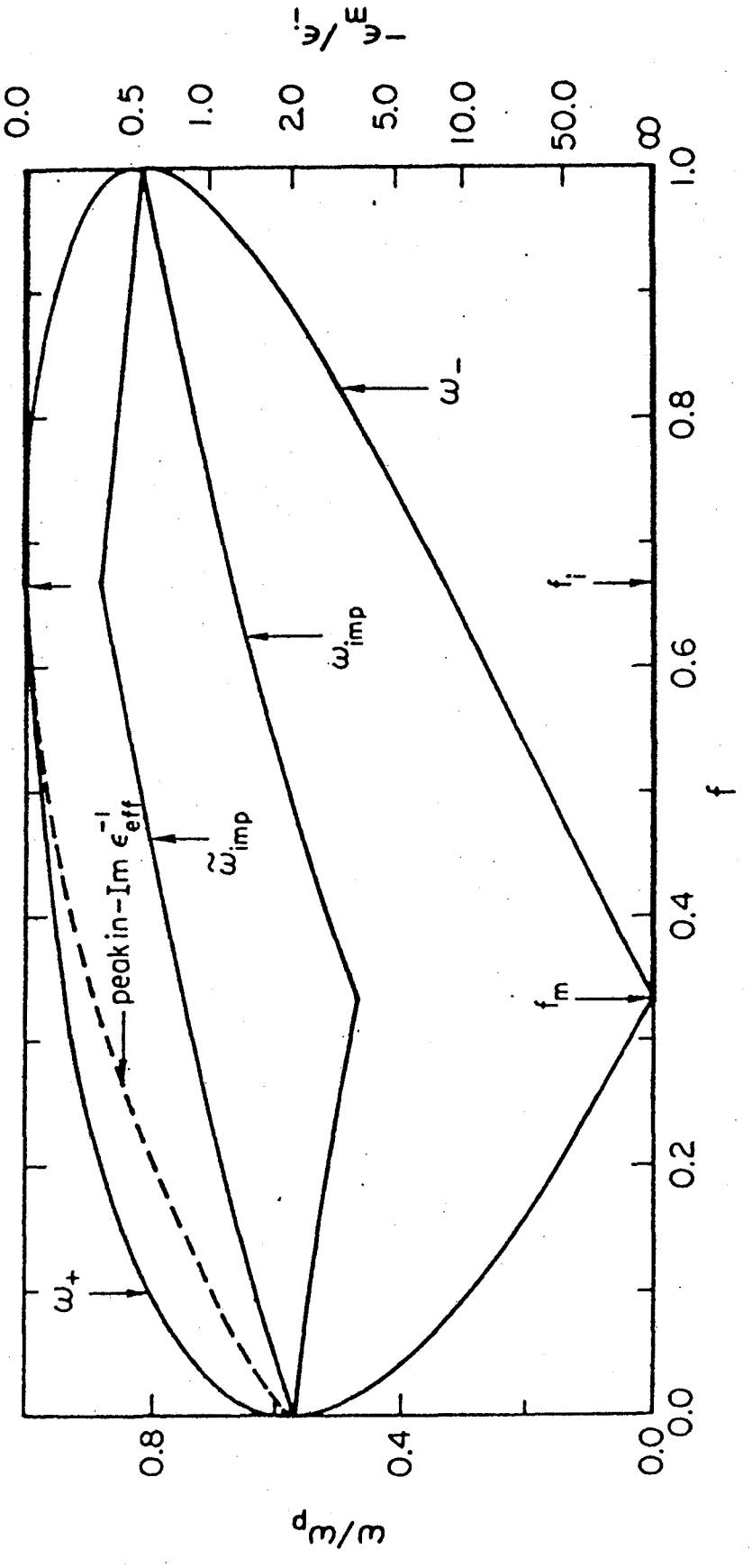
ω_p/ω
0.0
0.4
0.8
ω_+
peak in -Im ϵ_{eff}^{-1}
$\tilde{\omega}_{imp}$
ω_{imp}
ω_-
f_m
f_i
0.0
0.2
0.4
0.6
0.8
1.0
f
$-\epsilon_m/\epsilon_i$
0.0
0.5
1.0
2.0
5.0
10.0
50.0
∞

Figure 8

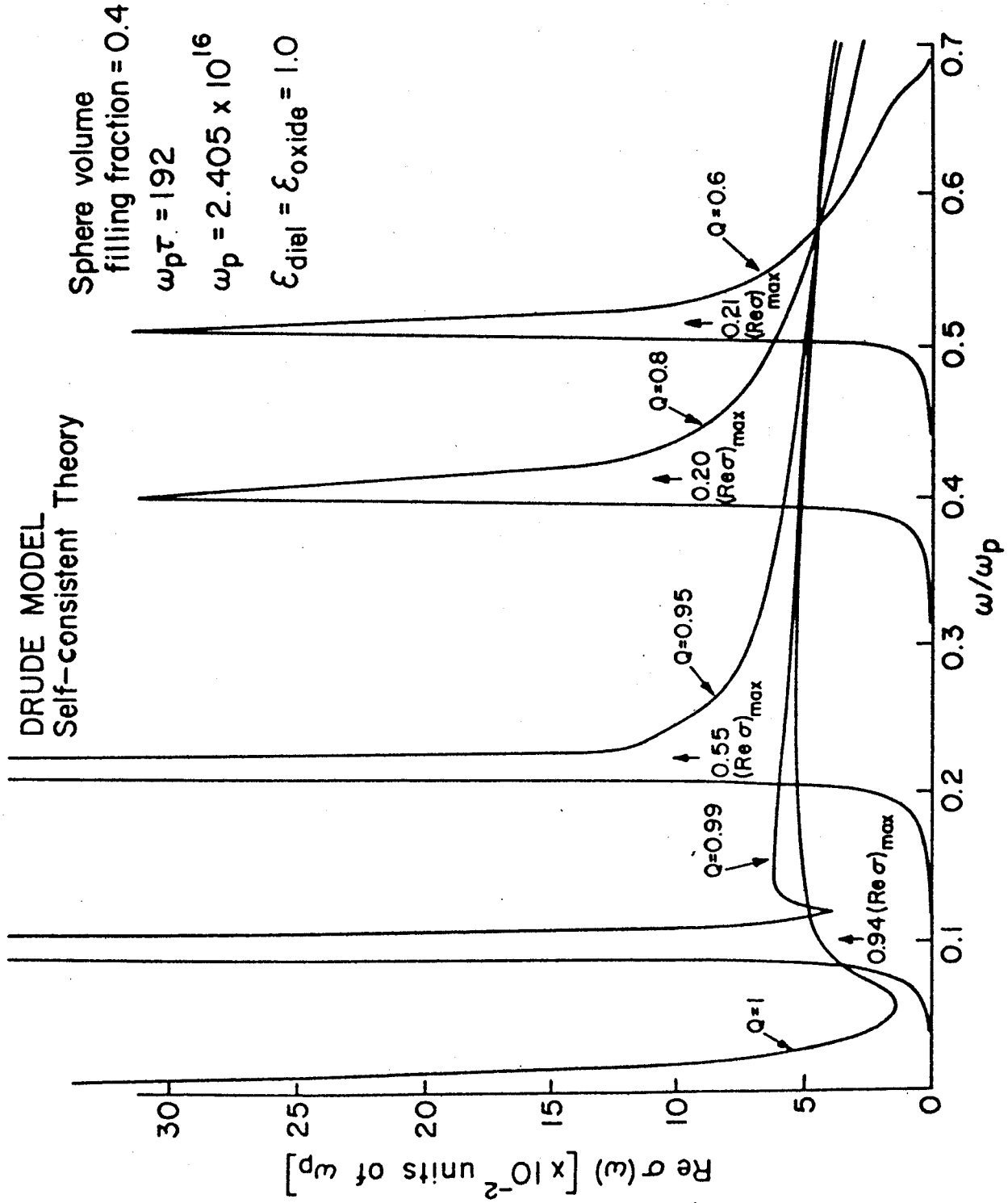
DRUDE MODEL
Self-consistent Theory
Sphere volume filling fraction = 0.4
$\omega_p\tau$ = 192
ω_p = 2.405 x 10^{16}
$\varepsilon_{diel} = \varepsilon_{oxide}$ = 1.0
Re σ(ω) [x 10^{-2} units of ω_p]
ω/ωp
Q=1
Q=0.99
Q=0.95
Q=0.8
Q=0.6
0.94 (Re σ)max
0.55 (Re σ)max
0.20 (Re σ)max
0.21 (Re σ)max

Figure 9.

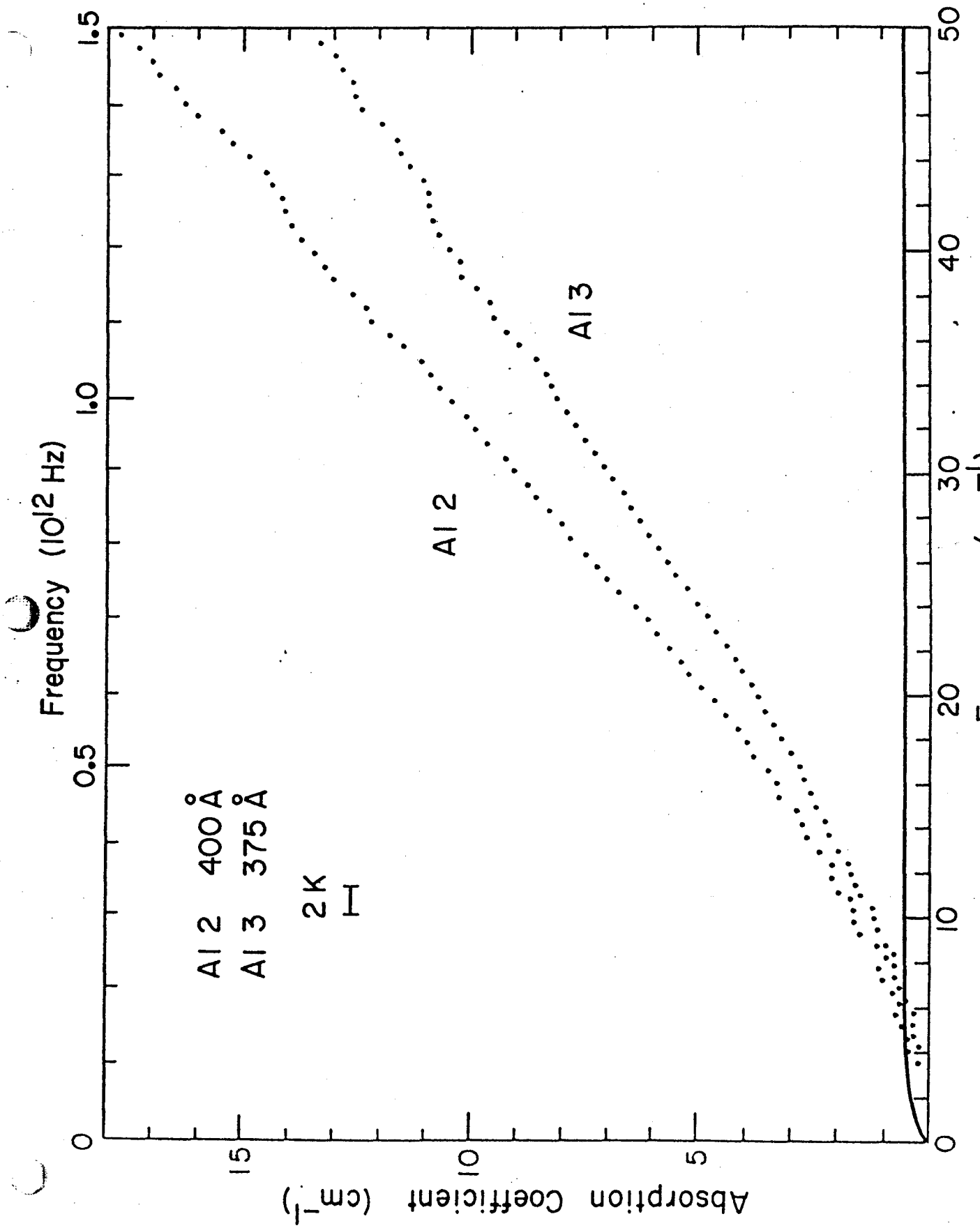

PRB15/FEB/BR401/FIG. 4/70 pp

Figure 10

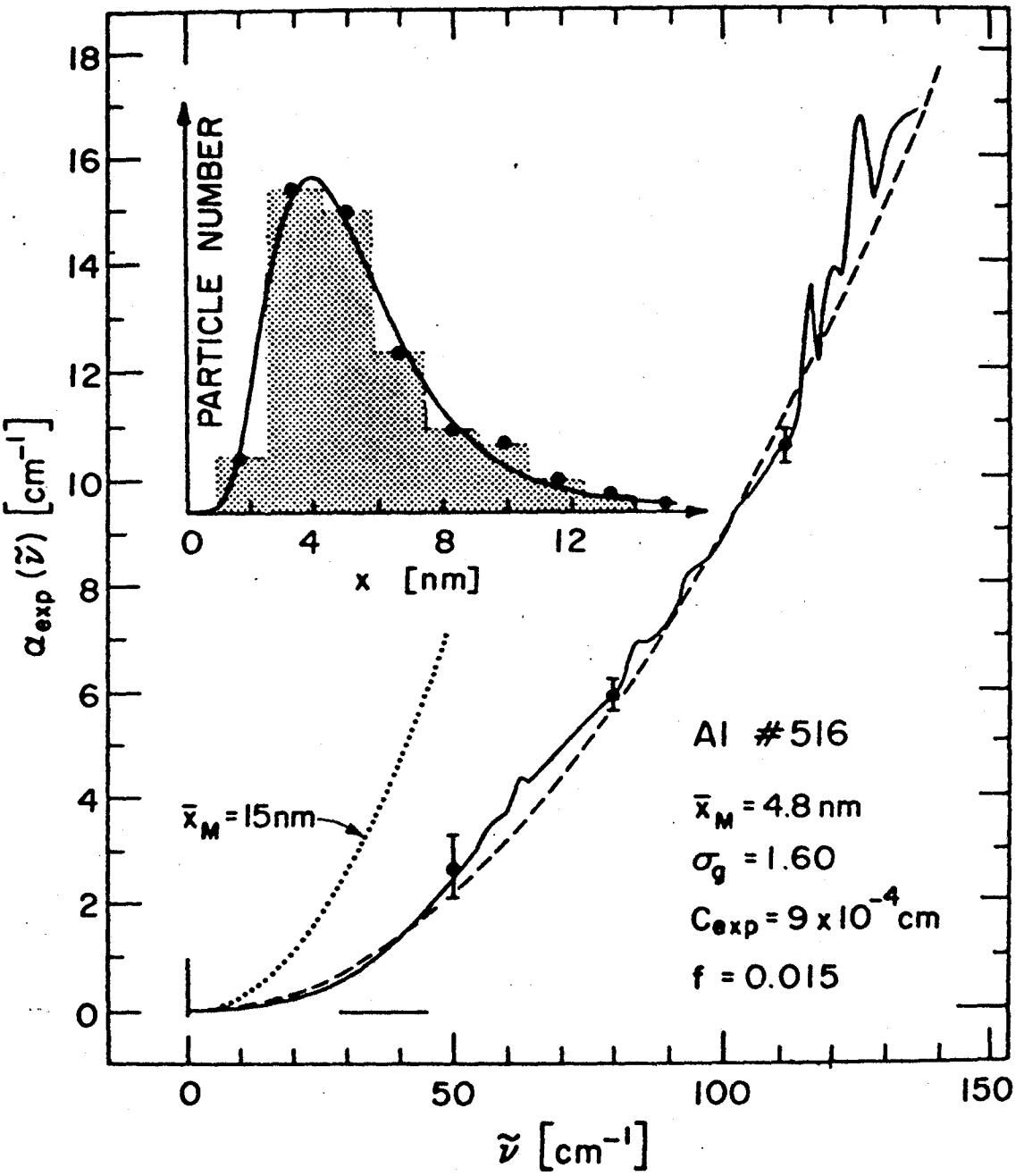
PARTICLE NUMBER
x [nm]
$\alpha_{exp}(\tilde{\nu})$ [cm^{-1}]
$\tilde{\nu}$ [cm^{-1}]
$\bar{x}_M$ = 15nm
Al #516
$\bar{x}_M$ = 4.8 nm
σ_g = 1.60
C_{exp} = 9 x 10^{-4} cm
f = 0.015

Figure 11

Fig. 12

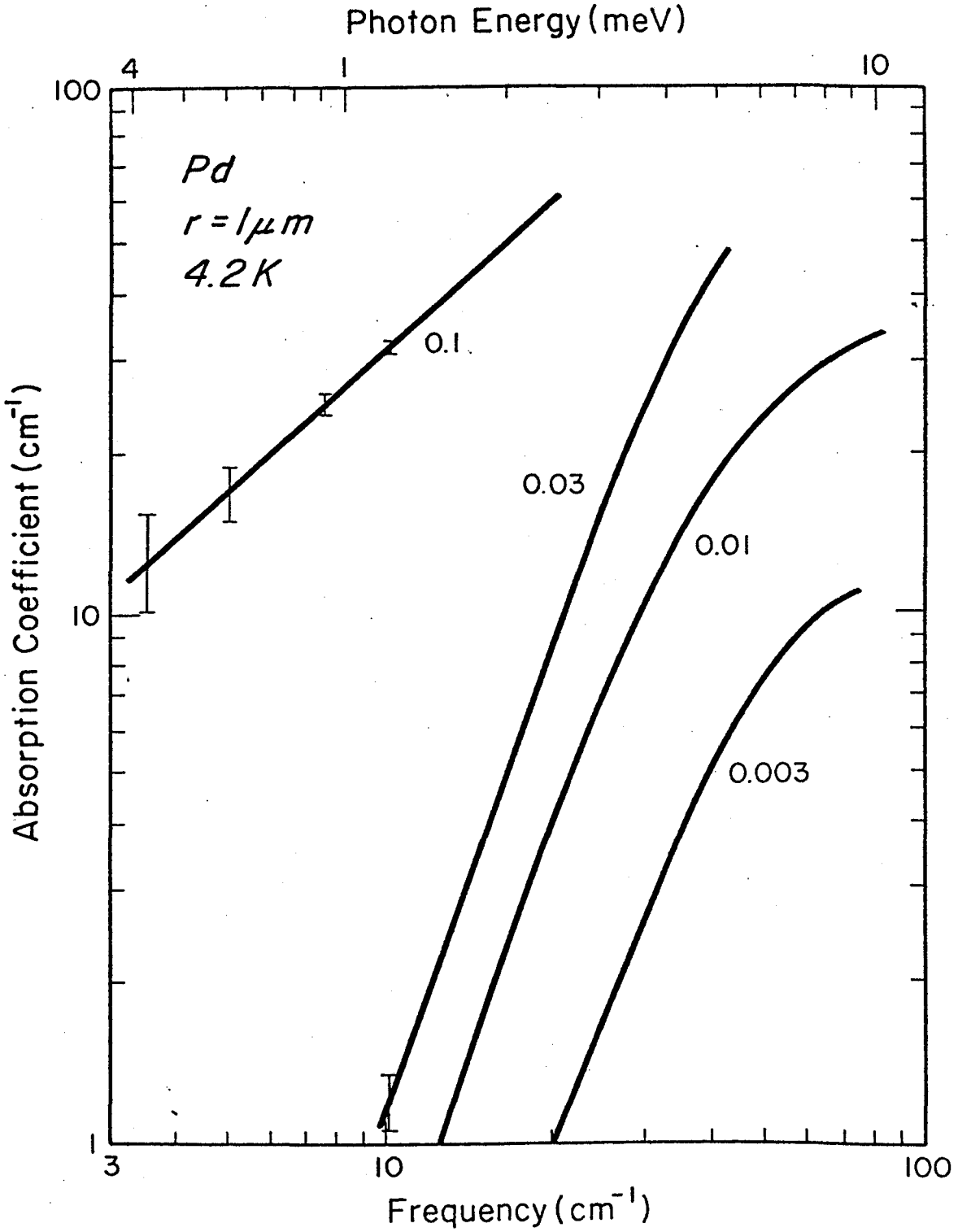

PRB1/BT 1416/JAN/FIG.3

50%

Figure 12

Fig. 13

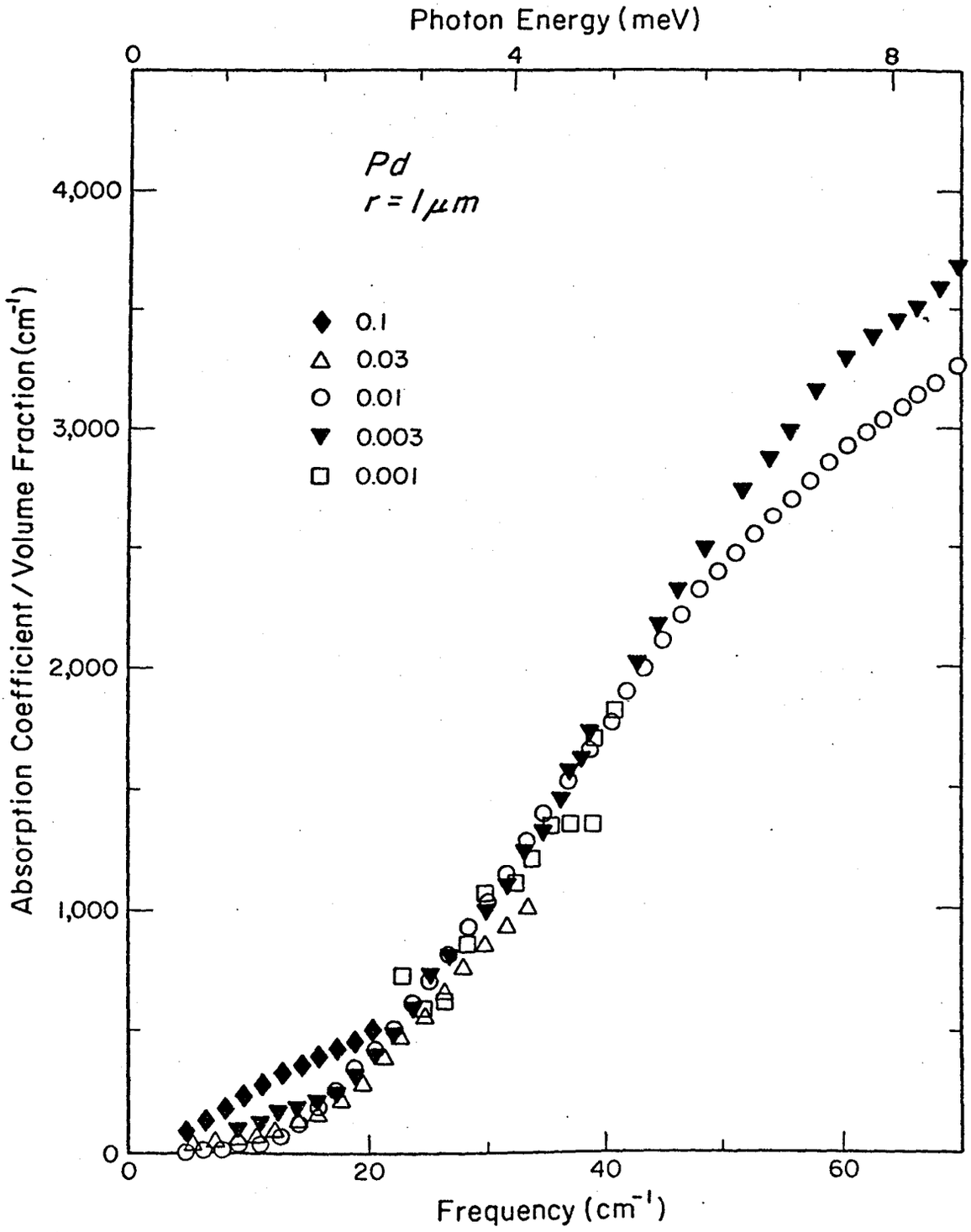

PRB1/BT 1416/JAN/FIG. 4

50%

Figure 13

Fig. 14

June 815/82/1407/k/ 50%

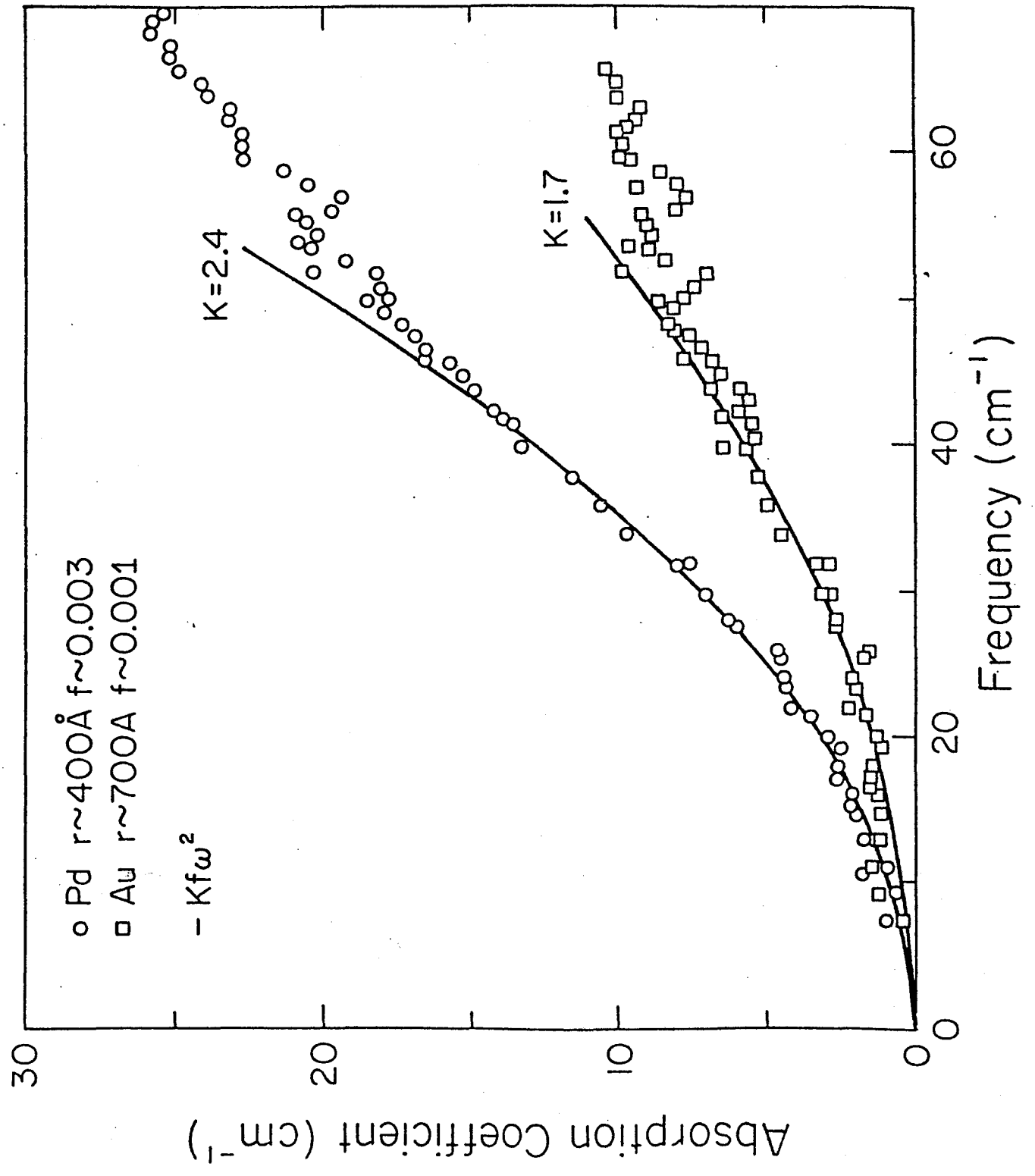

Figure 14

Fig. 15

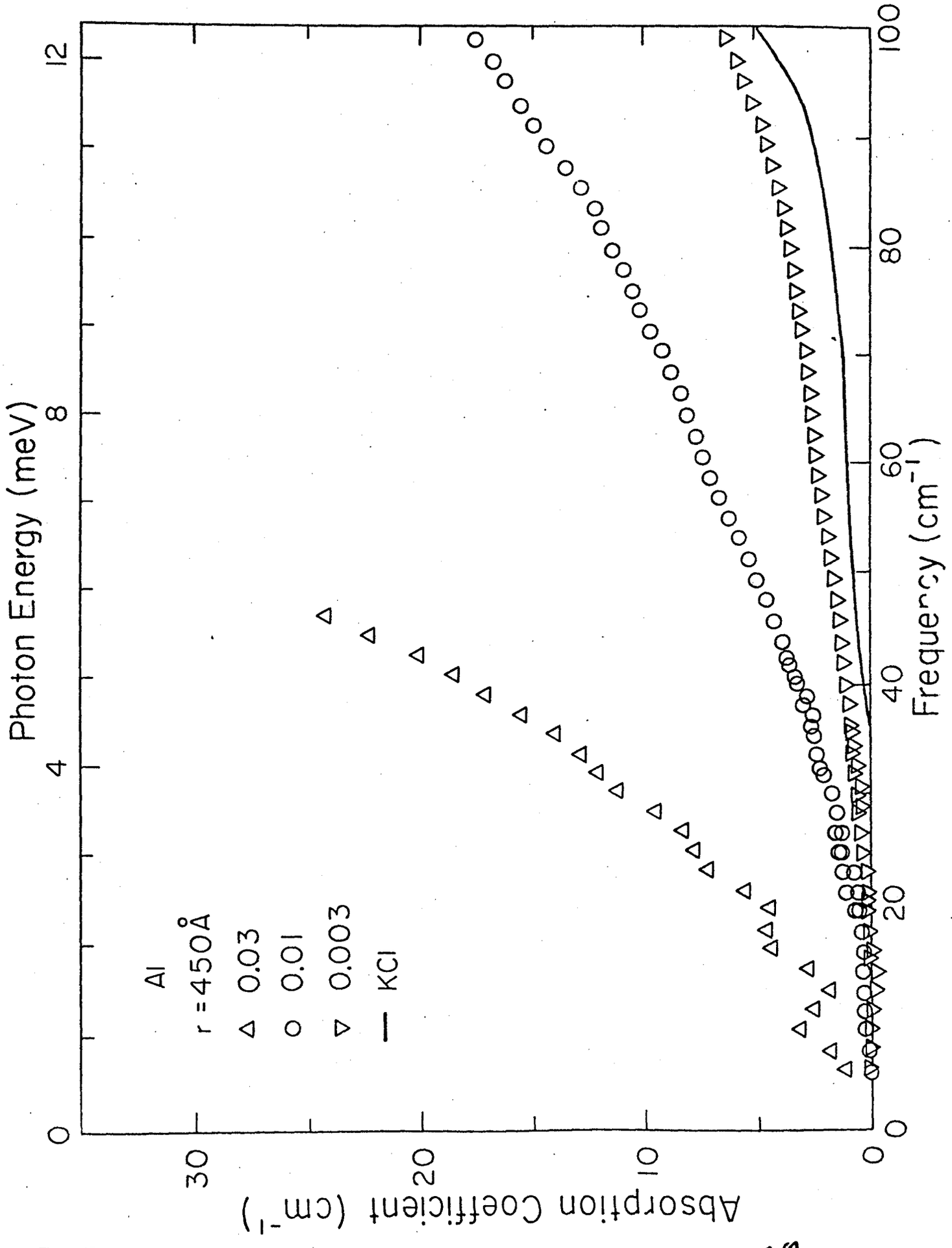

Figure 15

THE REFRACTION IS 45%

Fig. 16

June 815/82/1407/4/ 50%

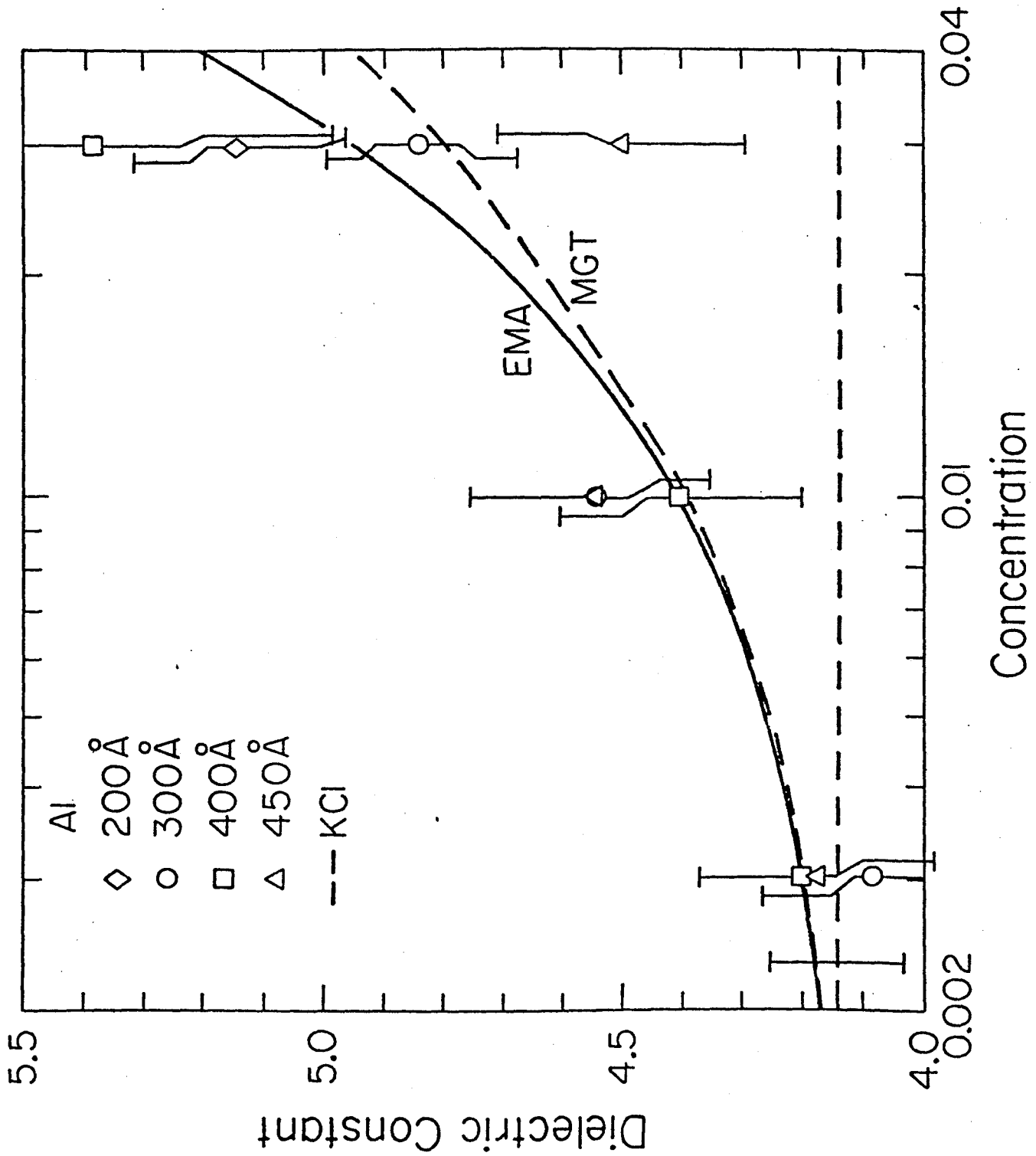

Figure 16

Fig. 17

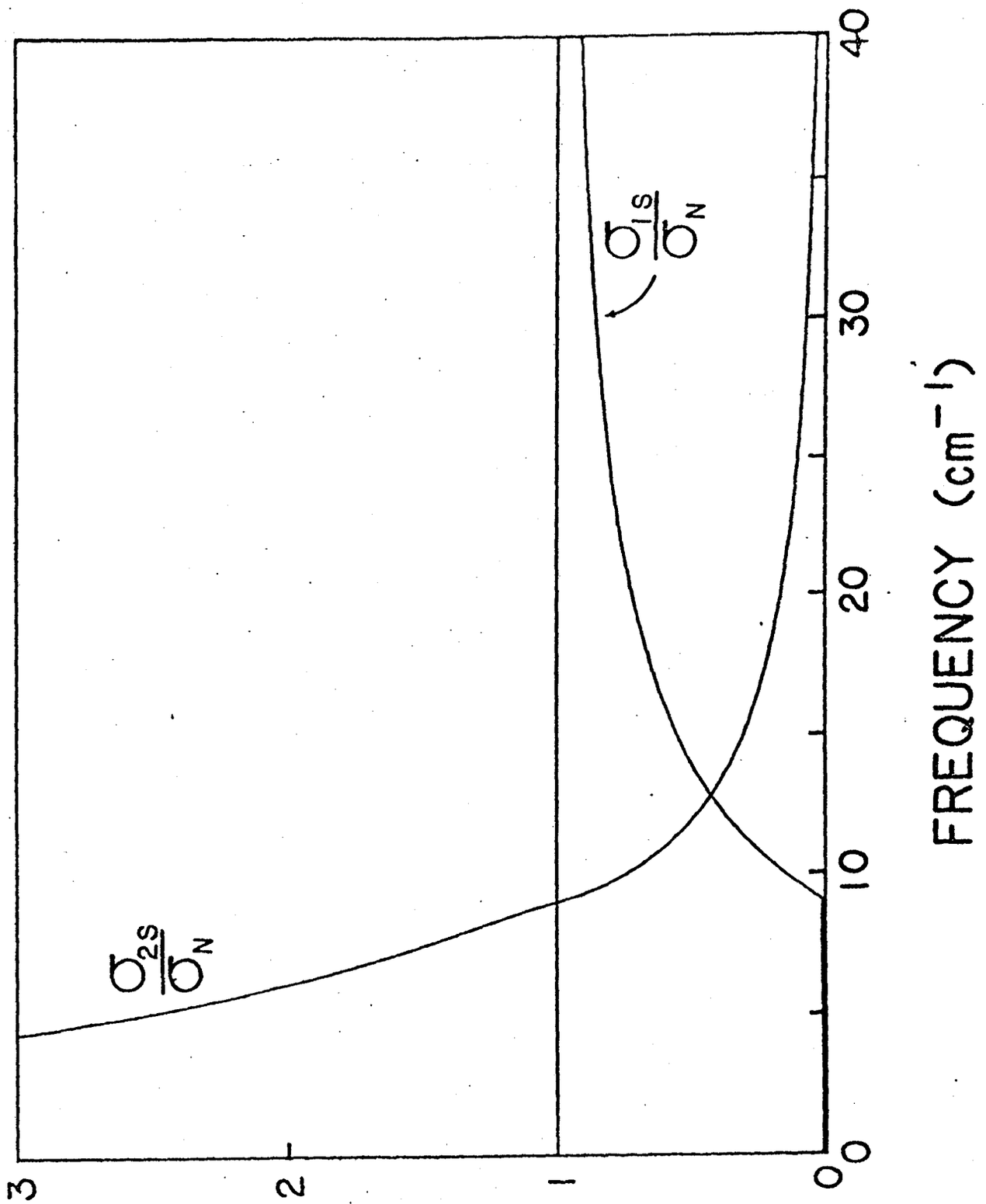

Figure 17

Fig. 18

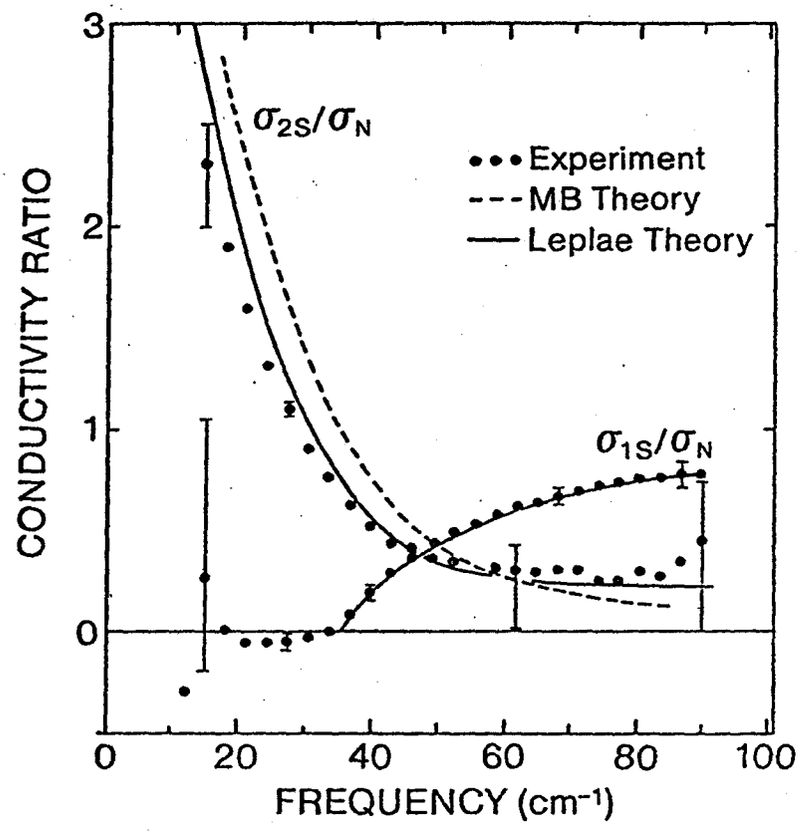

Figure 18

Fig. 19

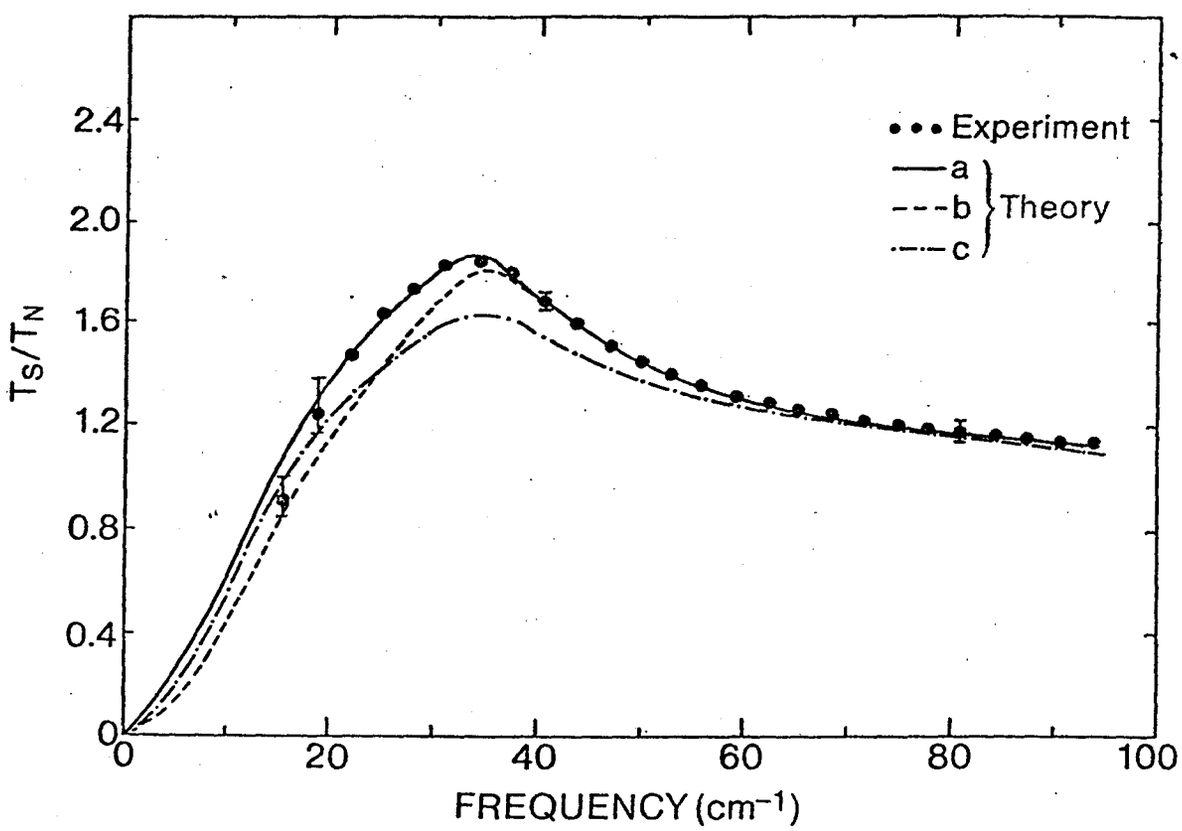

Figure 19

Fig. 20

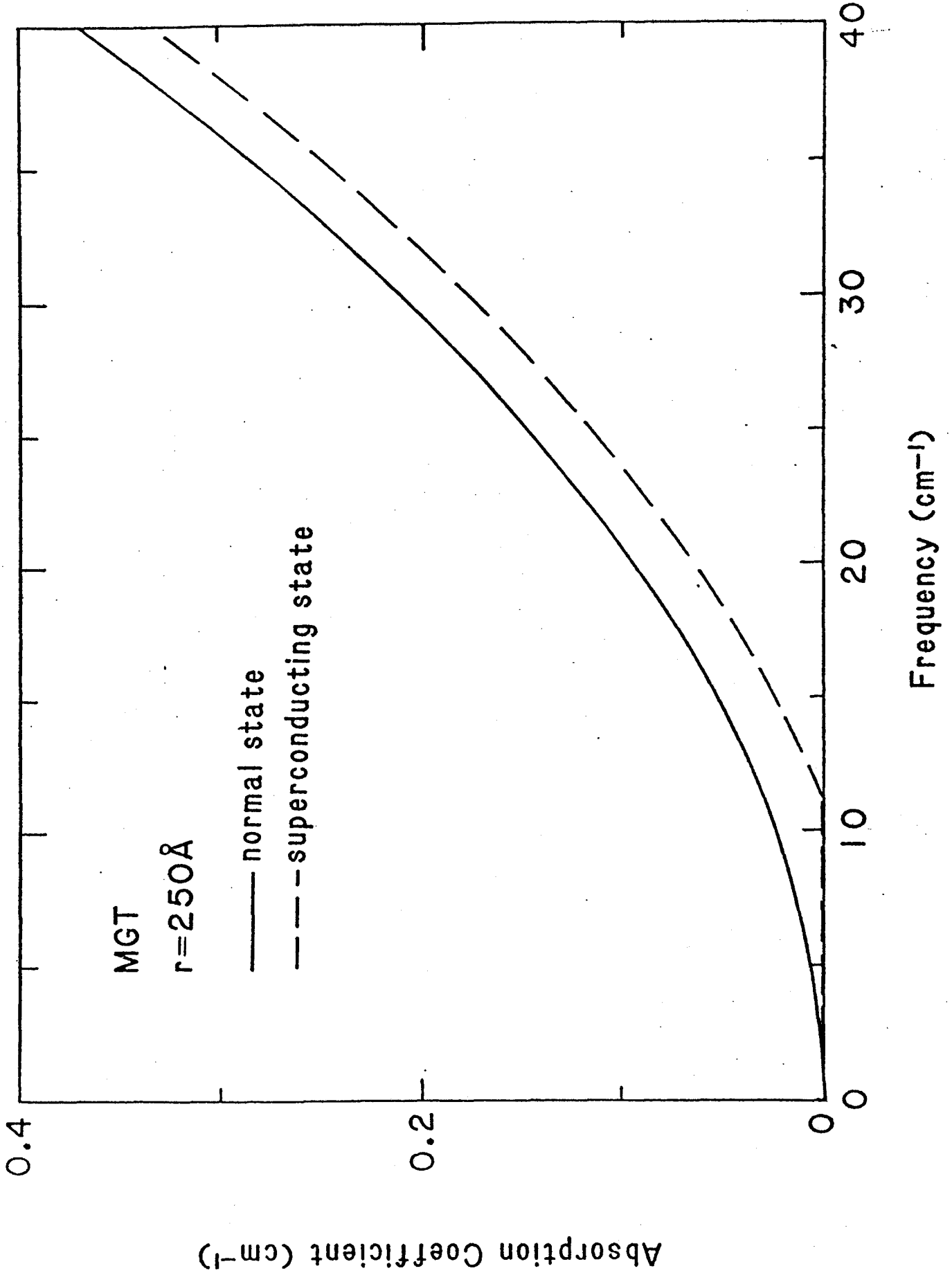

Figure 20

Fig. 21

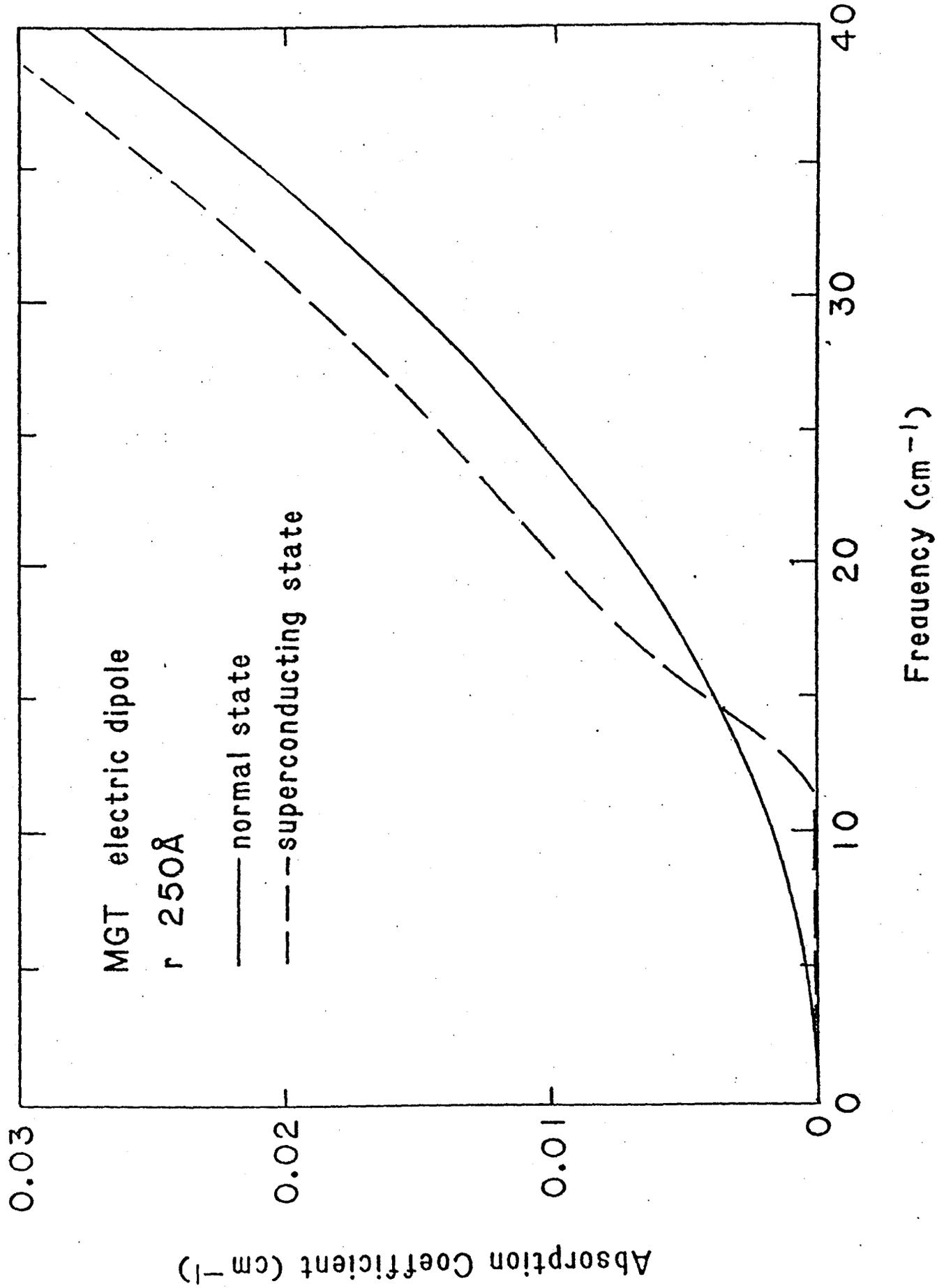

Figure 21

Figure 22

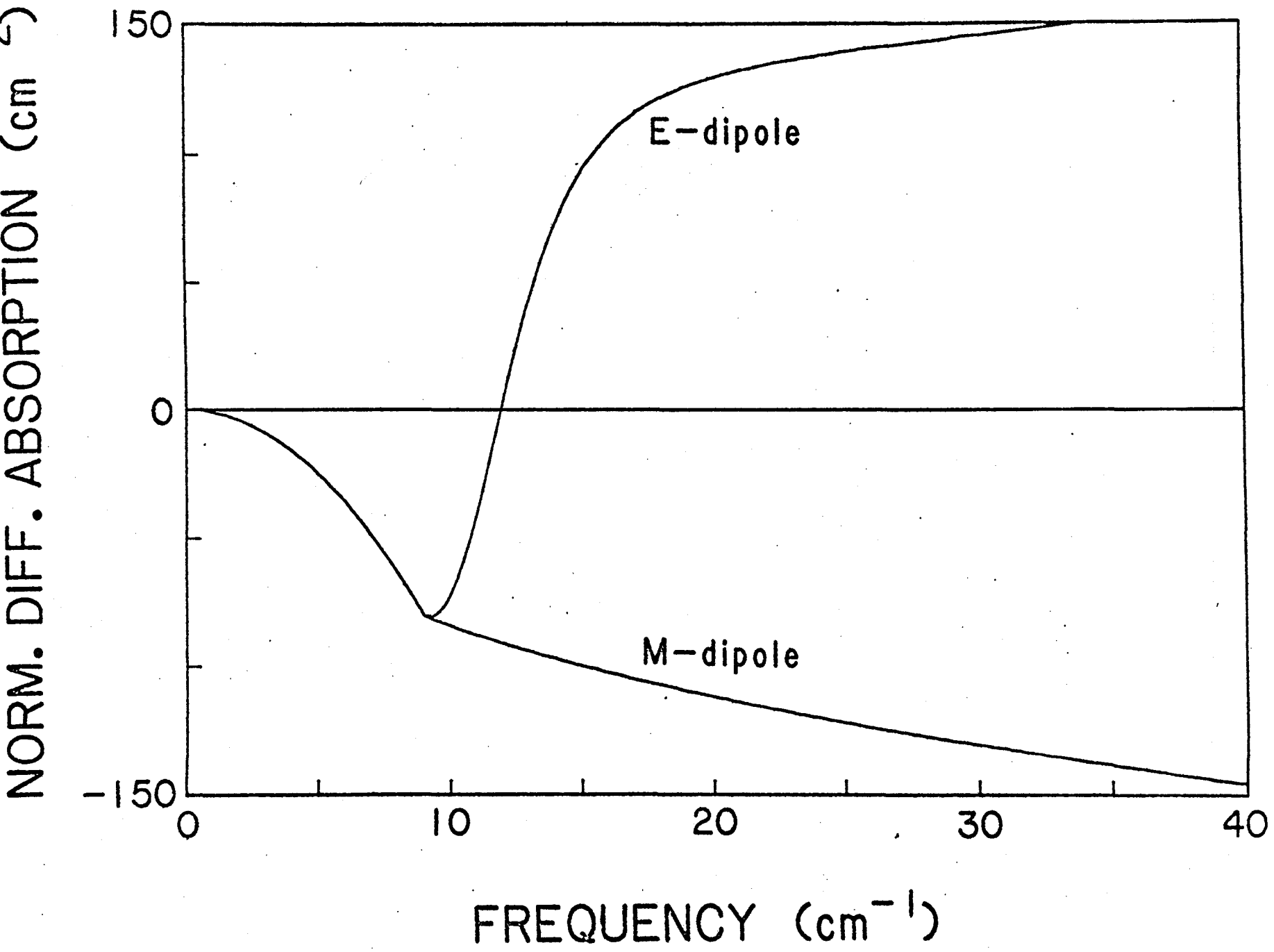
NORM. DIFF. ABSORPTION (cm^{-2})
150
0
−150
E−dipole
M−dipole
0
10
20
30
40
FREQUENCY (cm^{-1})

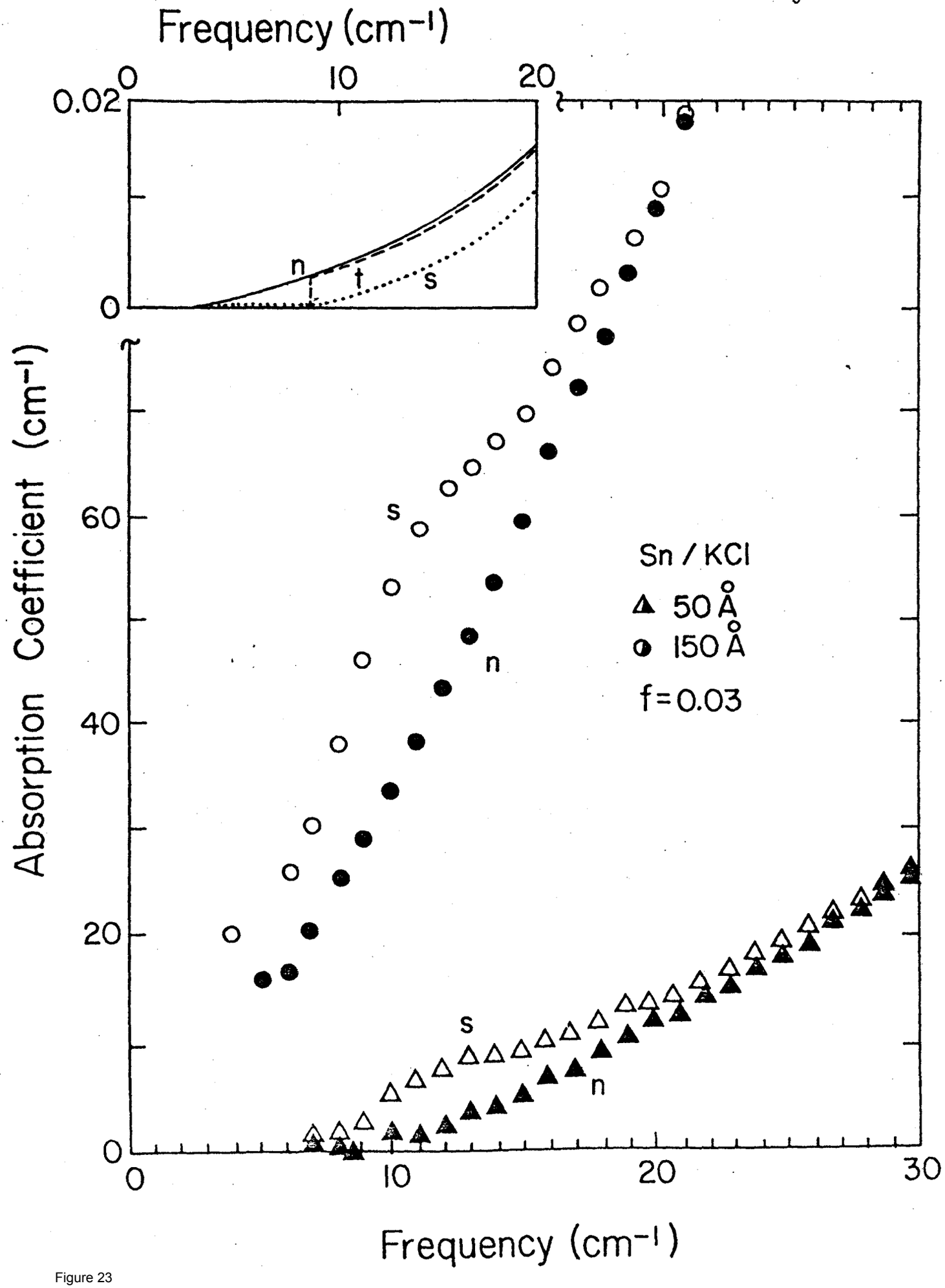
Frequency (cm⁻¹)
0
10
20
0.02
0
n
t
s
Absorption Coefficient (cm⁻¹)
60
40
20
0
s
n
Sn / KCl
50 Å
150 Å
f=0.03
s
n
0
10
20
30
Frequency (cm⁻¹)

Figure 23

Fig. 24

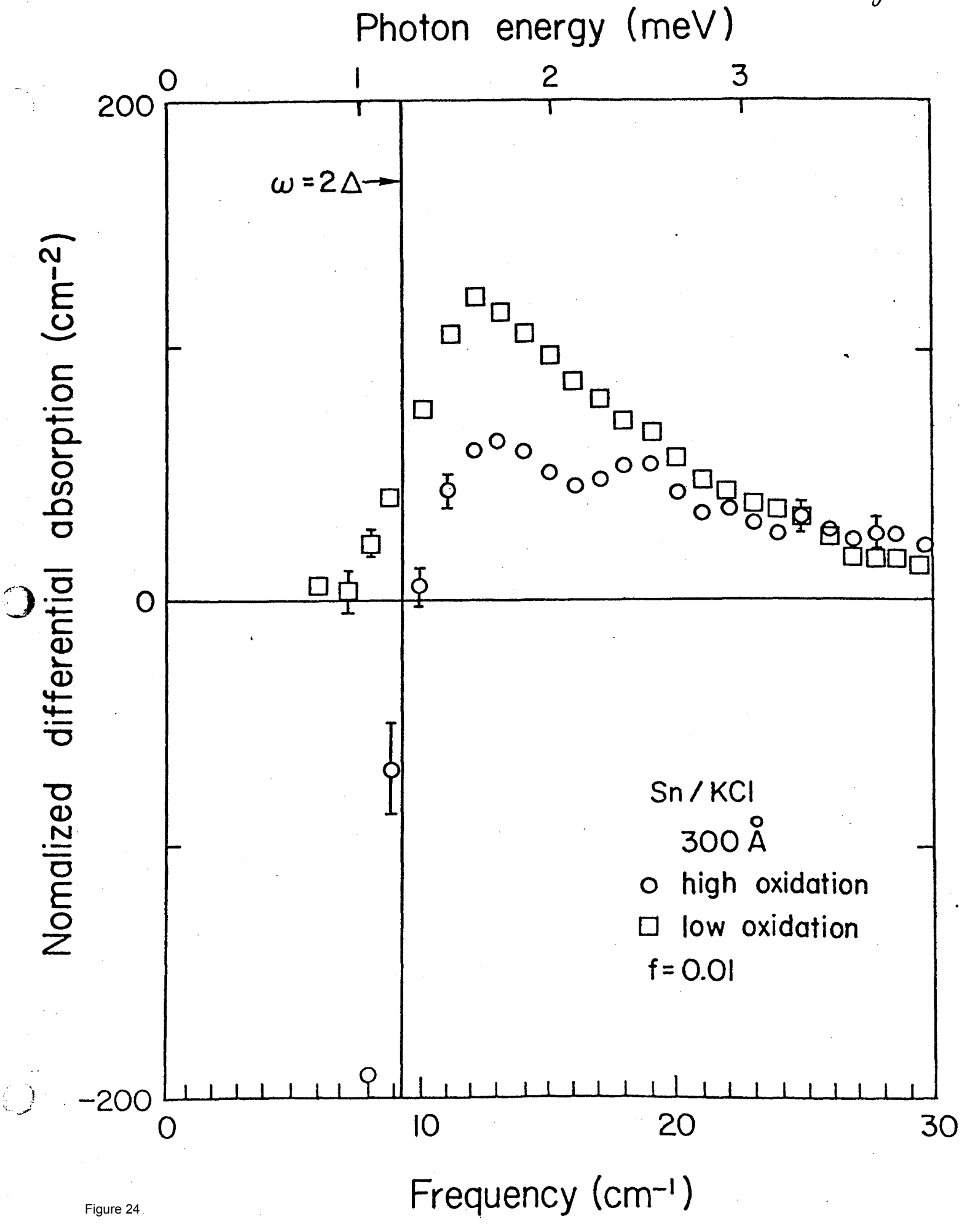

Figure 24

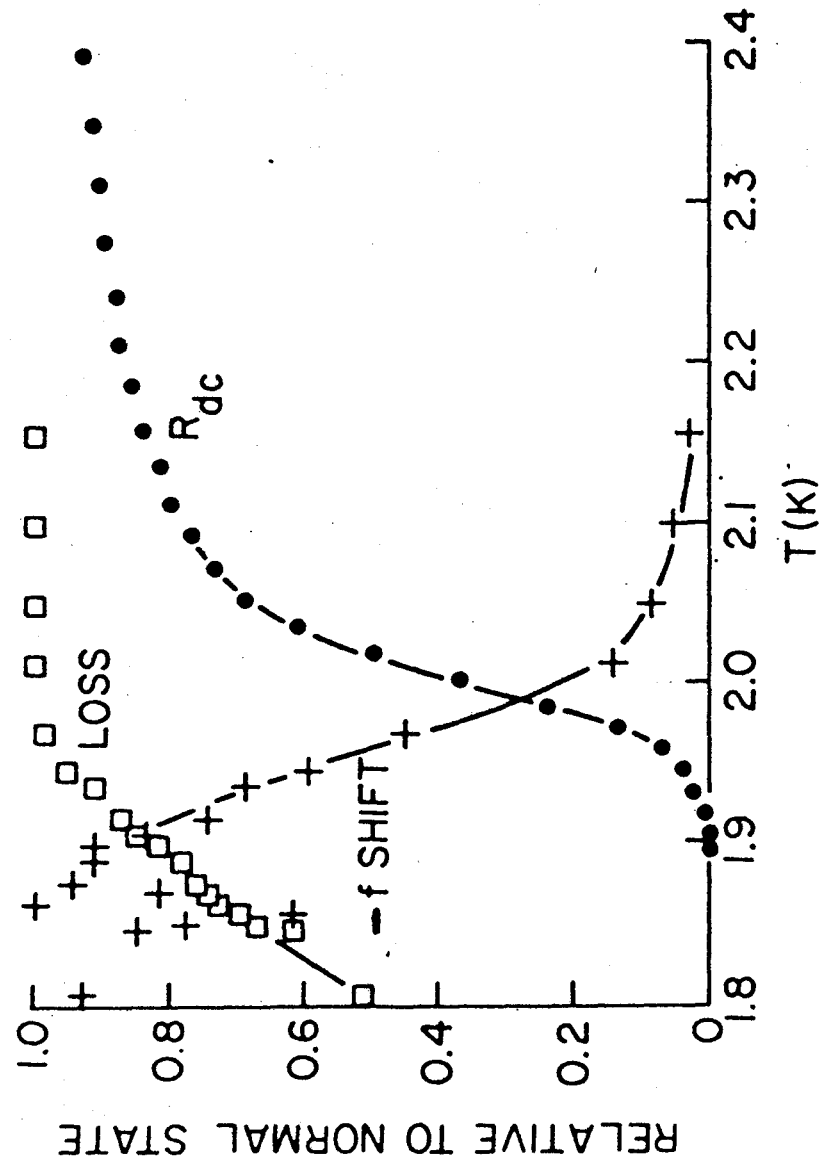
RELATIVE TO NORMAL STATE
1.0
0.8
0.6
0.4
0.2
0
1.8
1.9
2.0
2.1
2.2
2.3
2.4
T(K)
LOSS
R_{dc}
f SHIFT

Figure 25

Fig 26

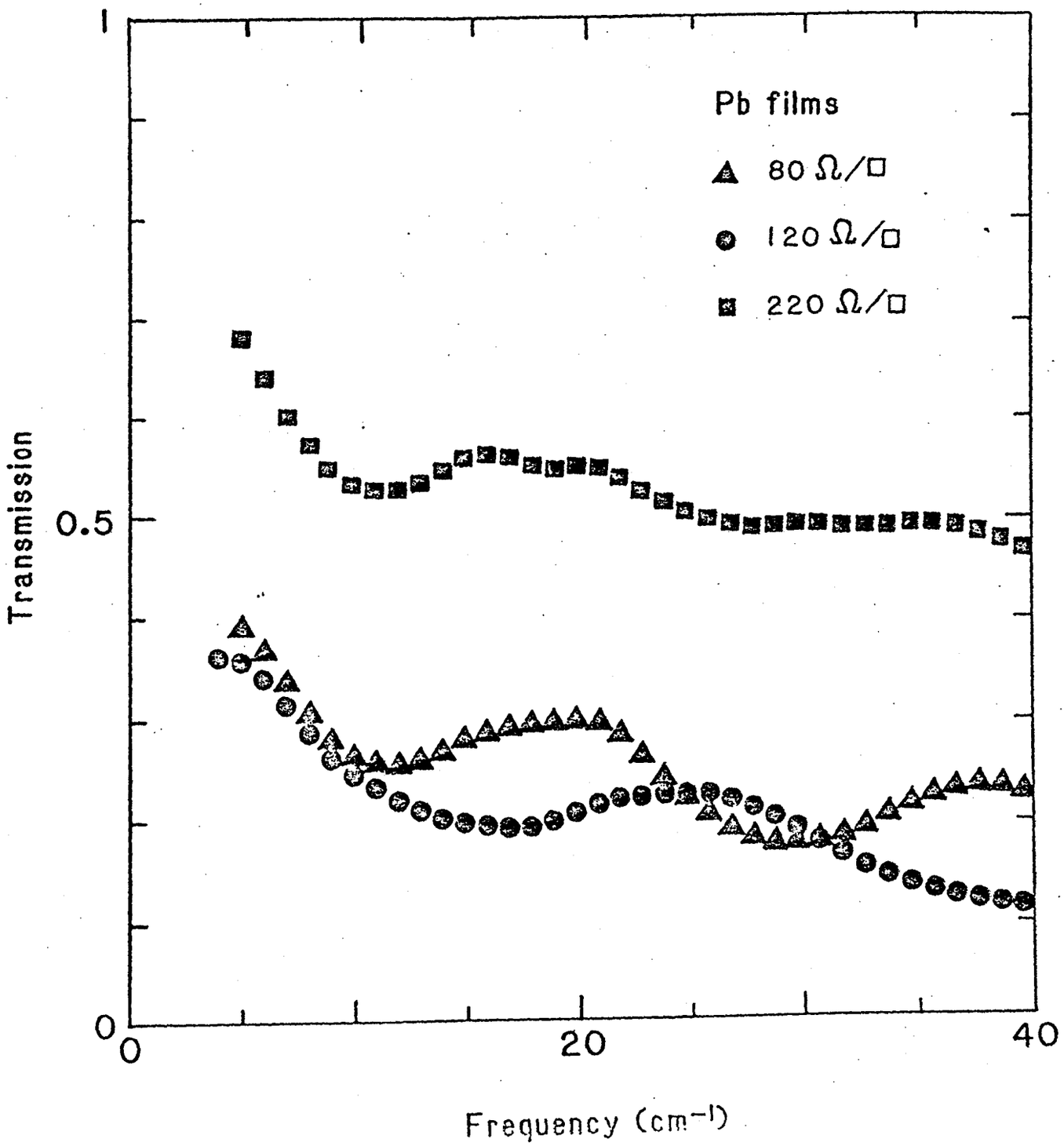

Figure 26

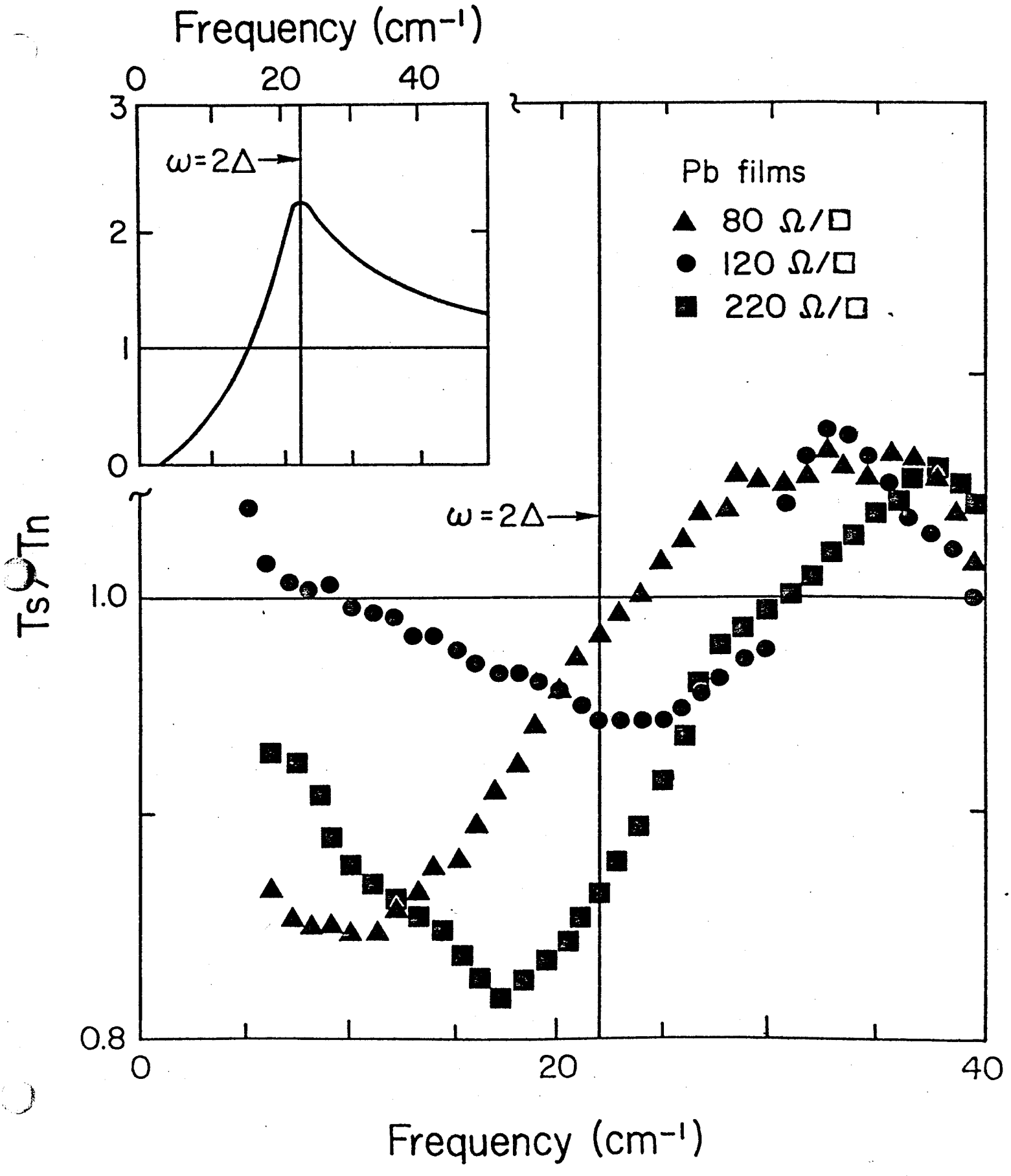
Frequency (cm⁻¹)
0
20
40
3
2
1
0
ω=2Δ
Pb films
80 Ω/□
120 Ω/□
220 Ω/□
Ts/Tn
ω=2Δ
1.0
0.8
0
20
40
Frequency (cm⁻¹)

Figure 27

Fig. 28

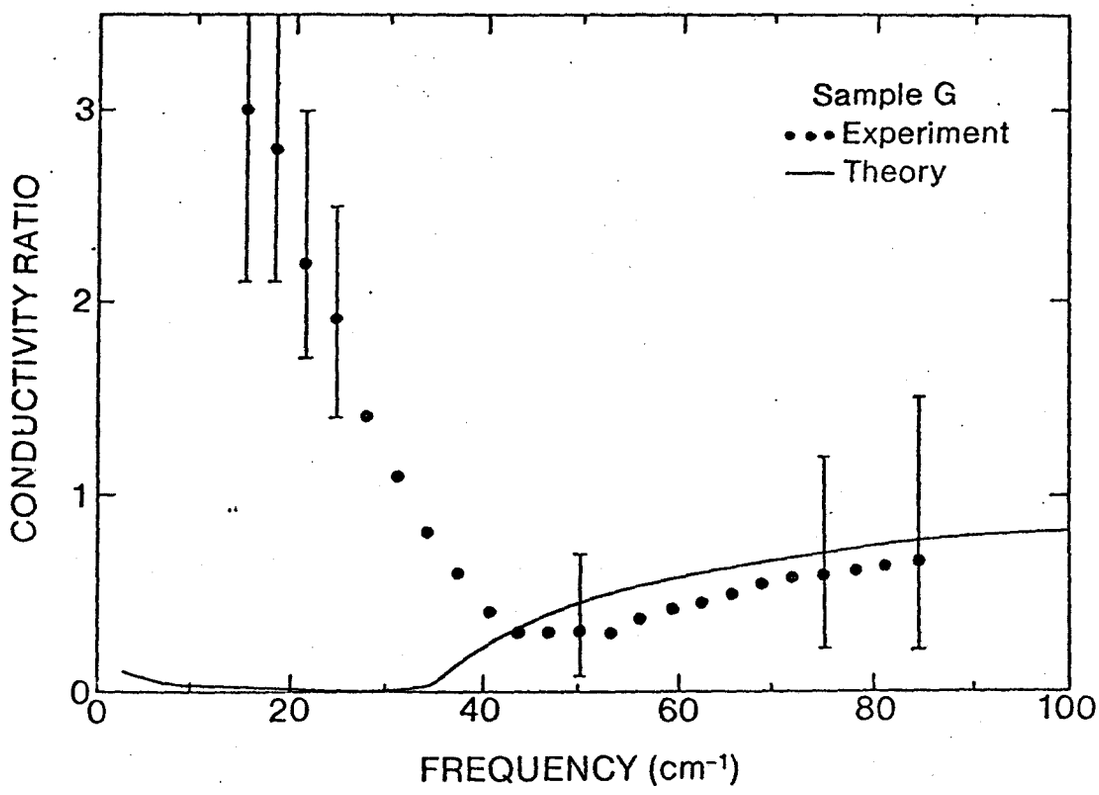

Figure 28

Fig 29

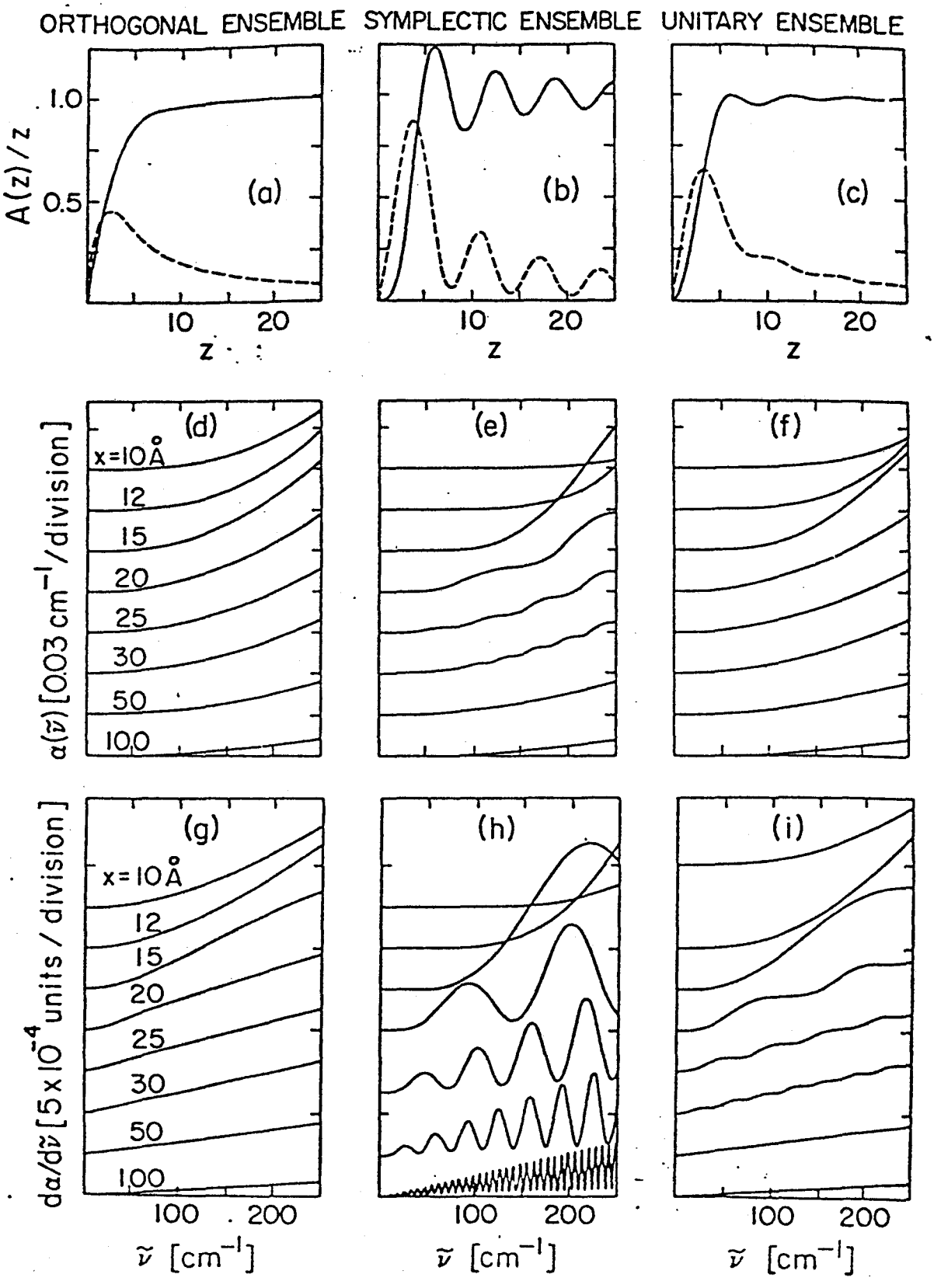

Figure 29

Fig. 30

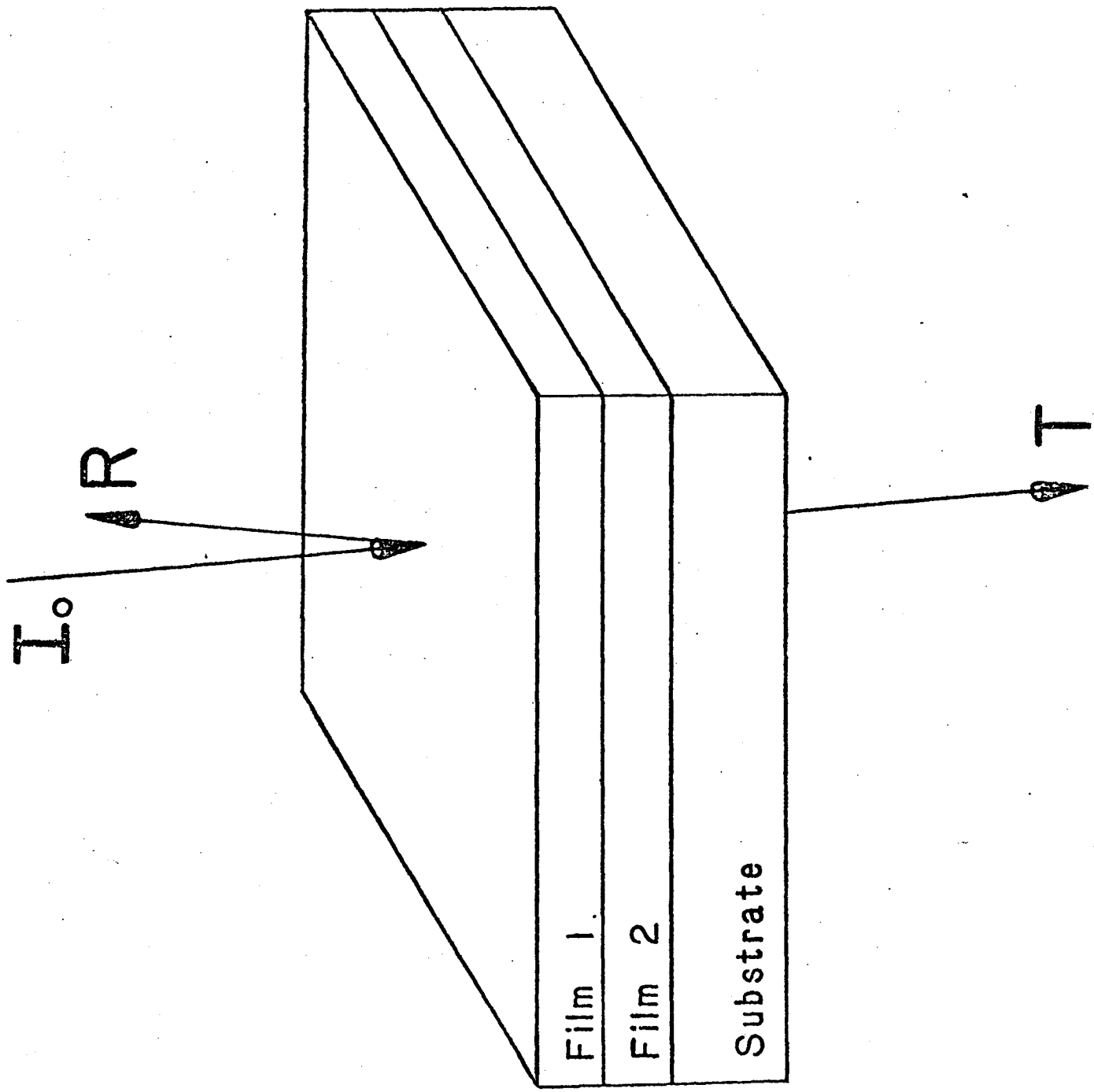

Figure 30

Figure 31

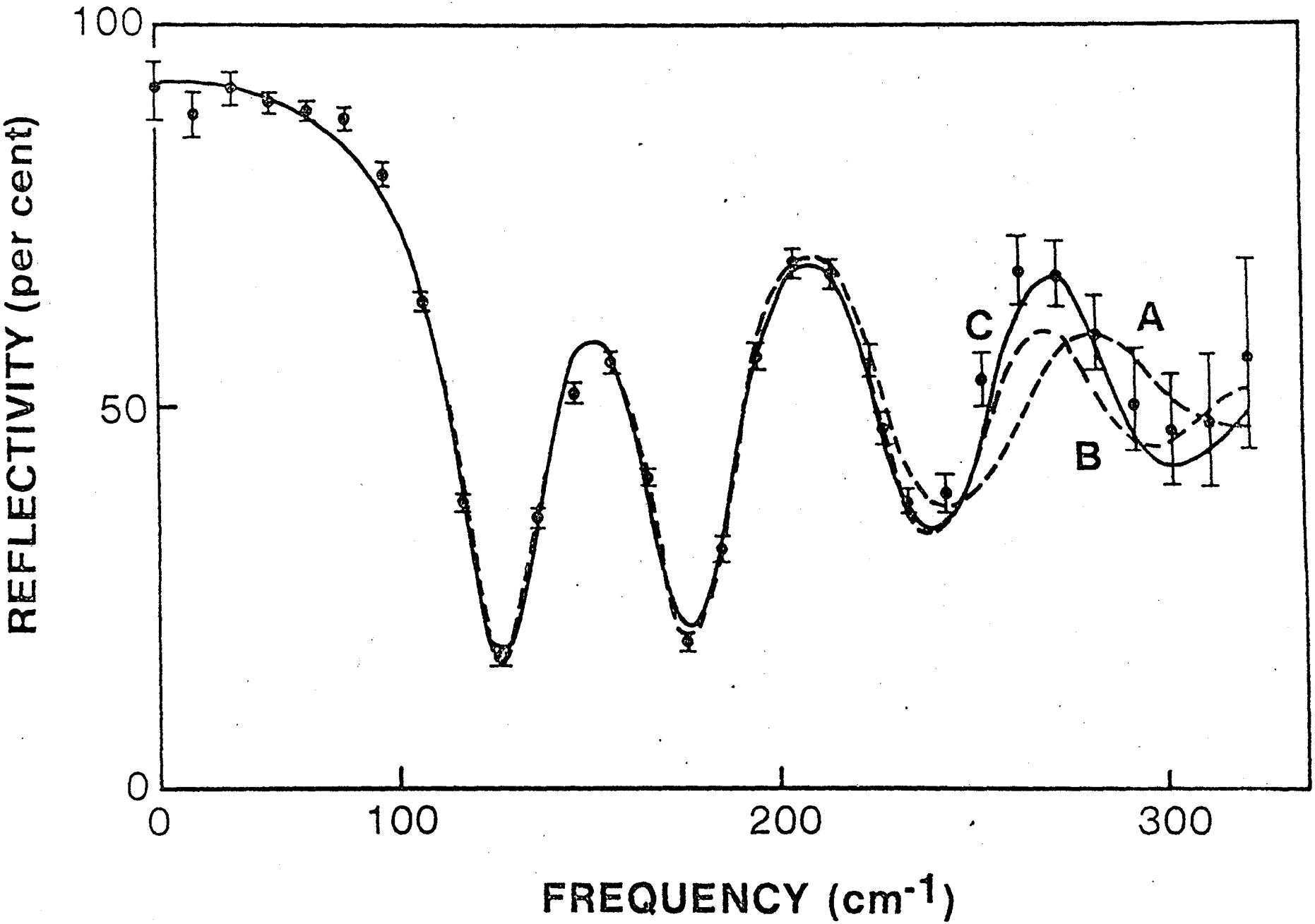
100
50
0
REFLECTIVITY (per cent)
0
100
200
300
FREQUENCY (cm-1)
A
B
C

Fig. 32.

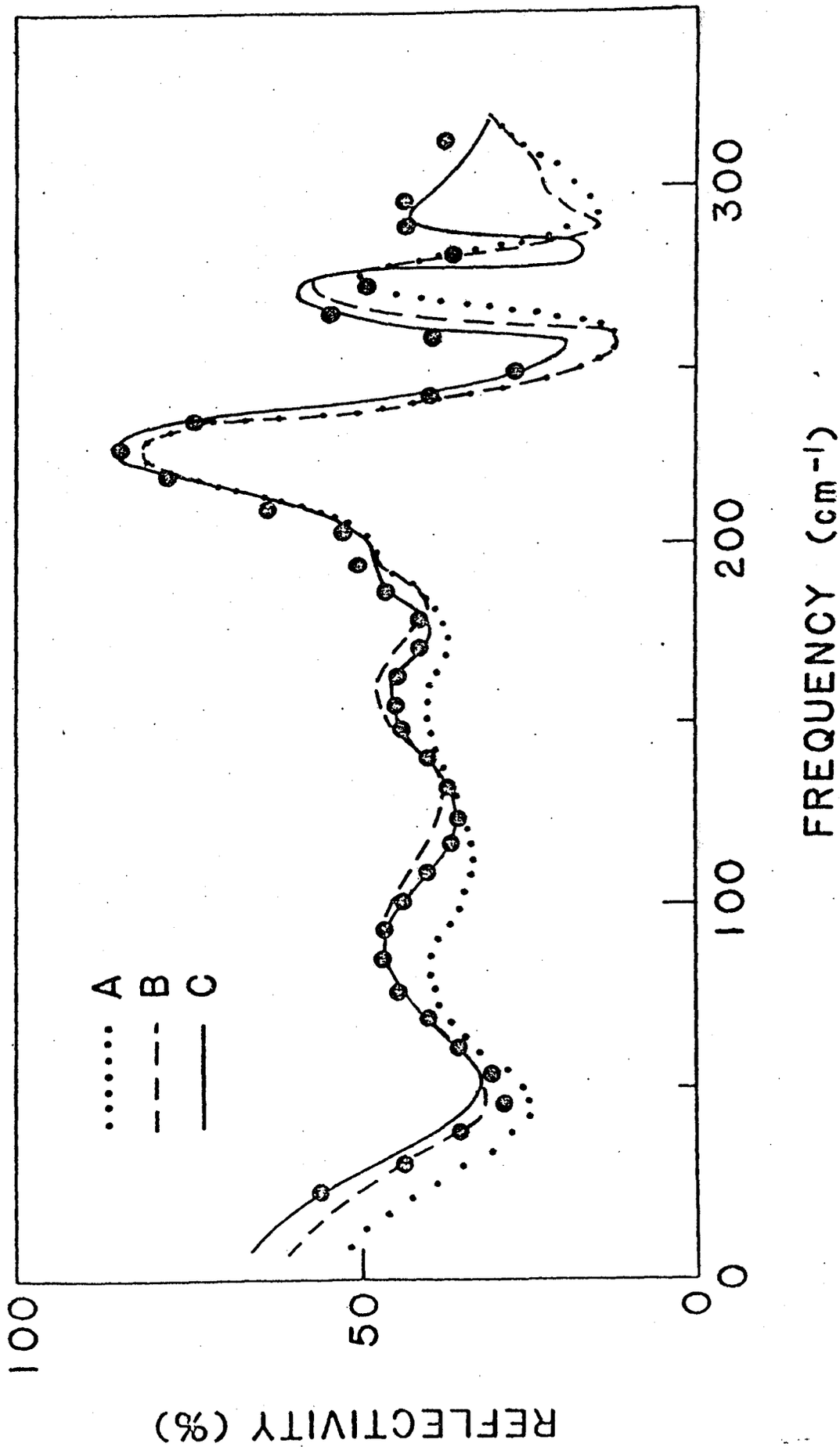

Figure 32